University of South Carolina
Scholar Commons

Theses and Dissertations

Spring 2020

Development, Validation, and Application of a Novel Method to Separate and Quantify Silver Intracellular Uptake in Pseudomonas aeruginosa

Mohammed A. Othman

Follow this and additional works at: https://scholarcommons.sc.edu/etd

 Part of the Environmental Health Commons

Recommended Citation

Othman, M. A.(2020). *Development, Validation, and Application of a Novel Method to Separate and Quantify Silver Intracellular Uptake in Pseudomonas aeruginosa.* (Doctoral dissertation). Retrieved from https://scholarcommons.sc.edu/etd/5936

This Open Access Dissertation is brought to you by Scholar Commons. It has been accepted for inclusion in Theses and Dissertations by an authorized administrator of Scholar Commons. For more information, please contact dillarda@mailbox.sc.edu.

Development, Validation, and Application of a Novel Method to Separate and Quantify Silver Intracellular Uptake in *Pseudomonas aeruginosa*

by

Mohammed A. Othman

Bachelor of Medicine and Surgery
Jazan University, 2010

Master of Science in Public Health
Tulane University, 2014

Submitted in Partial Fulfillment of the Requirements

For the Degree of Doctor of Philosophy in

Environmental Health Sciences

The Norman J. Arnold School of Public Health

University of South Carolina

2020

Accepted by:

Jamie R. Lead, Major Professor

Alan W. Decho, Committee Member

Mohammed Baalousha, Committee Member

Jim Hussey, Committee Member

Cheryl L. Addy, Vice Provost and Dean of the Graduate School

© Copyright by Mohammed A. Othman, 2020
All Rights Reserved.

DEDICATION

This dissertation is dedicated to my beloved parents, my wife Walaa the love of my life, my daughters, the apple of my eye, and my family and friends for their endless support.

ACKNOWLEDGEMENTS

I would like to express my deepest appreciation to Dr. Jamie Lead, for his expertise, assistance, guidance, and patience throughout my process of developing and writing this dissertation. The completion of this dissertation could not have been possible without your support. I am extremely grateful to Dr. Alan Decho for his invaluable support and guidance. I would like to extend my sincere gratitude to my committee members, Dr. Mohammed Baalousha, and Dr. James Hussey, for their support, suggestions, and encouragement.

I would like to thank my fellow graduate students in the CENR for their support and friendship. Heartfelt thanks to all my family, friends, and colleagues for their support, confidence, and belief in me. The author thanks Jazan University in Saudi Arabia for providing a scholarship and funding that support to complete my PhD.

ABSTRACT

Silver nanoparticles (AgNPs) have attracted tremendous attention as a potential broad-spectrum antimicrobial agent to overcome multidrug resistant (MDR) infections. However, a comprehensive understanding to AgNPs bactericidal mechanism of action and the relative role of particulate versus ionic Ag in AgNPs antibacterial activity is lacking but essential for their optimization for potential medical applications. Therefore, a novel method to separate and quantify Ag internalization in *P. aeruginosa* was developed and validated through multimethod approach. The methods used were optical density at 600 nm (OD600), LIVE/DEAD staining, transmission electron microscopy (TEM), and sorbed Ag liberation assays. After optimizing the method, it was applied to quantify Ag content in different bacterial fractions. To better understand the dynamic transformations of AgNPs upon exposure and the relative bioavailability/biouptake of different Ag species, bimetallic Au@Ag NPs was used and Ag:Au ratios were calculated in different bacterial compartments. Results showed a nearly constant OD600 within the first two hours of 50 mM EDTA treatment indicating complete bacterial growth cessation. However, bacterial density declined beyond this treatment condition indicating cell lysis. LIVE/DEAD staining images indicated intact bacterial membrane before- and after- EDTA treatment for six hours. Cell counts observed in untreated controls were statistically similar to cell counts after two hours exposure to EDTA. Whereas significantly (p <0.0001) fewer cells were observed in images after six hours EDTA exposure when compared to untreated controls. This suggested that complete disruption and lyses of cells may have occurred upon EDTA

exposures exceeding two hours rather than the simple cell membrane damage or/and increased permeability. TEM results indicated intact, smooth, and dense cell boundaries for untreated controls and cells exposed to EDTA for two hours. No membrane disintegrations were detected even after six hours EDTA treatment, but cells featured very light and thin surfaces near the cell edges compared to control. However, 50 mM EDTA treatment is a very high concentration and is expected to remove most of the periplasm. The plateau obtained in the Ag liberation curve, from the operationally defined sorbed fraction, within the first two hours of EDTA treatment suggested complete removal of sorbed Ag. Whereas the statistically significant (p <0.05) increase in Ag mass content after six hours EDTA treatment was likely as a result of cells lysis and/or increased membrane permeability. The weight of evidence across the multimethod approach suggested that two hours of EDTA treatment at a concentration of 50 mM provided a reproducible estimation of Ag uptake in the operationally defined internalized fraction approximating the accurate value in the Gram-negative bacterium *P. aeruginosa*. Therefore, this method was applied to quantify metallic distribution upon exposing bacteria to Au@Ag NPs. Ag distribution data indicated that the total Ag accumulated in the abiotic phase was mostly in dissolved form and was 45.5% and 54.8 % for 0.2 mg L^{-1} and 2.0 mg L^{-1} Au@Ag NPs exposure, respectively. The external cellular fractions after periplasm removal were 42.2% for 0.2 mg L^{-1} Au@Ag NPs exposure whereas for 2.0 mg L^{-1} Au@Ag NPs exposure it was 44.7%. The internalized fraction accumulated 16.2% ± 1.8 in 2.0 mg L^{-1} Au@Ag NPs exposure that was significantly greater (p = 0.0066) than 9.9% ± 1.1 in 0.2 mg L^{-1} Au@Ag NPs exposure. On the other hand, molar ratios were significantly greater consistently in all biotic phase fractions at lower exposure concentration except for internalized fraction.

Molar ratios detected in both abiotic phase (p >0.9999) and internalized fractions (p =0.9999) were not significantly different from pristine NPs. Ag:Au ratios indicated a significant concentration-dependent effect on Ag transformations and bioavailability. At higher exposure concentration, Ag was less bioavailable (in both external and internalized cellular fractions), and aggregation appeared to be the dominant process. In contrast, Ag was more bioavailable, and dissolution seemed to be the dominant process at lower exposure concentration. The weight of evidence suggests that Ag^+ preferentially adsorbed to the external cellular surface, whereas a complex mixture of depleted original Au@Ag NPs and dissolved Ag in either ionic or secondary NPs forms accumulated in the internalized fraction. However, these fractions were operationally defined and might not perfectly match their corresponding theoretical definitions. Consistent with previous studies, our results suggest that both AgNPs and dissolved Ag are bioavailable to bacterial cells and may interact with multiple cellular targets simultaneously.

TABLE OF CONTENTS

LIST OF TABLES

LIST OF FIGURES

CHAPTER 1

BACTERIA-NANOPARTICLE INTERACTIONS AND THEIR HEALTH IMPLICATIONS

1.1 INTRODUCTION

Nanotechnology is a multidisciplinary scientific field that is currently bringing revolutionary advances across wide array of fields including medicine, medical technology, engineering, electronics, and many others [1-3]. “There’s plenty of room at the bottom” titled Richard Feynman his famous lecture, in which he explained the potential of nanotechnology in a wide range of scientific fields by tailoring material properties at the atomic scale [4].

Nanoparticles (NPs) are the building blocks for the rapidly growing field of nanotechnology [5]. NPs are wide class of materials and typically defined to be of diameter range from 1 to 100 nm in at least one dimension [6]. At this size scale, materials can demonstrate novel properties compared to their bulk counterparts [7]. For instance, NPs tend to exhibit high chemical reactivity and unique optical properties that are attributed to the electronic confinement effects and the larger specific surface area (*i.e.,* surface area per unit mass) [8-10]. Consequently, NPs are attracting scientific community in a plethora of novel applications and research opportunities in a vast range of fields [11].

NPs are in the size scale of biological molecules [12] and can be produced with certain properties to fulfill certain intended functions [13] and therefore, they are potentially useful for medical applications [14]. Utilizing NPs unique properties for the purpose of diagnosing and treating health conditions is known as nanomedicine [15]. It is considered a relatively new area of nanotechnology that has demonstrated several high-quality benefits, and promises numerous medical advancement such as enhancing drug delivery and efficiency [16, 17], overcoming multidrug resistance (MDR) [18], enabling early detection of diseases [19], and improving imaging technology [20].

Nanotechnology exploits NPs tunable properties in designing highly functional agents with diagnostic and therapeutic capabilities [21]. Among those, NPs-based bacterial detection and treatment of bacterial-related conditions. In this review, various medical applications involving NPs-bacteria interactions and the current approaches available to study these interactions will be discussed. However, a key aspect of understanding these interactions is to understand bacterial envelope structure.

1.2 BACTERIAL CELL ENVELOPE

Bacteria are single-celled microorganisms that lack a nucleus and membrane-bound organelles. However, they possess highly sophisticated and multilayered structure (Figure 1.1). Typically, they fall into one of two main categories according to their cell envelope [22]. In both groups, cytoplasmic (*i.e.* plasma) membrane is surrounded by a rigid protective barrier layer that is the peptidoglycan cell wall (CW). In Gram-positive bacteria, this layer is relatively thick (10-20 nm), while in Gram-negative bacteria the CW is much thinner (2-7 nm) and is surrounded by an additional outer membrane layer that is a distinctive feature of Gram-negative bacteria [23]. The outer membrane is a lipid bilayer and is mainly composed of phospholipid from the inside whereas the outside leaflet is mainly composed of lipopolysaccharide (LPS). LPS molecules are cross-linked by divalent cations, mainly Ca^{2+} and Mg^{2+}, which is essential to outer membrane integrity [24].

The organization and composition of these multilayers are crucial determinants of bacterial interaction dynamics with various external factors [25, 26]. Bacterial cell envelope plays key roles in maintaining cells structure, controlling passage of molecules, and performing many other vital regulatory and physiological functions [27]. Primarily, the envelope serves as an efficient protective barrier against a wide range of physical,

chemical, and biological threats including antibiotics [28]. Along with cell envelope, bacteria have multiple strategies to ensure their survival against antibiotics called resistance mechanisms. Understanding those mechanisms is crucial for the imperative demand to developing agents to overcome MDR [29].

1.3 BACTERIAL RESISTANCE MECHANISMS

Bacteria typically develop multiple resistance mechanisms (Figure 1.2) that can be classified into two major categories: 1) intrinsic and 2) acquired resistance. These mechanisms include the use of enzymes to inactivate antibiotics, altering antibiotics uptake through efflux pumps or decreasing membrane permeability, modifying the antibiotics' cellular target (*i.e.,* receptor sites), developing alternative metabolic pathways, biofilm formation, and transferring resistance gene among microbial community, [30-32]. Bacterial genetic plasticity (e.g. chromosomal mutation, acquiring R plasmid, and transposons) allows them to cope and survive various modes of action of antimicrobial agents [33]. Natural selection favors resistance cells which then disseminate resistance traits across bacterial populations [34] vertically by replication of bacterial genetic material during cell division [35] and/or horizontally through genes exchange within bacterial population [36].

To enhance their resistance, the vast majority of actively functioning bacteria do not exist as individual isolated planktonic cells as it was traditionally believed but rather, they predominantly exist in an attached biofilm state [37]. This results in formation of metabolically integrated microbial communities [38] existing within a protective platform that facilitates cell-cell signaling and resistance genes transfer [39, 40]. Biofilms slow the

diffusion and penetration of antimicrobial agents and provide means for the bacterial community to inactivate antibiotics [41].

Conventional antibiotics affect bacterial viability through limited mechanisms (Figure 1.2) that are preventing regeneration of cell wall, interfering with cell membrane integrity and permeability, inhibiting nucleic acid synthesis, perturbing metabolic activity, and interfering with protein synthesis [42]. However, bacteria are highly adaptive organisms, and have found ways to ensure their survival. These adaptations result in the development of MDR bacterial infections, which pose serious public health threats [43]. It has therefore become urgently needed to develop alternative antimicrobial agents with novel modes of action to treat MDR infections [44].

1.4 NPs' MECHANISMS OF ANTIMICROBIAL ACTIVITY

Unlike conventional antibiotics, it is believed that NPs tackle bacteria through multiple mechanisms simultaneously and overwhelm bacterial resistance mechanisms [45]. Although NPs antibacterial activity is highly promising, the exact mechanism is poorly understood [46-49]. Many metal-based NPs exhibit potent biocidal activity through multiple mechanisms (Figure 1.3) [30, 50]. Recently, the growing interest of incorporating NPs into medical applications has led to an increasing demand for elucidating the NPs underlying modes of antibacterial action [51]. Table 1.1 and table 1.2 summarize antibacterial potencies and antimicrobial mechanisms of selected nanoparticles. A thorough understanding regarding the mechanisms of interaction between bacteria and NPs at the cellular level is lacking but is essential for the successful development of NPs applications in the medical field. Such data will be very useful in directing NPs optimization for potential medical applications [52-54].

In certain instances, NPs exert their antibacterial activity through direct physical contact with the bacterial cell. Researchers have suggested numerous forms of contact including receptor-ligand interactions [55], van der Waals forces [56], electrostatic attractions [57], and hydrophobic interactions [58]. NPs may also make their way into the inside of bacterial cells where they can perturb essential structural components [59], alter genetic expression, and disturb biological functions [60-62]. On the other hand, several reports attributed NPs antibacterial activity largely to being sustained reservoirs for continuous release of ions [63, 64]. However, the most commonly suggested mechanisms of NPs antibacterial activity are as follows.

1.4.1 ROS Production

Reactive oxidant species (ROS) are a natural byproduct of cellular metabolic activity and play a key role in cell homeostasis [65]. Excess ROS are generated as metallic NPs interact with bacteria leading to oxidative stress [66]. The rate of ROS generation is highly dependent on the NPs physicochemical characteristic such as size and coating [67] as well as on the exposure media contents and conditions such as pH [68]. Numerous biologically significant ROS could be generated including superoxide ($O_2^{\bullet -}$), singlet oxygen ($^1O_2$), hydroxyl ($HO^{\bullet}$), and hydroperoxyl ($HO_2^{\bullet}$) ions [65, 69].

Several reports attributed engineered NPs toxicity in a wide range of microorganisms mainly to their capability of ROS generation [70]. Arakha and his colleagues examined the antimicrobial activity of iron oxide NPs (FeONPs) with two different coatings, they found that FeONPs that generated higher ROS was associated with more potent antimicrobial activity against *E. coli* and *Bacillus subtilis* [71]. Similarly,

silver NPs (AgNPs) antimicrobial activity have been also demonstrated to be associated with ROS generation [72].

1.4.2 Interaction with Cytoplasmic Components

Many metal-based NPs exert their biocidal effect through interacting with the internal cellular components of bacteria, in both metallic and ionic forms [73]. The antibacterial activity of AgNPs, zinc oxide NPs (ZnONPs), and copper oxide NPs (CuONPs) [74] have been demonstrated toward a broad spectrum of bacterial strains [75-78]. Metallic NPs might release dissolved ions as they come in contact with the exposure medium [30, 79]. Free ions have been found to readily cross cell membranes and perturb vital physiological processes [80, 81]. Several cytoplasmic targets for NPs have been suggested including disruption of bacterial gene expression [82] and protein synthesis [83]. Furthermore, it has been shown that these NPs perturb cell wall permeability and lead eventually to leakage of cytoplasmic contents [84].

1.4.3 Sorption and Penetration through Barriers

Interaction kinetics by which NPs kill bacteria remain poorly understood. This is especially true for the bacterial uptake of NPs and whether or not this involves their internalization [30]. Several studies suggested NPs accumulation and deposition over bacterial surface [85-88]. Other reports demonstrated evidence suggesting NPs penetration and internalization into bacterial cytoplasm [89-92]. NPs internalization might be preceded by NPs surface sorption that perturb membranes permeability [86]. In fact, it was found that, NPs' capability to adhere to a cell surface is directly proportional to their uptake efficiency [93]. For example, quantum dots (QDs) found to be readily adsorbed to the surfaces of both

Gram-positive and Gram-negative bacteria probably due to electrostatic forces followed by internalization [94].

A recent study demonstrated the internalization of ZnONPs and titanium dioxide NPs (TiO_2NPs) into the cytoplasm of the Gram-negative bacterium *Salmonella typhimurium* [95]. A research group studied AgNPs mechanisms of antimicrobial activity against *E. coli* and found formation of "pits" in the bacterial cell wall. These pits were suggestive of AgNPs creating holes in the membrane to penetrate and destroy bacterial cells [83]. Several studies addressed adsorption of AuNPs over the outer bacterial surface during interaction between AuNPs and bacteria [96, 97]. However, in-depth understanding to the antibacterial mechanisms of NPs is yet to be elucidated [85, 98]. Although multi-modal mechanisms were proposed to be involved in NPs antibacterial activity [63, 99-101], developing clear understanding is crucial particularly for NPs potential medical application [102].

1.5 NPs MEDICAL APPLICATIONS

While some NP-based medical applications are already in use, several applications are still in the research and development phase and are yet to be clinically approved [103, 104]. For instance, only one NPs, namely iron oxide NPs (FeONPs), have been approved and currently in use for diagnostic purposes in clinical practice [105]. Whereas the vast majority of NPs-based therapeutic applications that are currently undergoing clinical trials, are NPs-based formulations to enhance the activity of previously approved drugs [106]. The difficulty in clinically approve NPs-based formulations may be attributed to the tedious and tremendously challenging approval process for new drugs [107]. Granting a clinical approval requires extensive and comprehensive preclinical steps including

conducting extensive research, using appropriate design of clinical trials, and successfully completing all these clinical trials [108, 109].

NPs offers a highly versatile multifunctional platform in which potential dual applications of same NP can be achieved [110, 111]. For instance, positively charged silver shelled gold core-shell NPs (Au@Ag NPs) tend to aggregate on the surface of negatively charged bacteria, which make them of greater medical use. Au@Ag core-shell NPs exhibited both potent antimicrobial activity against *Staphylococcus aureus* and enhanced two-photon photoluminescence effect [112], which make them suitable for theranostic applications (*i.e.,* therapeutic and diagnostic). Similarly, QDs, which are fluorescent nanocrystals, tend to have high affinities for cellular proteins and could be functionalized for both bacterial detection and treatment [94, 113].

On the other hand, researchers are currently developing new NPs-based protease sensors that concurrently distinguish bacterial from other forms of lung infection and monitor the effectiveness of prescribed antibiotic [114]. This technique enables identifying the nature of causative agent, and hence avoiding unnecessary administration of antibiotics that might potentially contributes to MDR [115]. Additionally, it enables monitoring the effectiveness of the drug which allow for "course correction" and implementation of an alternative effective therapeutic plan [116, 117]. This multifunctionality is projected to potentially revolutionize the current approach in diseases management for a wide variety of health conditions. In this section, various potential medical applications of NPs in pathogenic bacteria-related arena will be briefly discussed.

1.5.1 Therapeutic Applications

1.5.1.1 NPs as Antimicrobials

Over the last years, treatment and control of infectious diseases have been achieved predominantly through antibiotics administration [118, 119]. However, bacterial versatility along with misuse of antibiotics have contributed to the emergence of MDR [120]. Recently, NPs exhibited promising antibacterial potential toward multiple MDR strains [121]. Certain NPs have novel intrinsic antimicrobial activity and have been studied extensively. Among all NPs, AgNPs were the most studied for potential use against MDR infections [122].

Numerous studies have been conducted to evaluate the bactericidal effect of AgNPs against major MDR strains, including those termed the ESKAPE pathogens [123]. ESKAPE is an acronym for six serious and clinically important human pathogens that exhibit MDR properties: *Enterococcus faecium*, *Staphylococcus aureus*, *Klebsiella pneumoniae*, *Acinetobacter baumannii*, *Pseudomonas aeruginosa* (*P. aeruginosa*), and *Enterobacter spp.* [124]. AgNPs are found to be effective as potential broad-spectrum antibiotics against both Gram-negative and Gram-positive bacteria [125].

Furthermore, NPs are being studied for their antibiofilm activities and have been incorporated to prevent biofilm formation and nosocomial device-associated infections [126, 127]. Metal and metal oxide NPs, such as AgNPs, ZnONPs, CuONPs, FeONPs, and many others are exhibiting inherent toxicity to microorganisms at concentrations lower than those are toxic to human cells, and therefore can be applied for this purposes [50, 128]. For example, ZnONPs and AgNPs have been widely used as broad spectrum anti-biofilm agents for coating implants and medical devices [129-131]. Topical applications of AgNPs

in wound dressings hastened the healing process of wounds and resulted in a better cosmetic appearance when applied to animal models [132].

1.5.1.2 Drug Delivery

Traditional medical treatment strategies carry many pitfalls that can be improved upon by modern technological advances and strategies. For instance, administration of non-targeted drugs requires using higher doses in order to have the adequate concentration received at the target site(s) [133, 134]. Cytotoxic side effects of non-targeted drugs are usually more severe and occur more frequently when compared with targeted drugs [135]. Limited drug bioavailability remains a further significant drawback of non-targeted therapeutic strategies [136]. Therefore, targeted therapeutic approaches are more desirable as they can increase drug efficiency and minimize cytotoxicity.

Targeted drug delivery provides controlled, long-lasting release of specific drugs at specific sites [134, 137, 138]. NPs are particularly useful in drug delivery due to their high specific surface area, which confers them the capability to adsorb and bind multiple molecules [139]. Interestingly, NPs were engineered not to carry medications only, but to bind cell membrane penetrating agents, and stimulus-sensitive agents. As a result, NP are planned to carry more than one treatment, deliver it specifically to the target where a stimulus could be applied, such as ultraviolet or infrared irradiations for photosensitive agents, to stimulate drug release [140]. This therapeutic approach will enhance specificity, efficacy, and minimize toxicity of the drug [141]. Drug accumulation around target sites increases their efficiency and subsequently improves drug safety by improving their resulting therapeutic index [142, 143].

NPs are also employed as vehicles for the efficient delivery of vaccines [144]. For example, silica NPs, a biocompatible non-degradable form of NP, have been structured and fine-tuned for the purpose of immune engineering in vaccine formulation [145]. Furthermore, NPs were designed to potentiate and/or manipulate immune cells for specific immune responses by modulating an important group of immune cells called antigen presenting cells [146]. NPs-based drug delivery holds promising potential to considerably advance therapeutic healthcare strategies in preventing and controlling a wide range of infectious diseases [147, 148].

1.5.2 Diagnostic Applications

NPs-based diagnostic modalities in the medical field are projected to vastly enhance healthcare through enabling early detection of diseases and providing means for rapid, sensitive, and minimally invasive testing [149-151]. Rapid screening tests allow physicians to diagnose and initiate treatment plans immediately at point-of-care [152]. Early, sensitive, and specific detection plays an essential role in controlling the spread of infectious diseases [153]. Furthermore, diseases detected at early stages usually have higher chances for successful treatment and better prognosis [154-156]. Therefore, incorporating these techniques into medical diagnostic practice will contribute to an overall improvement of healthcare systems and public health.

NPs are set to be a powerful diagnostic tool as they can be fine-tuned through manipulating their physiochemical properties such as diameter, coating, and concentration [157]. NPs enhance the sensitivity of certain diagnostic modalities by labelling specific cellular components [158]. AuNPs, in particular, possess a unique plasmon resonance properties which make them excellent for fluorescent-based labelling that can be detected

by numerous fluorescence techniques [159, 160]. Additionally, they have been demonstrated as a very useful contrast agent in photoacoustic imaging (*i.e.,* a type of imaging that utilizes both optical and acoustic imaging) [161]. Greatly amplified photoacoustic signals and better images with higher contrast were achieved by modifying AuNPs coating from polyethylene glycol (PEG) to silica [162]. Furthermore, their surface is relatively easily functionalized with various targeting agents to monitor or localize specific biological targets [163].

Several other NPs have shown promising features that might be potentially translated into clinical application such as QDs [164], silica NPs [165], and FeONPs [166]. Recently, these NPs and many others integrated with various imaging and bacterial detection techniques resulted in faster and improved sensitivity of bacterial identification. In fact, certain approaches are capable of highly efficient and simultaneous detection of multiple biomarkers within relatively short amount of time [150]. However, all these are still in the developing phase and are being tested for their reproducibility and safety.

1.6 BIOAVAILABILITY AND BIOUPTAKE

Biouptake of NPs in bacteria depends mainly on the bioavailability (biological availability) of NPs in the exposure medium [167]. The bioavailable portion of a given material is the fraction that is available to be taken up by a certain organism under a defined set of conditions [168]. Considering factors affecting NPs bioavailability in exposure media cannot be overlooked in toxicity and biouptake studies. For the purpose of this dissertation, we will focus on factors influencing AgNPs bioavailability.

Exposure media tend to have complex chemical compositions that influence AgNPs bioavailability [169-171]. Bioavailability has a key role in dictating the bactericidal activity

of AgNPs. Greater bioavailability is presumed to correlate with enhanced antibacterial activity and vice versa [172, 173]. AgNPs biocidal activity is strongly influenced by dynamic physical, biochemical transformation and speciation in exposure media. Therefore, understanding the factors affecting bacterial bioavailability and biouptake of AgNPs is crucial to their applications in the medical field [172].

Factors influencing AgNPs bioavailability can be grouped into two main categories: 1) initial physicochemical characteristics of the AgNPs such as size, capping agent, dispersion, and concentration [174] and 2) chemical composition of the system where exposure is taking place including pH, ionic strength, protein, and electrolyte contents) [175, 176].

Dispersed and smaller AgNPs tend to remain in the aqueous phase and have a higher mobility than larger, agglomerated AgNPs, which tend to settle down and therefore become less bioavailable [172]. Sterically stabilized AgNPs (e.g., PVP-coated) generally feature higher colloidal stability than electrostatically stabilized AgNPs (e.g. citrate-coated) in terms of both aggregation and dissolution [177]. Both dissolution and aggregation of AgNPs are concentration dependent processes. The presence of AgNPs at high concentrations increases their potential to aggregate whereas they tend to be in dissolution-dominant regime at low exposure concentrations [178, 179]. Dissolved Ag might reprecipitate to form secondary NPs or speciate to another form of Ag compounds such as silver-chloro- (Ag-Cl) complexes [179]. Furthermore, NPs biouptake is a morphology and size-dependent process. Smaller as well as spherical NPs are more likely to efficiently penetrate into cells compared to larger and differently shaped NPs [180-182].

Ionic strength and pH of experimental media will also influence the colloidal stability of AgNPs. Lower pH and higher ionic strength are associated with increased rates of aggregation especially in electrostatically stabilized AgNPs [175, 183]. AgNPs interact readily with proteins and electrolytes and therefore their presence in culture media should be considered [175]. Ag ions (Ag^{+}) has very high affinity to bind chloride (Cl^{-}) and form Ag-Cl complexes, which alter the bioavailability and bactericidal activity of Ag [184]. AgNPs instantly acquire a protein layer in protein-rich exposure media called protein corona. Formation of protein corona modifies AgNPs surface characteristics and consequently their antimicrobial activity [185].

1.7 CURRENT APPROACHES TO INVESTIGATE INTERACTIONS BETWEEN BACTERIA AND NPs

Interactions of NPs with bacteria are quite complex and controversial in the literature. It is widely believed that multiple interactions take place simultaneously [30, 45] including cell wall adhesion, internalization, and oxidative stress, resulting ultimately in perturbing vitally essential functional and structural components [186]. To date, interactions of NPs with bacteria are poorly understood especially from mechanistic perspectives [98]. Studies usually provide partial or limited information due to the complexity of interactions in exposure systems and inability of available techniques to quantify such interactions [46, 187, 188]. However, understanding the interactions is crucial for assessing the NPs risks and benefits for potential medical applications [189]. In this section, current techniques used to evaluate underlying mechanisms involved in bacteria-NPs interaction will be discussed. Several assays have been used to assess interactions, which can be classified into two major categories: 1) toxicokinetic (TK) and 2) toxicodynamic (TD) approach.

1.7.1 Toxicokinetic Approach

In the TK approach, interactions are typically analyzed by high-resolution imaging techniques, which can provide direct and quantitative essential information about NPs and cells such as proximity, penetration, and aggregation [190, 191]. These techniques include, but are not limited to, transmission electron microscopy (TEM) [192], scanning electron microscopy (SEM), energy-dispersive X-ray spectroscopy (EDX) [193], conventional fluorescent microscopy, confocal laser scanning microscopy (CLSM) [61], nuclear magnetic resonance (NMR) [150], flow cytometry [192], and reflection-based imaging [194, 195].

Imaging technologies help localize NPs at the cellular level and determine whether the interactions involved NP sorption to bacterial cell walls and/or internalization. Concurrently, these tools help to simultaneously characterize structural changes in bacteria as well as morphological changes in NPs upon exposure. However, these techniques have certain limitations. For example, TEM examinations require that specimens are dehydrated then observed in a vacuum, which may introduce artifacts leading to misinterpretation of data [196]. Sample fixation, dehydration and embedding are essential steps in TEM sample preparation, which hinder the possibility of monitoring interaction on living cells [197]. EDX, which is a multi-elemental analysis technique that generate characteristic peaks indicative of element presence in tested specimens [198], detection limits may underestimate NPs composition in different cellular compartments [199]. For all these techniques, data can only be partially obtained as investigators can only analyze a limited areas of the sample due to time and cost constraints [196, 200]. Furthermore, real-time

monitoring and analysis of actual biological interactions usually obscured as images are not taken directly from environment where NPs and bacteria co-occur [201].

In addition to imaging techniques, quantitative multielement information with high precision capacity and low detection limit are obtained from spectroscopic analytical techniques, which are becoming dominant source of NPs-bacteria interaction data [202, 203]. These techniques include inductively coupled plasma optical emission spectrometry (ICPOES) [204] and inductively coupled plasma mass spectrometry (ICPMS) [205]. More detailed information about the interactions (*i.e.,* inferences on the presence of NPs in different bacterial compartments) are obtained when combined with separation techniques such as ultrafiltration and centrifugation [200]. Although mass analytical tools are widely used, they have some limitations such as an inability to distinguish particles from ions, difficult sample preparation, and elemental interference [206]. However, operating ICPMS in a single particle mode (SP-ICPMS) could overcome some of these limitations. SP-ICPMS is a powerful tool that enables the distinguishing among elements in particulate and ionic forms using relatively simple requirements [207-209].

1.7.2 Toxicodynamic Approach

The TD approach tend to assess toxicity of NPs to bacteria by determining their antimicrobial activity in term of bacteriostatic and bactericidal effect. Toxicity are usually investigated by viability-based [210] and growth-based [211] assay techniques. Key information may be obtained by comparing cells before and after treatment or against controls. These tools include absorbance measurements at 600 nm (OD600) [212], disc diffusion assays [213], broth dilution assays, time-kill tests, plate count methods, TEM

[214], and fluorescent-based imaging (such as CLSM and flow cytometry) coupled with two-color fluorescent stain (LIVE/DEAD staining kit) [215, 216].

The LIVE/DEAD *Bac*Light stain kit is composed of equal combinations of nucleic acid stains SYTO9 and propidium iodide (PI). SYTO9 fluoresces green and penetrates into all cells due to its relatively small molecular size and surface charge. Whereas PI, which is relatively larger in molecular size, fluoresces red and is only able to penetrate cells with compromised membranes where it will displace the green fluorescence. These differences allow easy microscopical assessment of bacterial viability as a function of cell membrane integrity where intact cells appear green whereas compromised cells appear red in color [217, 218].

Antimicrobial susceptibility assays are usually conducted using standardized protocols in accordance with two main institutions: the Clinical and Laboratory Standards Institute (CLSI) and the European Committee on Antimicrobial Susceptibility Testing (EUCAST) [219]. Methodologies for testing should be standardized as outcomes of susceptibility testing are greatly influenced by type of culture media, inoculum density, incubation conditions such as temperature and speed of agitation, and other components of experiments [220]. Essential toxicity data obtained through a toxicodynamic approach such as minimum inhibitory concentration (MIC) and minimum bactericidal concentration (MBC).

Antimicrobial assays have been routinely used in microbiology to assess the bacteriostatic and bactericidal properties of drugs. However, there are certain drawbacks to these techniques. For example, determining the best therapeutic concentration is not attainable using dilution method as it does not compare antimicrobial potencies, and it is

designed to only determine MIC and MBC [221]. Cell membrane integrity could be induced during sample processing when assessing cell viability with TEM [222]. OD600 absorbances do not directly measure bacterial densities but rather measures bacterial suspension turbidity through detection of light scattering and absorbance at 600 nm. Thus, OD600 measurements are only a rough estimate of bacterial density and can be easily affected by bacterial suspension matrices [223]. Plate counting method allow only a relatively narrow range for the limit of quantification (25-250 CFU/plate) [224]. Additionally, the assumption that a single colony was founded by single viable microbial cell is not always correct and may underestimate the actual microbial density [225].

1.8 DISSERTATION OVERVIEW

Although nanotechnology hold a promising potential in counteracting MDR bacterial infections, a comprehensive understanding to the mechanism(s) of interaction is lacking, but mandatory to optimize their use in medical applications. However, this appeared to be quite intricate given the lack of standardized methodology and analytical techniques to quantify such a complex interaction. Therefore, the overall aim of this dissertation was to develop a chemical extraction method to separate and quantify the internalized and sorbed fractions of Ag to the surface of selected Gram-negative bacterium *P. aeruginosa*.

A method employing novel application of EDTA to separate surface sorbed from truly internalized Ag was developed and validated. EDTA is a chelating agent with high affinity to divalent cations that stabilize bacterial outer membrane. We hypothesized that, under appropriate treatment conditions, EDTA will specifically remove the periplasm along with sorbed Ag and separate it from the internalized Ag without significantly

affecting inner membrane integrity. To validate this, four different analytical and imaging techniques were used, to investigate the effect of different EDTA treatment conditions.

To better understand the dynamic AgNPs transformations and their influence on NPs bioavailability and biouptake, the previously validated method was applied after exposing bacteria to bimetallic Au@Ag NPs. These NPs are particularly useful because they have Au core that is protected from direct interactions with exposure media and remains in particulate form throughout exposure duration. Therefore, it could be used as an internal standard for this study purpose. We hypothesized that bacteria take up (*i.e.,* internalize) the dissolved Ag from AgNPs. To test this hypothesis, metallic molar ratios were calculated and analyzed in abiotic and biotic phases in different bacterial fractions.

The ultimate goal of this dissertation is to provide a well validated method to separate and quantify the internalized fraction of Ag. Furthermore, to provide insights on the influence of AgNPs dynamic transformations in the exposure media on NPs bioavailability and biouptake.

Table 1.1 Antimicrobial activity of selected nanoparticles toward selected microorganisms.

Nanoparticle type	Size (nm)	Organism	MIC/MBC	References
Silver	20-25	*P. aeruginosa* ATCC 27853	MIC = 0.4 µg/mL	[226]
		E. coli ATCC 25922	MIC = 0.5 µg/mL	
		S. aureus ATCC 25923	MIC = 0.7 µg/mL	
Zinc oxide	9.5	*S. mutants*	MIC = 4 µg/mL	[227]
	19	*E. coli*	MIC = 50 µg/mL	[228]
Titanium dioxide	250–300	*P. aeruginosa* ATCC 27853	MIC = 20 µg/mL	[229]
	25	*E. coli*	MIC = 100 µg/mL	
Copper Oxide	20-95	*S. aureus*	MBC = 100 µg/mL	[230]
	40	*S. mutans*	MIC50 =1-10 µg/mL	[231]
		L. acidophilus	MIC50 =< 1 µg/mL	
		L. casei	MIC50 =10 µg/mL	

Table 1.2 Antimicrobial mechanisms of selected nanoparticles.

Nanoparticle type	Antimicrobial mechanism
Silver	-Perturb cell membrane permeability and integrity [83, 84]. -Alter genetic material [82, 84]. -ROS generation [72]. -Disrupt protein synthesis [83]. -Antibiofilm activity [227].
Zinc oxide	-Interfere with cell membrane [232]. -ROS generation [233]. -Internalize into bacteria [95] - Release of Zn^{2+} [234]
Titanium dioxide	-Cell membrane disruption [235]. -Produce ROS [236].
Copper Oxide	-Produce ROS [230]. -Cell membrane damage [237]. -Antibiofilm activity [238].

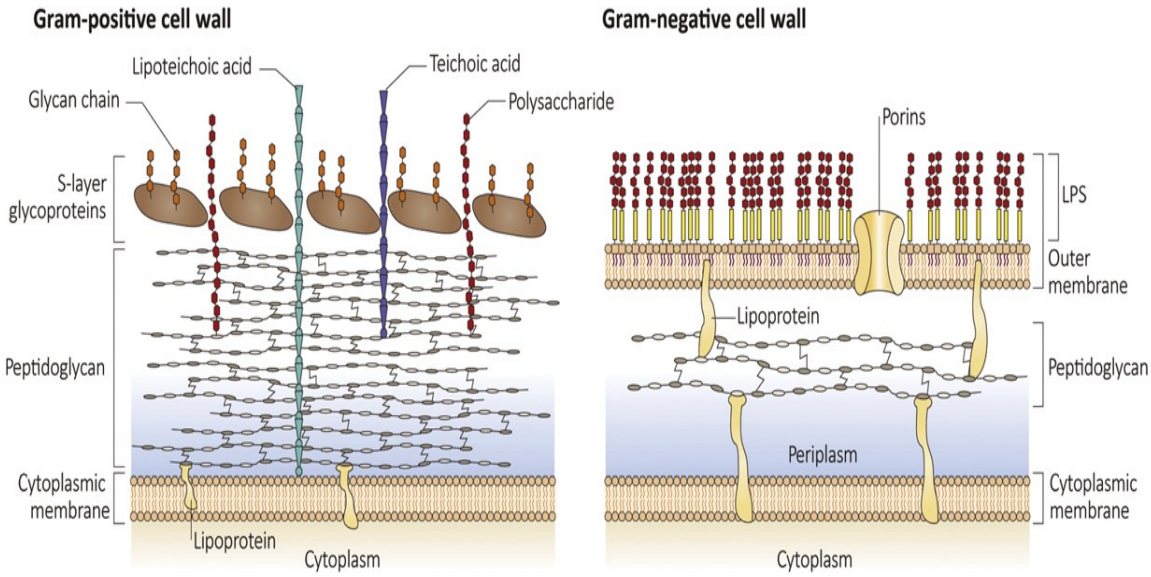

Figure 1.1 Schematic representation of bacterial cell envelopes of Gram-positive and -negative bacterial cells. LPS = Lipopolysaccharides. Obtained from Depelteau et al, 2019 [239]

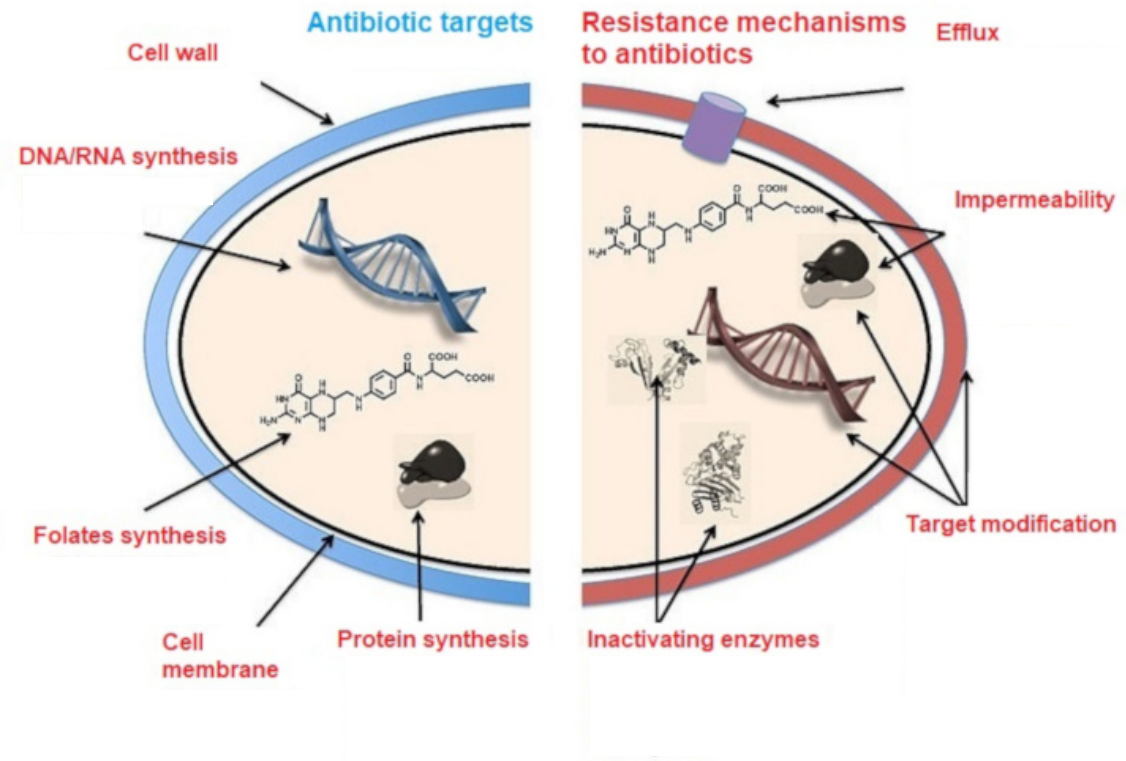

Figure 1.2 Schematic representation for conventional antibiotics cellular targets and various bacterial resistance mechanisms. Obtained from Maurin, 2020 [240].

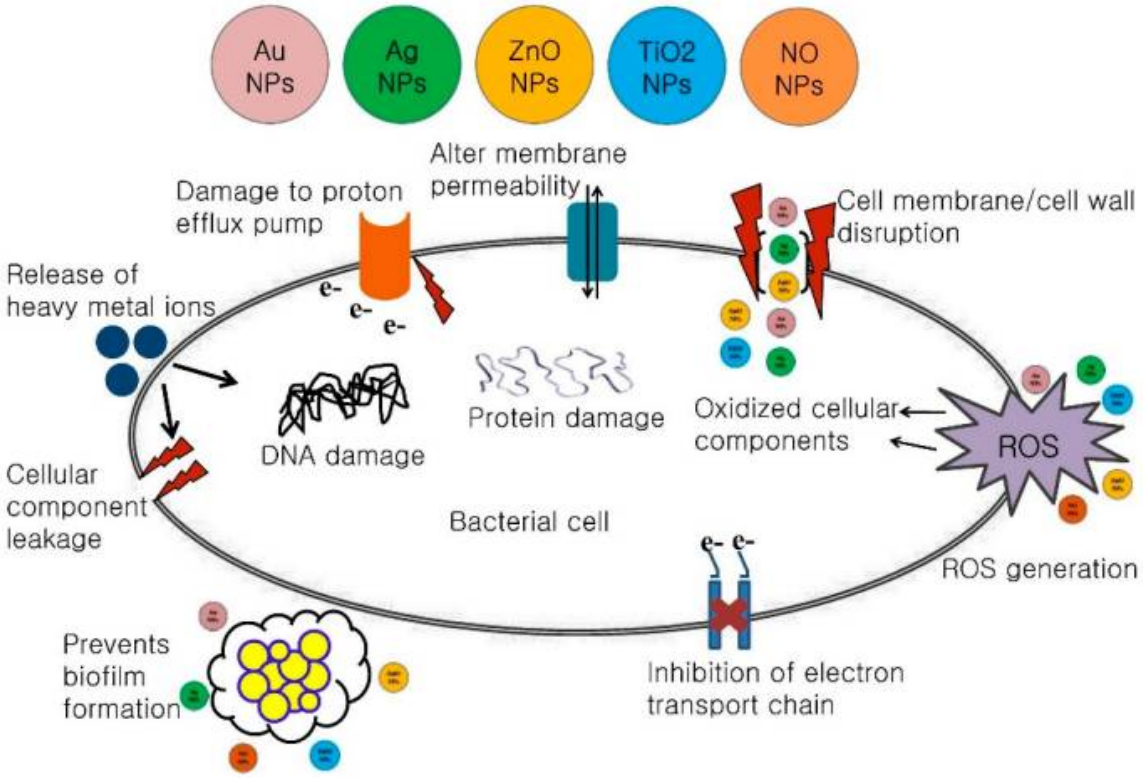

Figure 1.3 Diagram showing several proposed antimicrobial mechanisms of selected nanoparticles. Obtained from Shaikh et al., 2019 [79].

CHAPTER 2

DEVELOPING AND VALIDATING A NOVEL PROTOCOL TO SEPARATE AND QUANTIFY THE INTERNALIZED FRACTION OF SILVER IN THE GRAM-NEGATIVE BACTERIUM *PSEUDOMONAS AERUGINOSA*

2.1 ABSTRACT

Multidrug resistance (MDR) is an emerging significant public health issue that is associated with increased mortality, morbidity, and healthcare costs. Silver nanoparticles (AgNPs) is regarded as a potential broad-spectrum antimicrobial agent against MDR infections. However, the exact mechanism(s) of AgNPs antimicrobial activity is yet to be fully elucidated. Although there are many studies on Ag biouptake, quantitative data remain limited. In the present study, a method using EDTA to separate truly cellular internalized fraction of Ag was developed and validated. EDTA is a chelating agent that disrupt bacterial periplasm by binding to divalent cations that maintain outer membrane integrity. Accordingly, it is expected to specifically remove the periplasm and leave cell inner membrane intact under appropriate treatment conditions. This method was validated through multimethod approach. The result showed that, 50 mM EDTA Inhibited bacterial growth during the first 2 hours of treatment. However, evidence of cell lysis beyond these conditions were observed. OD600 data indicated decreased cells density at longer exposure duration and higher EDTA concentrations. Confocal micrographs showed significantly fewer cell counts (p <0.001) after six hours EDTA exposure suggesting significant influence on bacterial viability. Furthermore, TEM images showed thin cell surfaces near edges compared to two hours EDTA exposure. Ag liberation curve showed a plateau within the first two hours of exposure to 50 mM EDTA while significantly higher Ag masses were observed beyond that (p <0.05) likely due to increased permeability or cells rupture. Therefore, 50 mM EDTA for two hours suggested the complete removal of outer membrane while preserving viable cells reproducibly and consistently across the multimethod approach. Based on the weight of evidence, this method is reliable to be

utilized for its stated purpose. By using this method, accurate approximation to the estimated internalized cellular fraction of Ag in Gram-negative bacterium *P. aeruginosa* can be obtained.

2.2 INTRODUCTION

Antimicrobial agents have been helpful in combating bacterial infections since their discovery in 1920s [120]. However, a significant proportion of human pathogenic bacteria have developed MDR owing to misuse as well as overuse of antibiotics. This represents an emerging major public health concern that is resulting in increased severities of infections, prolonged hospital stays, increased mortality [122, 124] and limited treatment options for infected individuals [241]. It is estimated that 50,000 lives are lost in the United States and Europe only [242] and at least 700,000 lives across the world each year [241] due to MDR infections. Therefore, there is an urgent demand for developing new antimicrobials with new modes of actions [243-245].

Recently, NPs received attention as a potential future treatment against MDR pathogens [246]. AgNPs, particularly, are considered the most promising of all NPs due to their broad-spectrum and potent antimicrobial activity [247]. Silver (Ag) has been used widely as antimicrobial for thousands of years [248]. More recently, AgNPs are attracting substantial interest in the medical field as a new class of antimicrobial agents [122, 249] that bacteria are less likely to develop resistance against [250]. AgNPs have been incorporated into many medical applications such as wound dressings [251] and coatings to implanted devices [252]. Although the antimicrobial activities of AgNPs has been extensively studied, the exact mechanism is not yet fully understood [253, 254]. A thorough understanding regarding the mechanism(s) of interaction between bacteria and

AgNPs at the cellular level (e.g. biouptake processes) is lacking [246, 255] but essential for the successful development of AgNPs in potential medical applications. [255, 256].

The complex interaction between AgNPs and bacteria have been widely studied [257-259]. Biouptake mechanisms have been suggested to involve (strong or weak) sorption onto the bacterial cell surface [83], and/or intracellular compartmentalization [82]. The outer portion of a Gram-negative bacterial cell, called the periplasm, is the space between the outer cell membrane and the inner plasma membrane. The inner plasma membrane represents the barrier to differentiate between the uptake of NPs into the bacterial cytoplasm, and those that are outside of this border [22]. Measurements of AgNPs at different cellular compartments will enhance our understanding to bacterial uptake processes of AgNPs.

To our knowledge, no standard method to date applied to Ag allowing such differentiation. Therefore, the aim of this study was to develop a methodology to quantify AgNPs internalization into the Gram-negative bacterium, *P. aeruginosa*. In this project, a chemical extraction method was successfully developed and data differentiating the cellular internalized portion, and externally sorbed fraction were reported. The results will provide very useful methodology to help better understand biouptake processes involved in NPs-bacteria interaction.

2.3 MATERIALS AND METHODS

2.3.1 AgNPs synthesis and characterization

AgNPs were synthesized using a standard chemical reduction method of silver nitrate ($AgNO_3$ Sigma-Aldrich; CAS No. 7761-88-8) by sodium borohydride ($NaBH_4$; Alfa

Aesar; Cat. No. 88983) in the presence of the capping agent, trisodium citrate (TSC; VWR; CAS No. BDH0288), following slight modifications to a previously established and standard procedures [260]. Briefly, solutions of 1.7 mL $AgNO_3$ (0.25 mM), 2.9 mL TSC (0.31 mM), and 1 mL $NaBH_4$ (0.25 mM) were prepared using ultrapure water (UPW; 18.2 MΩ-cm). 400 mL of UPW was heated to boiling in a conical flask with vigorous stirring. $AgNO_3$ and TSC were added simultaneously to the boiling water and mixed for an additional three minutes. Then, 0.5 mL of $NaBH_4$ was slowly added to the mixture in a drop-wise manner at the rate of one drop (~15 uL) every five seconds. Finally, the mixture was further heated while stirring vigorously for 30 minutes and then allowed to cool in darkness at room temperature (25 °C) overnight.

The synthesized batch was washed three times to remove excess unreacted reagents and ions using diafiltration (Amicon; 3 kDa regenerated cellulose membrane; Millipore). Nanoparticles were resuspended in TSC solution to avoid dryness and formation of secondary nanoparticles. To enhance NPs stability, an aliquot of the citrate coated AgNPs was further coated with polyvinylpyrrolidone (PVP) by adding PVP_{10} (Mw 10,000; Sigma Aldrich; CAS Number 9003-39-8) while stirring in darkness for one hour. The number of PVP molecules needed to cover the entire nanoparticles is calculated to be eight molecules per nm^2 [261, 262].

Stock AgNPs were comprehensively characterized using multimethod approach. The mean z-average diameter and polydispersity index (PDI) were obtained by replicate measurements using dynamic light scattering (DLS) (Malvern Instruments, MA, USA). Ultraviolet and visible light (UV–vis) spectra were measured in triplicate over the

wavelength range of 200-800 nm using a UV-Vis spectrophotometer (UV-2600, Shimadzu Co., Kyoto, Japan). Zeta potential, a measure of colloidal stability, was measured by laser Doppler electrophoresis (Malvern Zetasizer NanoZS, MA, USA). AgNPs TEM images were collected using Hitachi HT7800 TEM. Samples were prepared by ultracentrifugation of AgNPs suspension on a copper grid at 30,000 (150,000 x g) rpm for one hour at 4 °C [263] in Sorvall MTX 150 micro-ultracentrifuge (Thermo Scientific) with an S52-ST rotor. Size and size distribution were analyzed with the National Institutes of Health (NIH) ImageJ Version 1.46r software (https://imagej.nih.gov/ij/) package.

2.3.2 Antibacterial activity

To prepare bacterial cells for experiments, *P. aeruginosa* (ATCC 27853) was cultured in tryptic soy broth (TSB) media and incubated at 37 °C with shaking at 180 rpm. AgNPs antibacterial activities against *P. aeruginosa* were investigated using the broth microdilution assay [264] to identify the MIC. Briefly, *P. aeruginosa* stock culture was inoculated into sterile TSB medium and incubated at 37 °C with shaking. OD600 of microbial suspensions was measured and adjusted at 0.1 equivalents to 0.5 McFarland standard and diluted to 1 X 10^6 CFU/mL. Antibacterial activities of citrate coated AgNPs (Cit-AgNPs) and PVP coated AgNPs (PVP-AgNPs) were tested in triplicate using sterile 96-well microtiter plates. 100 uL of microbial suspension, combined with 100 uL of each type of Ag at the desired concentrations, were added to each well using sterile technique. Sterility controls (broth only; no bacterial inoculum) and growth controls (no Ag) were also applied. Then, 96-well plates were sealed with parafilm to prevent evaporation and were incubated (20 hours) in darkness at 37 °C with shaking (80 rpm). MIC values were

determined as the lowest concentration of Ag that was sufficient to prevent bacterial growth.

2.3.3 Chemical extraction method validation

The proposed chemical extraction method was validated using four different approaches: 1) measurements of OD600 of bacterial suspension upon exposure to varying concentrations of ethylenediaminetetraacetic acid (EDTA) over time, 2) bacterial viability assays using CLSM, 3) structural change assays using TEM, and 4) sorbed Ag liberation assays using ICPMS.

OD600 measurements were obtained as a quantitative measure of growth dynamics of bacterial cells under different EDTA concentration treatments. The optimum concentration of EDTA was determined to be the highest treatment concentration/duration that inhibited bacterial growth without impacting bacterial cell viability. Failure to inhibit growth indicated lower than needed concentration and vice versa.

Confocal micrographs were analyzed to assess the viability of bacterial cells in terms of cell membranes integrity. TEM was used to visualize changes in bacterial morphology and microstructures at different timepoints of EDTA treatments and to quantify internalized AgNPs, if any. At the optimal treatment conditions, EDTA will only remove the bacterial periplasm (*i.e.,* outer cell membrane, cell wall, and molecules contained within this space) along with sorbed NPs, but will do so without influencing bacterial viability or leading to major structural changes.

Finally, the Ag free/weakly bound fractions, sorbed fractions, and internalized fractions were separated (see section 2.4.4) and masses for each fraction were plotted against time. A plateau in sorbed fraction indicated release of all periplasm and surface

sorbed Ag. In contrast, an increased mass value indicated lysis of cells or increased permeability of the cell membranes. The details of these methods and their outcome are discussed further below.

2.3.3.1 Optical density

Initially, a rangefinder experiment was conducted to determine the optimum bacterial exposure conditions (concentration and exposure time) to EDTA that would remove the bacterial outer membrane and cell wall without influencing cell viability. Bacterial cultures were exposed to varied concentrations of EDTA, 20, 30, 50, 75 and 100 mM, in triplicate and the OD600 was monitored over time. Cells viability and the removal of outer membrane was further verified through imaging with CLSM and TEM.

2.3.3.2 Bacterial viability assay

Samples were collected after EDTA exposure at different timepoints (t): t1.5, t2 and t6 hours, for both controls, and cells exposed to different forms of Ag (Cit-AgNPs, PVP-AgNPs, and Ag^{+}) and then stained using LIVE/DEAD *Bac*Light bacterial viability kit and imaged with CLSM (Leica TCS SP5; HCX PL Apo 63×/ 1.40 oil-immersion objective) to determine the viability of cells over the different durations of exposure. Confocal images were further analyzed using ImageJ. At least five images were randomly taken for each timepoint and number of cells per field of view (FOV), which was 238x238 μm, were counted using "Analyze Particles" procedure [265]. Mean cell counts at each time point were compared using one-way analysis of variance (ANOVA). Where differences were significant, Tukey's test was used for pairwise comparisons of the means at a significance level of $p < 0.05$.

2.3.3.3 Structural changes assay

TEM images were obtained to verify the removal of bacterial outer membrane following EDTA treatment and to characterize detectable structural changes at the same timepoints. Samples were placed over 15 nm X 25 nm slot formvar-filmed copper grids (Ted Pella; Product # 01813-F) and were examined under TEM. When the desired treatment time was reached, a 1 mL sample was collected and washed three times by centrifugation (13,200 rpm; 3 min.) to remove EDTA and other cellular residuals. Pellets were then resuspended in 0.5 ml phosphate-buffered saline (PBS) and 0.5 ml 4% paraformaldehyde for fixation and refrigerated at 4 °C in darkness. Following fixation, samples were washed three times and then resuspended in PBS. A small drop from each sample was placed over copper grids and allowed to air dry at room temperature and were examined by TEM.

To further investigate bacterial structural changes, samples were collected and fixed with 2% glutaraldehyde/2% paraformaldehyde in PBS. Ruthenium red (final conc. 0.1%) was added and samples agitated for one hour in darkness then rinsed with PBS to remove excess ruthenium red. Secondary fix were added with 2% osmium tetroxide (PBS) for three hours and agitated for three more hours in darkness then rinsed with water and embedded in 2% agar and thin sliced (<1 mm). The pellets were dehydrated through an ascending concentration series of ethanol and then embedded in polybed 812. Ultra-thin sections (~90 nm thick) were obtained by ultramicrotome (Leica Ultracut R), placed over copper grids, stained with 1% uranyl acetate for 40 min and with Hanaichi's lead citrate for four minutes, and imaged with TEM [266]. EDX analyses were also performed to qualitatively test for the presence of Ag inside bacterial cells using ultra-high resolution scanning electron microscope (Hitachi SU9000) equipped with EDX.

2.3.3.4 Ag liberation curve

Overnight *P. aeruginosa* cultures (15 hours) were harvested during late exponential growth phase (OD600=1.00 ± 0.2) by centrifugation (4,000 rpm for 10 min; 25 °C). Cells were washed then resuspended in fresh TSB. Bacterial suspensions were then exposed in separate containers to 2 mg L^{-1} from each form of Ag (Cit-AgNPs, PVP-AgNPs, and Ag^{+}) in nutrient media (TSB) for 24 h in darkness under similar culture conditions. When the exposure time were completed, suspensions were washed three times by centrifugation under same conditions (Figure 2.1). Pellets were resuspended in PBS and treated with 50 mM EDTA. Aliquots were taken from each sample at t1.5, t2, and t6 hours and washed by centrifugation three times (13,200 rpm; 3 min). This gave rise to three different fractions for each sample at each sampling timepoint as follows: 1) initial washes before treating with EDTA representing both free- and weakly-bound Ag to bacterial cells combined, 2) supernatant from washes after EDTA treatment representing the Ag fractions that were strongly sorbed to bacterial outer membranes and subsequently liberated by EDTA, and 3) pellets after EDTA treatment representing the assumed internalized fraction contained in the bacterial cytoplasm.

Finally, all samples were acidified with concentrated acid (70% HNO_3) for 24 hours and then dilutions were made to a 1% HNO_3 final concentration across all samples. Ag concentrations measured by ICPMS (Finnigan MAT, Germany). Results were statistically analyzed using ANOVA (p <0.05) and subsequently Tukey test where ANOVA was significant.

2.4 RESULTS

2.4.1 AgNPs characterization

The synthesized batch of AgNPs was pale yellow in color. Table 2.1 summarizes the characteristics of synthesized batches. The increased hydrodynamic sizes obtained by DLS, and the shift in surface plasmon resonance (SPR) to longer wavelengths confirmed the conversion of AgNPs coatings from citrate to PVP [261] (Table 2.1). Images obtained by TEM indicated that AgNPs were spherical in shape and the sample had a narrow size distribution (15.2 nm ± 3.5) (Figure 2.2). The total Ag concentration in the stock solution was 18.5 mg L^{-1} as determined by ICPMS measurements.

2.4.2 Antibacterial activity

The antimicrobial activities of both Cit-AgNPs and PVP-AgNPs toward *P. aeruginosa* were determined. Our results indicated stronger antibacterial activity was exhibited by Cit-AgNPs. The MIC values were 5 mg L^{-1} and 7 mg L^{-1} for Cit-AgNPs and PVP-AgNPs, respectively. Therefore, 2 mg L^{-1} was selected as the sublethal dose to be applied to avoid the antibacterial effect of AgNPs for this study.

2.4.3 Optical Density

Effect of EDTA on bacterial growth was estimated using OD600. At concentration of 50 mM, stable OD600 was observed during the first two hours indicating total inhibition of the growth. However, OD600 measurements was subsequently decreased beyond this exposure duration likely due to cell lysis (Figure 2.3). At exposure concentrations higher than 50 mM EDTA, the OD600 began to considerably decrease on or before the first one hour of exposure suggesting decreased number of viable cells. In contrast, increased

OD600 was observed for lower concentrations (<50 mM) indicating failure of bacterial growth inhibition by these EDTA concentrations.

2.4.4 Bacterial viability assay

Confocal cell imaging, for cells treated with LIVE/DEAD stain, visualized cells as green when their cell membrane integrity was maintained or as red otherwise. The results showed intact membranes for cells before- and after- exposure to EDTA for six hours (Figure 2.4). Although there was no detectable evidence for loss in membrane integrity, significantly fewer green cells (p <0.0001) were observed in images after six hours exposures when compared to untreated controls. No significant differences were found after two hours exposure (p =0.9656). Mean cell counts ± SD were 660 ± 43, 650 ± 35, and 306 ± 78 cells/ FOV for untreated control, exposed to EDTA at t2 hours, and t6 hours, respectively.

2.4.5 Structural changes assay

Cell pellets collected before, at t2 hours, and at t6 hours after EDTA exposure were analyzed using TEM. Similar results were observed for non-exposed controls and exposed after two hours of exposure (Figure 2.5). Cells had intact, dense, and smooth cell boundaries. Even after six hours exposure, cells were largely intact with no detectable lyses, but featured very light and thin surfaces near the cell edges compared to control. TEM thin sections analyses (Figure 2.6) showed no morphological changes in bacteria exposed to EDTA at t2 hours. In contrast, bacteria exposed to EDTA at t6 hours were unequally affected. Some cells showed irregular edges and relatively less dense cell walls.

2.4.6 Ag liberation curve

All Ag content detected in washes before EDTA treatment was considered as free/weakly bound Ag, while Ag detected in washes after EDTA treatment was considered as sorbed

fraction. All detected Ag in bacterial pellet was considered as the truly internalized fraction that was contained within the bacterial cytoplasm. Bacterial strains were exposed to sublethal doses of 2 mg L^{-1} for 24 hours then treated with EDTA. An Ag liberation curve was obtained by plotting Ag mass over time after EDTA treatment for sorbed fractions (Figure 2.7).

A mass balance for Ag was constructed for these data and recovery rates were calculated (Table 2.2). Free/weakly bound Ag was found to constitute about 24%, 33%, and 54% of the total exposure mass for Cit-AgNPs, PVP-AgNPs, and Ag^{+}, respectively. In contrast, sorbed fractions ranged from 2% to 4% while internalized fractions ranged from 12% to 37% from the total exposure mass in all types of Ag (Table 2.3). Statistically similar mass values were detected in first two hours of exposure to EDTA for both sorbed and internalized fractions for all types of Ag (Table 2.4). Whereas after six hours exposure, higher concentrations were detected in sorbed fractions while lower concentrations were detected in internalized fractions.

2.5 DISCUSSION

A novel chemical extraction method using EDTA for separating internalized and sorbed Ag was developed and validated through multi-laboratory analyses and imaging techniques. EDTA is a chelating agent that is known to sequester divalent cations, most especially calcium (Ca^{2+}) and magnesium (Mg^{2+}). These same ions bridge together LPS molecules in the outer membrane of Gram-negative bacteria [24]. Many studies of Gram-negative bacteria, have demonstrated outer membrane disintegration and release of large quantities of LPS upon exposure to EDTA [24, 267-269]. Therefore, under appropriate conditions, EDTA is expected to completely remove the periplasm of *P. aeruginosa* along

with sorbed Ag without significantly impacting inner plasma membrane (*i.e.,* phospholipid bilayer) [270].

Ideally, the appropriate treatment conditions for this study purpose would be the maximum EDTA concentration and exposure time under which complete cessation of bacterial growth is achieved without significant influence on bacterial cells survival. In this study, exposing *P. aeruginosa* to 50 mM EDTA temporally (*i.e.,* within first two hours) inhibited cell division, likely due to stress-response pathway activation [271-273]. However, stress-response pathways seem to start failing and cells lysed beyond these exposure conditions (*i.e.,* longer times and higher concentrations).

As indicated by confocal micrographs, bacterial membrane integrity and cell counts were preserved within first two hours of exposure compared to six hours exposure. While confocal images revealed no red cells, the significantly lower cell counts suggested that complete disruption and lyses of cells may have occurred upon EDTA exposures exceeding two hours rather than the simple cell membrane damage or/and increased permeability. These findings support our initial determination.

Thin and disrupted surfaces near cell membranes suggested that removal of the periplasm was occurring as indicated by TEM micrographs (Figure 2.5). This further supports the optical density measurements and CLSM results in showing that this method was working as proposed. Even though TEM images showed unequal EDTA impact on all cells, the 50 mM EDTA is a relatively high concentration and was expected to remove all sorbed Ag by weakening periplasm structures. Dense spherical particles were found inside cells (Figure 2.6), however, no Ag signals were detectable using EDX analyses. This could

be due to the low Ag concentrations of individual NPs, which are below the detection limits (of EDX) of 0.1% for total elements.

For practical considerations, we were able to show only two data points in the Ag liberation curve within the proposed maximum time for treatment. Both points showed statistically identical values and a resulting plateau was obtained (Figure 2.7). Although the plotted data did not produce an observable plateau for the suggested maximum treatment duration, the plateau obtained suggested that most sorbed Ag was liberated and separated from the internalized fractions. Two possible reasons might relate to the increased concentrations in sorbed fractions after applying EDTA for six hours, lysis of cells, or more likely increased permeability of the cell membranes. This conclusion is conducive to the known properties of EDTA as a permeabilizer, in addition to our finding here that bacteria still possessed intact membranes after six hours of exposure to EDTA.

Mass balance calculations after 24 h exposure to AgNPs indicated that Ag accumulated in all fractions (free/weakly bound, strongly sorbed to cell surface, and internalized). The highest fraction of Ag was the free/weakly bound which constituted up to 54% of total Ag. Whereas, sorbed Ag that was liberated by EDTA constituted only 4% at highest measurements (the lowest accumulating fraction). These data suggested that Ag multi-target mode of action against bacteria [30].

The weight of evidence across the multimethod approach utilized in this study to validate the proposed method suggested that the method for periplasm removal in Gram-negative bacterial cells was reliable and could be used for its stated purpose of differentiating Ag that was sorbed externally (weakly or strongly) vs that which was taken up by the (internal) cytoplasmic fraction. The consistency between results obtained by

optical density, TEM, CLSM, and ICPMS (Ag liberation curve) support our view that by using this method we are approximating the internalized fraction. Therefore, two hours of EDTA treatment at a concentration of 50 mM provided a reproducible estimation of internalized cellular fraction approximating the accurate value in the Gram-negative bacterium *P. aeruginosa*. However, the optimal exposure conditions may vary with organism and require further validation.

Table 2.1 Summary of AgNPs physiochemical characterization data for pristine nanoparticles. Data represented as mean (SD) of at least three consecutive measurements.

	UV-vis absorbance	**DLS**	
Sample	Peak Position (nm)	Diameter (nm)	PDI
Citrate-Coated	389.5 (1.0)	24.1 (0.5)	0.1 (0.01)
PVP-Coated	393.0 (1.0)	34.1 (0.4)	0.2 (0.01)

Table 2.2 Recovery rates % for all types of Ag at different sampling timepoints obtained by ICPMS. Data represented as the sum of mean percent recovery (SD) from free/weakly bound, strongly sorbed to the surface, and internalized fractions.

Timepoint (hours)	Citrate-coated (%)	PVP-coated (%)	Ag^+ (%)
1.5	75.2 (2.1)	67.8 (1.7)	70.2 (2.6)
2	65.5 (1.8)	79.7 (1.8)	72.9 (2.9)
6	42.9 (3.3)	51.3 (4.0)	82.2 (3.8)

Table 2.3 Summary of % Ag mass distribution collected at each timepoint for all forms of silver. Data are presented as means (SD). BDL = below detection limit.

		Ag Type			
	Timepoint (hours)	**Control (No Ag)**	**Citrate-Coated AgNPs**	**PVP-coated AgNPs**	**Ag^+**
Unbound and weakly bound fraction (%)	**0**	BDL	23.96 (0.10)	33.15 (0.15)	53.75 (0.10)
Strongly sorbed fraction (%)	**1.5**	BDL	2.06 (0.03)	1.68 (0.41)	2.62 (0.38)
	2	BDL	1.75 (0.22)	1.76 (0.21)	2.85 (0.15)
	6	BDL	3.28 (0.57)	3.95 (0.35)	3.75 (0.01)
Internalized fraction (%)	**1.5**	BDL	36.55 (6.76)	29.50 (0.10)	13.85 (6.40)
	2	BDL	22.97 (0.87)	33.20 (13.85)	16.35 (1.15)
	6	BDL	15.65 (11.35)	18.94 (4.15)	11.60 (6.55)

Table 2.4 One-way ANOVA test and Tukey multiple comparison test comparing the mean masses of strongly sorbed Ag to the outer membrane of *P. aeruginosa* and liberated by 50 mM EDTA at 1.5-hour exposure, 2-hour exposure, and 6-hour exposure to EDTA. Data representing p values at significance level of $p = 0.05$ *. Results revealed insignificant difference between masses of Ag at 1.5-hour exposure and 2-hour exposure but significant differences otherwise.

Ag Type	ANOVA	Tukey Test		
		1.5 h vs 2 h	1.5 h vs 6 h	2 h vs 6 h
Cit-AgNPs	0.005*	0.670	0.009*	0.007*
PVP-AgNPs	0.006*	>0.999	0.007*	0.010*
$AgNO_3$	0.011*	0.622	0.010*	0.023*

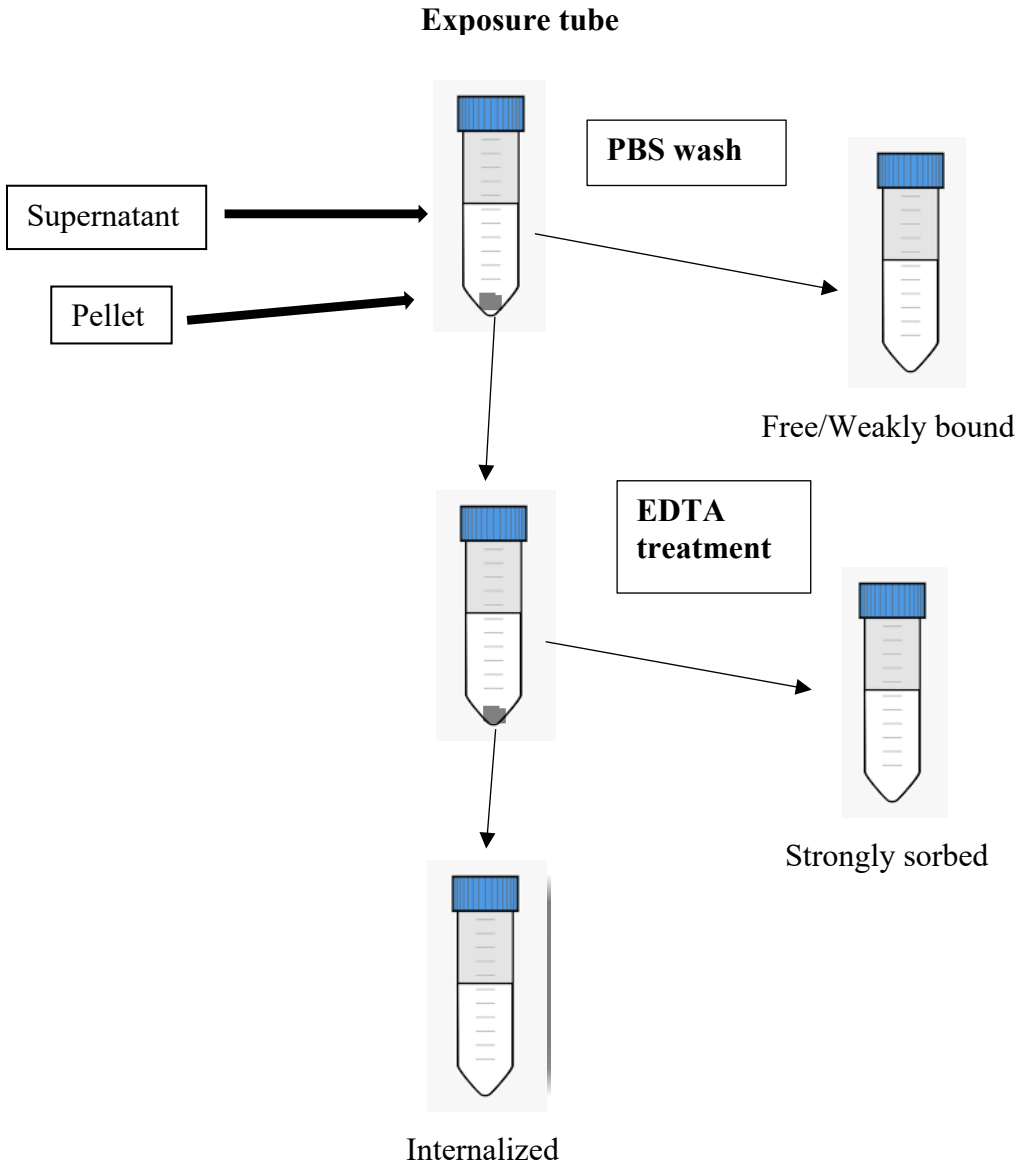

Figure 2.1 Schematic representation for experimental approach showing all fractions and their operational extraction method.

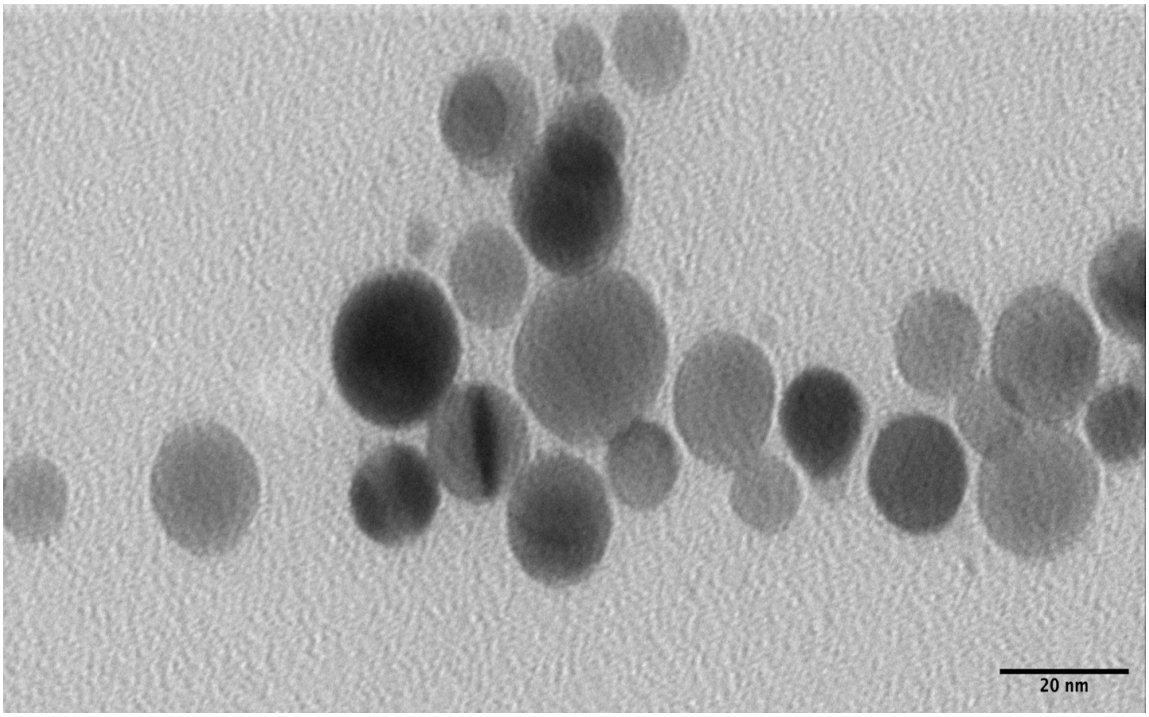

Figure 2.2 TEM micrograph of pristine stock AgNPs placed on formvar-filmed copper grid by ultracentrifugation (15.2 ± 3.5 nm).

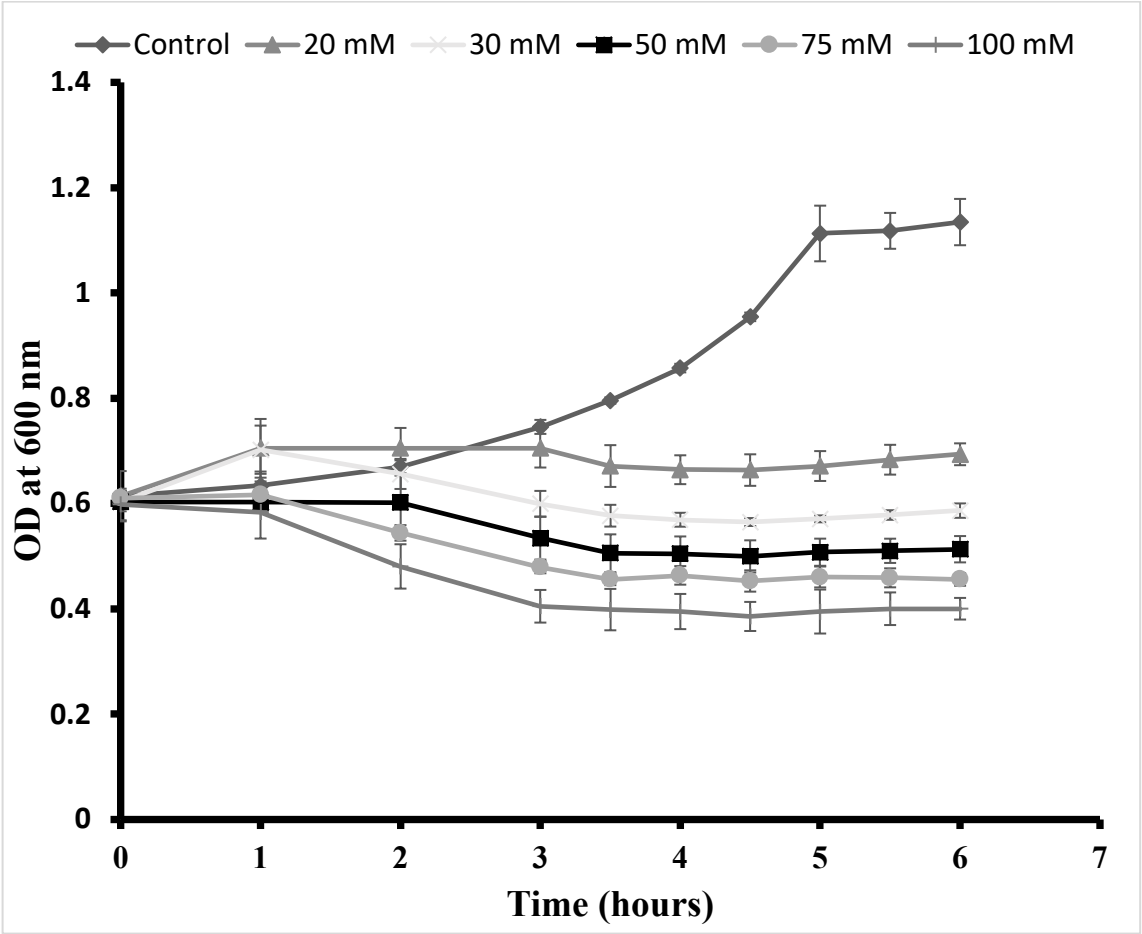

Figure 2.3 The effect of different EDTA concentrations on bacterial growth over time compared to untreated controls. Mean absorbances at 600 nm for at least three replicates were used as to estimate changes in cell densities. Error bars represent standard deviation. EDTA concentrations used were 20 mM, 30 mM, 50 mM, 75 mM, and 100 mM.

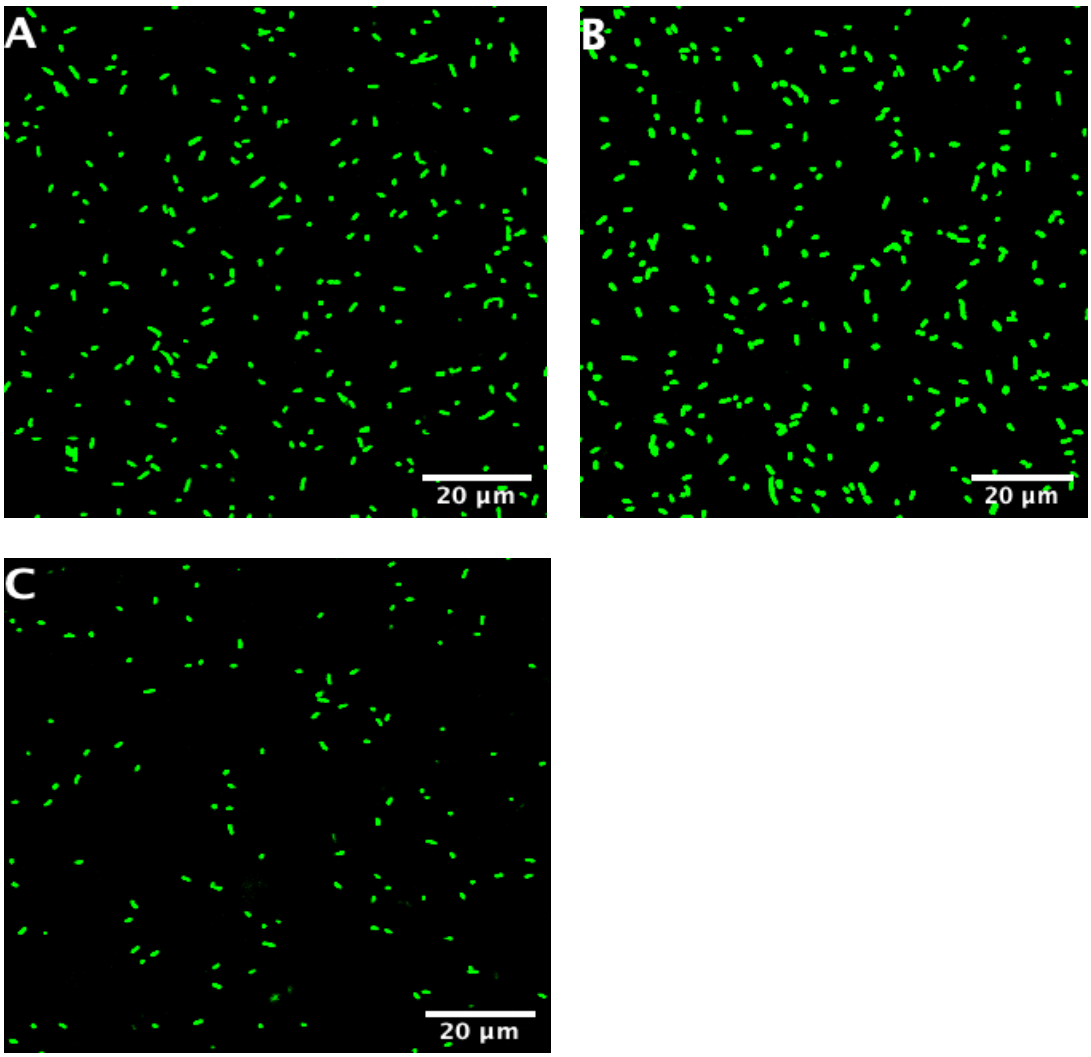

Figure 2.4 Confocal laser scanning microscopy (CLSM) images of fluorescent-stained (LIVE/DEAD *Bac*Light viability kit) *P. aeruginosa* cells at different timepoints after 50 mM EDTA treatment. (A) untreated controls; (B) cells after 2-hour exposure to EDTA; (C) cells after 6-hour exposure to EDTA. Green fluorescence indicates cells with intact membranes (Live cells).

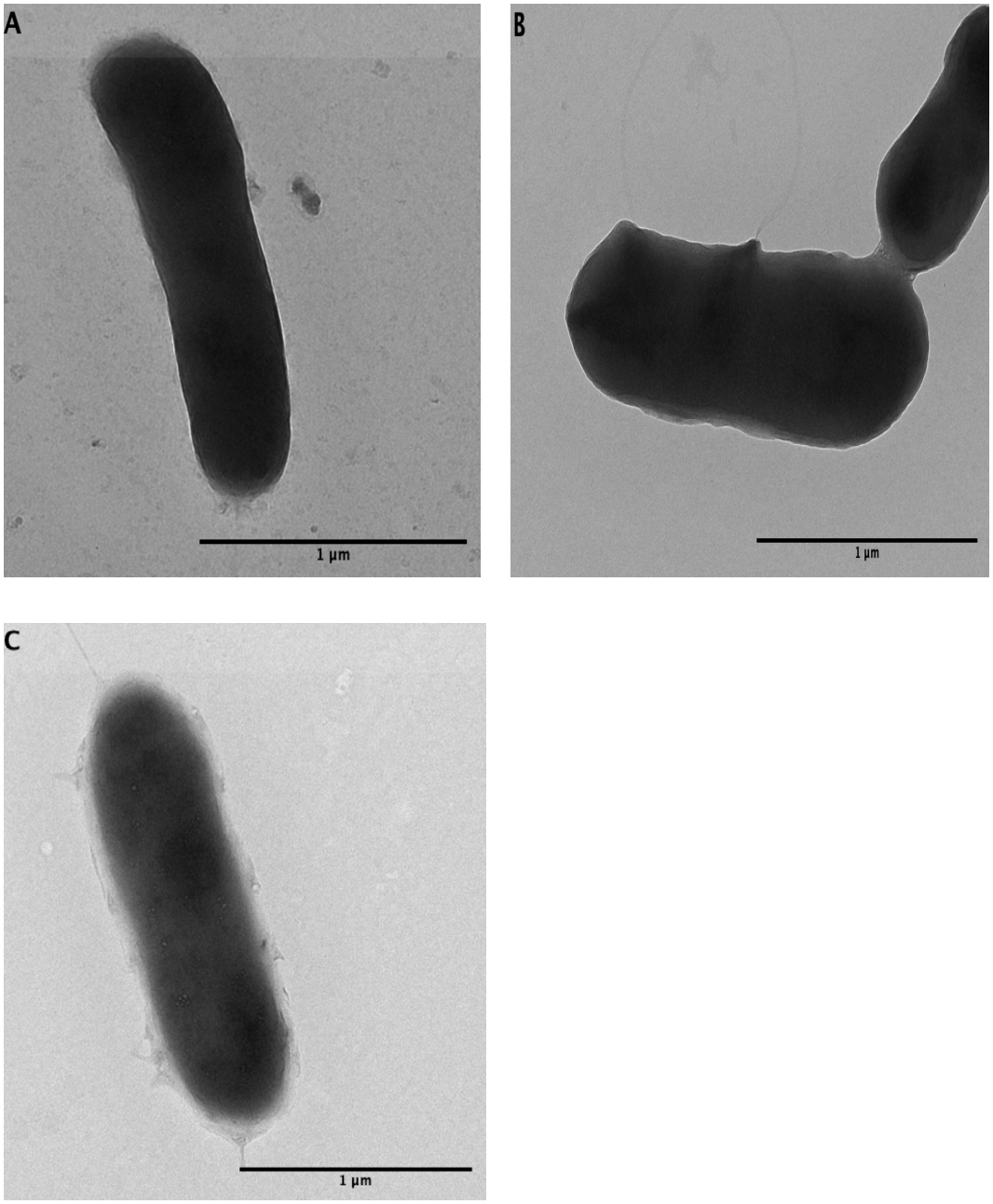

Figure 2.5 TEM micrographs showing *P. aeruginosa* cells at different timepoints after 50 mM EDTA treatment deposited on a grid by drop-deposition method. (A) untreated controls; (B) cells exposed to EDTA for 2-hour; (C) cells exposed to EDTA for 6-hour.

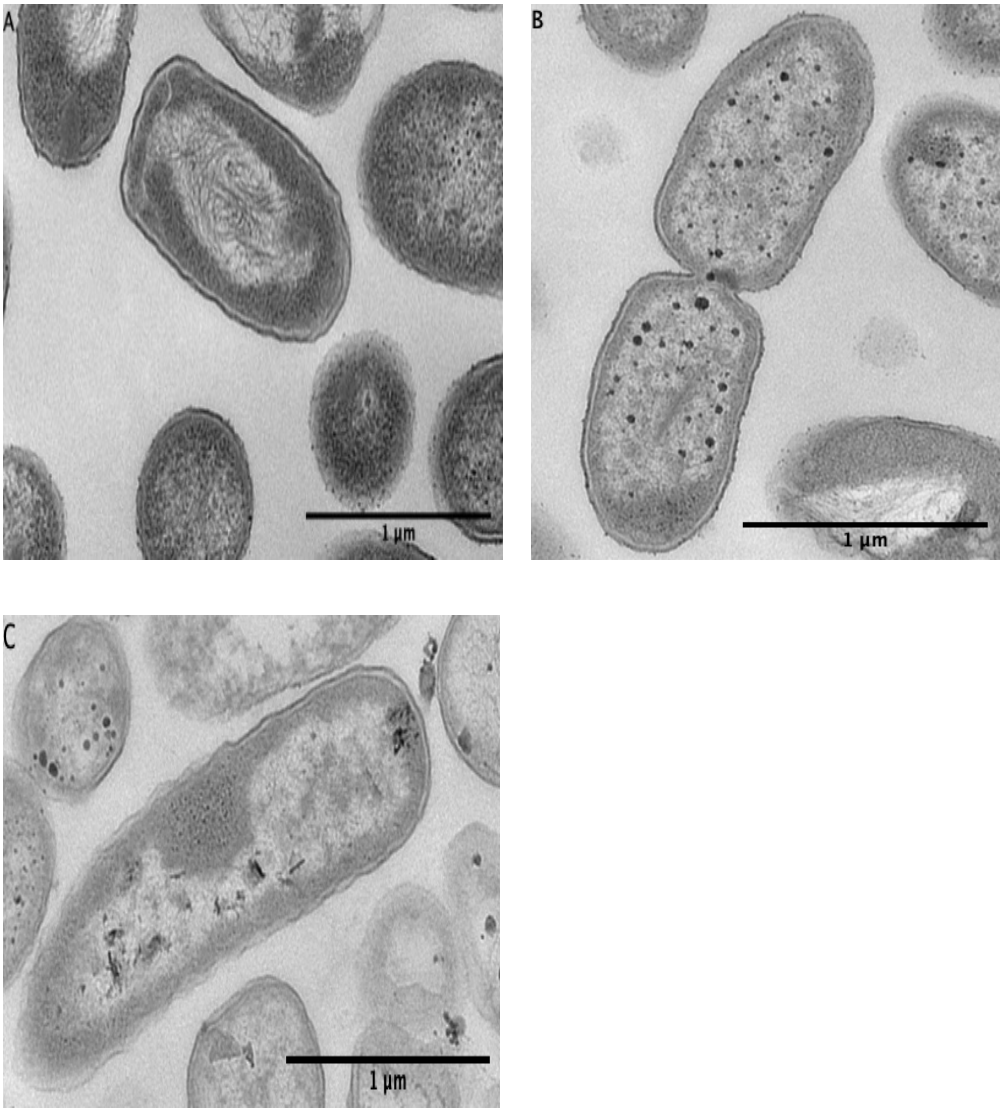

Figure 2.6 TEM ultra-thin sections (~90 nm thick) micrographs for *P. aeruginosa* post-stained with uranyl acetate and lead citrate at different timepoints after 50 mM EDTA treatment. (A) untreated controls; (B) cells exposed to EDTA for 2-hour; (C) cells exposed to EDTA for 6-hour.

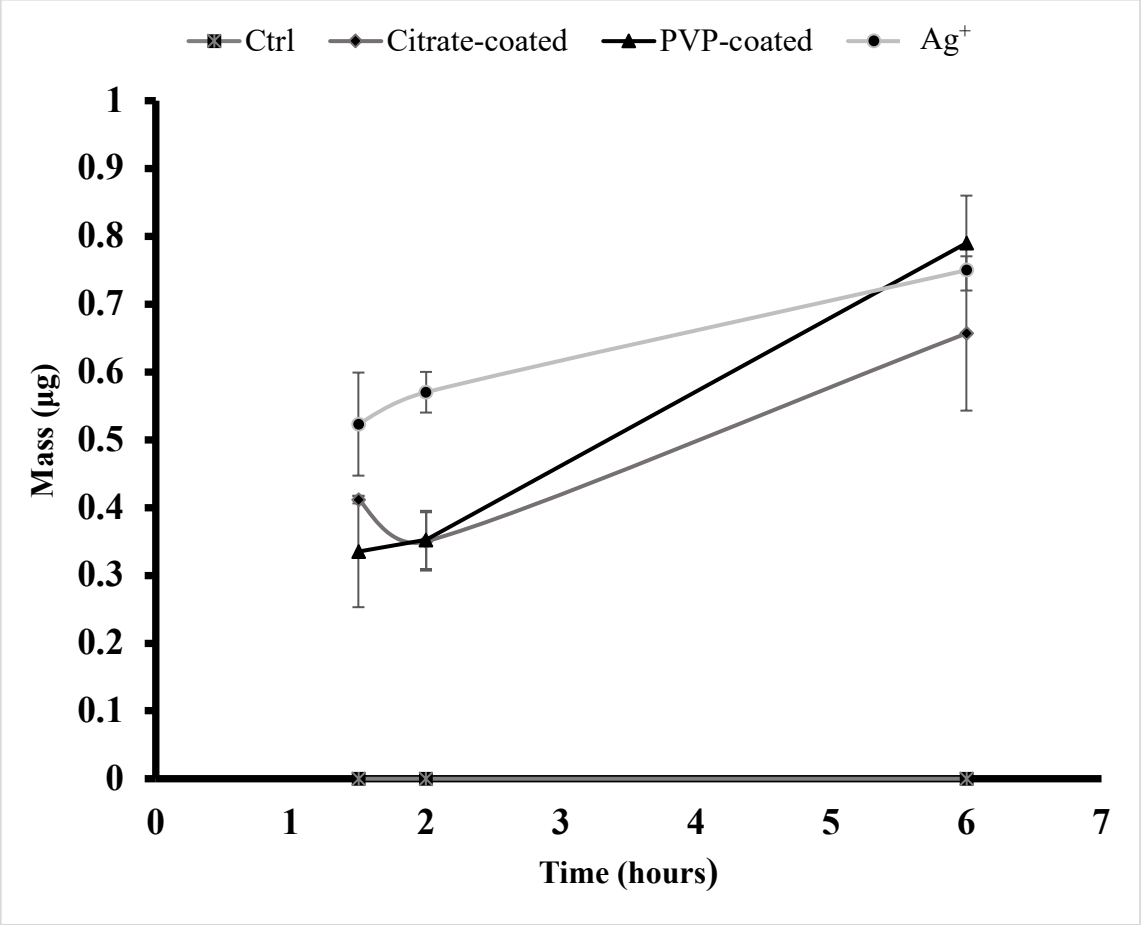

Figure 2.7 Strongly sorbed fraction of Ag that liberated by 50 mM EDTA at 1.5-hour exposure, 2-hour exposure, and 6-hour exposure to EDTA. Ag masses determined by ICPMS for negative controls, exposed to citrate coated AgNPs, PVP coated AgNPs, and Ag^{+}.

CHAPTER 3

THE ROLE OF SILVER NANOPARTICLES TRANSFORMATIONS IN SILVER UPTAKE BY GRAM-NEGATIVE BACTERIA *PSEUDOMONAS AERUGINOSA*

3.1 ABSTRACT

AgNPs hold a great potential as a NPs-based therapeutic agent against multidrug resistant (MDR) bacterial infections. However, a comprehensive understanding to the relative role of particulate versus dissolved Ag in AgNPs antimicrobial activity is poorly developed. AgNPs undergo numerous transformations in exposure media that significantly influence their bioavailability, and consequently uptake and toxicity. In the current study, we exposed a selected Gram-negative pathogenic bacterial strain *P. aeruginosa* to bimetallic Au@Ag NPs and quantified metal distribution and Ag:Au ratio in different bacterial compartments, to better understand Ag complex transformations and subsequent bioavailability and biouptake. The result showed that concentration is a major factor governing overall NPs transformations and bioavailability. As indicated by relatively higher ratios in all biotic phase fractions at lower exposure concentration, there was greater bioavailability of Ag at lower concentration where dissolution seems to be the dominant process whereas less bioavailability was observed at higher concentration where NPs were in aggregation-dominant state. Ag^+ is enriched and preferentially adsorbed to cell surface. For all forms of Ag exposure, 42.8% to 54.8 % of Ag original exposure mass was detected in abiotic phase and was mostly in dissolved form. Weakly/strongly sorbed fractions accumulated 35.9% to 44.7% of Ag original exposure mass. At 2.0 mg L^{-1} Au@Ag NPs exposure, 16.2% ± 1.8 accumulated in the operationally defined internalized fraction. This was significantly greater (p =0.0066) than same fraction at 0.2 mg L^{-1} Au@Ag NPs exposure which accumulated 9.9% ± 1.1. Ag:Au molar ratios of both total abiotic phase (p >0.9999) and operationally defined internalized fractions (p =0.9999) were statistically equivalent to pristine NPs. The weight of evidence suggests that the internalized portion is a mixture of

depleted original Au@Ag NPs, dissolved Ag in ionic and/or re-precipitated form. The relative contribution of ionic versus particulate Ag in NPs-bacteria interaction are still poorly understood although, in this study, it seems that Ag is bioavailable in both forms and may interact with multi-subcellular targets in bacteria simultaneously.

3.2 INTRODUCTION

Engineered NPs in its simplest definition are regarded as intentionally produced particles with diameter between 1-100 nm in at least one dimension [254]. Particles at this size scale usually manifest properties that are significantly different from bulk sizes of the same material [274]. The novel properties of NPs have attracted researchers and scientists to study NPs for their potential applications in a wide range of fields including medicine, biomedical devices, microbiology, and cosmetics [10, 275]. Among them, the application of AgNPs is gaining an increasing interest. AgNPs by far are considered the most promising NPs in NPs-based therapeutic approach against microbial infections [276]. However, the relative bioavailability and biouptake of particulate versus ionic Ag, which is essential toward understanding AgNPs toxicity, have not been fully quantified [249, 254, 277-279].

AgNPs readily undergo numerous physiochemical transformations in exposure media such as dissolution, agglomeration, and formation of protein corona [280, 281]. These transformations are dynamic and can be influenced by various factors related primarily to the nature of the AgNPs, exposure media compositions, as well as exposure conditions [280, 282]. Consequently, AgNPs transformations will influence NPs-bacteria interaction and cellular uptake and toxicity [283]. Therefore, it is crucial to consider AgNPs complex transformations in order to evaluate their bioavailability, and biouptake.

However, it is still very difficult to develop a comprehensive understanding to these processes likely due to the complexity of interaction and lack of standardized analytical methodologies and techniques [179, 284].

Recently, bi-metallic NPs have become attractive to researchers due to their higher functionality by combining two different metals with each featuring unique properties [285]. Au@Ag NPs provide the advantage of having Au core that is more stable (*i.e.,* remains in particulate form) than the outer shell Ag and protected from direct interaction with organism and exposure media [286]. Thus, Au can be used as internal standard [179] to help better understand the complicated Ag transformation as well as bioavailability. Compared to mono-metallic NPs, more information regarding NPs-bacteria interactions can be obtained using Au@Ag NPs, which may enhance our understanding to bioavailability, bioaccumulation, and Ag solubility [286].

Developing an understanding to these mechanisms and cellular internalization is essential for NPs potential use and applications [287]. Therefore, we aim in this study to quantify the biouptake and bioaccumulation of nanoparticulate and ionic Ag based on the molar ratios of Ag to Au being taken up. The results will provide very useful insights in directing AgNPs optimization for therapeutic purposes.

3.3 MATERIALS AND METHODS

3.3.1 Silver NPs and silver shelled gold NPs

Two different NPs suspensions were purchased from nanoComposix Inc. (San Diego, CA, USA): 1) 60 nm bi-metallic Au@Ag capped with sodium citrate (30 nm Au core; 15 nm Ag shell) at a concentration of 0.95 mg mL^{-1}, and 2) 60 nm mono-metallic Cit-AgNPs at a concentration of 0.02 mg mL^{-1}.

3.3.2 NPs Characterization

Stock NPs solutions were analyzed through multimethod approach for their average diameter, PDI, colloidal stability, absorbance spectra, and metals (Au and Ag) concentrations. Detailed characterization methods were discussed previously (see section 2.3.1).

3.3.3 NPs toxicity testing

The antibacterial activities of both Au@Ag and Cit-AgNPs toward *P. aeruginosa* (ATCC 27853) were investigated to determine the MICs (illustrated in detail in section 2.3.2). Briefly, broth microdilution assay was conducted using range of concentrations (2, 5, 7, and 10 mg L^{-1}), and the minimum concentration needed to completely inhibit bacterial growth was determined as the MIC. Using bi-metallic AgNPs with Au core might affect the antibacterial activity of Ag. To account for that, mono-metallic Cit-AgNPs of comparable physiochemical characteristics were investigated and their antimicrobial activities were compared.

3.3.4 Bacterial exposure to NPs

Bacterial cultures grown under similar conditions (see section 2.3.4), harvested, and resuspended in fresh TSB media. To investigate the concentration-dependent transformations and biouptake [178], bacterial suspensions were exposed to two 10-fold different concentrations of Au@Ag in separate containers, 2.0 and 0.2 mg L^{-1} in dark for 24 hours. Additionally, bacterial suspensions exposed to 2.0 mg L^{-1} of mono-metallic AgNPs of comparable diameter and coating (as a control for the effect of Au core), and $AgNO_3$ (as a positive control for the effect of dissolved Ag) under similar conditions.

3.3.5 Bacterial microscopy assessment

Samples prepared and examined under CLSM and TEM to assess cell viability and structural changes. Detailed sample preparations were discussed previously (see section 2.3.3.2 and 2.3.3.3). Samples collected before- and after- periplasm removal and then stained with LIVE/DEAD *Bac*Light bacterial viability kit. At least five randomly taken images obtained with CLSM and cell counts per FOV (FOV = 238x238 μm) were quantified in each acquired micrograph using ImageJ software. Samples mean cell counts for both before- and after- periplasm removal were statistically compared using paired t-test for each exposure type. Mean cell counts were also compared between different NPs exposure at each sampling timepoint using paired t-test to further investigate the effect of Au core in AgNPs toxicity. Additionally, ultra-thin sections (~90 nm thick) were prepared as previously illustrated (section 2.3.3.3) and were analyzed with TEM.

3.3.6 Bacterial exposure to EDTA and different fractions quantification

Exposures were performed for 24 hours in triplicate at a concentration of 2.0 mg L^{-1} for Cit-AgNPs and $AgNO_3$ exposure types whereas for Au@Ag NPs exposure were performed at concentrations of 2.0 mg L^{-1} and 0.2 mg L^{-1}. When exposure time was completed, exposed bacteria were washed three times by centrifugation under similar conditions. Supernatants of these initial washes representing abiotic phase (*i.e.,* aqueous fraction) were accumulated. Each pellet was resuspended in PBS and divided into two separate tubes of equal volumes. First group of tubes were further washed with PBS three times, the supernatants of these washes, representing weakly bound fraction, were accumulated. Pellets then resuspended in PBS and this fraction represent both strongly sorbed and internalized fractions combined. The other group of tubes were treated with 50 mM EDTA

and bacterial suspensions were incubated under similar growth conditions. Two hours post EDTA treatment, suspensions were washed three times by centrifugation under same conditions. Supernatants of post-EDTA-treatment washes, representing cellular external fractions (weakly bound and strongly sorbed), were accumulated (Figure 3.1). All separated fractions were sampled, digested, and analyzed for their total metals content (illustrated in detail in section 2.3.3.4). Abiotic phase was analyzed for both total and dissolved metals content after separating particles from dissolved forms for both Ag and Au using centrifugal ultrafiltration devices (Pall Corporation, Microsep Advance with 3kDa omega) and centrifuged at 4000 rpm for 30 minutes at 25°C. Particle form was calculated by the difference between these two fractions. Moles and molar ratios were calculated from Ag and Au masses obtained by ICPMS. Results were statistically analyzed using ANOVA ($p \leq 0.05$) and subsequently Tukey multiple comparison test where ANOVA was significant.

3.4 RESULTS

3.4.1 NPs characterization

Absorption spectra, size distribution and TEM images of pristine NPs suspensions are shown in Figure 3.2 and 3.3. Characterization resulted in UV-vis absorption peaks at 433.0 nm ± 1.0 and 439.0 nm ± 1.5, average hydrodynamic sizes were 63.4 nm ± 1.0 and 66.5 nm ± 1.8, PDIs were 0.2 ± 0.01 and 0.1 ± 0.01 for Au@Ag NPs and Cit-AgNPs, respectively (Table 3.1). Total metal concentrations for pristine Au@Ag NPs resulted in an Ag:Au mean mass ratio of 2.8 ± 0.3 that corresponds to a molar ratio of 5.1 ± 0.6. Stock NPs characterizations provided by manufacturer indicated that Ag:Au mean mass ratio is 3.0 that corresponds to 5.4 molar ratio.

3.4.2 Antibacterial activities

The antimicrobial activities of Au@Ag NPs and Cit-AgNPs, with average diameters of ~ 60.0 nm, toward *P. aeruginosa* were determined by the standard microdilution method. The obtained results suggested identical antimicrobial potency of > 10.0 mg L^{-1} for both NPs types. To avoid the antibacterial effect of NPs for this study, 2.0 mg L^{-1} and 0.2 mg L^{-1} were selected as the sublethal doses to be investigated for their interactions.

3.4.3 Bacterial viability and structural changes assessment

Figure 3.4 shows CLSM micrographs of *P. aeruginosa* before- and after- periplasm removal. Samples were stained with LIVE/DEAD fluorescent viability kit which visualizes live bacterial cells as green or red otherwise as a function of cell membrane integrity. However, all visualized cells (for both NPs exposure at both sampling timepoints) fluoresced green indicating bacterial integrity in all samples. As summarized in Table 3.2, the mean numbers of viable cell counts were not significantly different (p = 0.2105) for cells exposed to Au@Ag NPs before- and after- periplasm removal at values of 1493 ± 109 and 1449 ± 157 cells/ FOV, respectively. Similarly, statistically insignificant difference (p = 0.6033) was found in the mean numbers of viable cell counts before- (1361 ± 189 cells/FOV) and after- (1475 ± 123 cells/ FOV) periplasm removal in group exposed to Cit-AgNPs. Mean number of viable cell counts in bimetallic Au@Ag NPs-exposed cells was not significantly different from mean number of viable cell counts in group exposed to monometallic AgNPs at both sampling timepoints (p = 0.3046 before periplasm removal versus p = 0.8313 after periplasm removal). No structural changes were detected in the TEM images (Figure 3.5).

3.4.4 Metal accumulation

3.4.4.1 Quantification of metals distribution

In all exposure types, fractions were defined operationally based on our experimental approach and extraction methodology as follows (Figure 3.1). Fraction separated by initial PBS washes were referred to as abiotic phase (*i.e.,* aqueous fraction) whereas pellets were referred to as biotic phase fraction. The biotic phase further fractionated into external cellular fractions (either weakly or strongly sorbed to the cell surface) and internalized fraction. Fraction separated by second PBS washes were referred to as weakly bound fraction while pellets of these washes were referred to as strongly sorbed and internalized fractions combined. The EDTA-extracted fraction here referred to as strongly sorbed and internalized fractions combined (*i.e.,* cellular external fractions) whereas metal accumulated in the pellets after periplasm removal were defined as internalized fractions.

Molar concentrations were calculated for all fractions in both biotic and abiotic phases (Table 3.3). For all forms of Ag exposure, nearly one-half (the highest accumulating fraction) of the total added Ag accumulated in the aqueous fraction (*i.e.,* abiotic phase) ranging from 42.8% to 54.8 %. The detected Ag in this fraction was mostly in the dissolved form ranging from 46.0% to 80.0% for all forms of Ag. The weakly bound fraction was the highest in 2.0 mg L^{-1} Au@Ag NPs exposure (42.4% ± 4.5), followed by 0.2 mg L^{-1} Au@Ag NPs exposure (33.9% ± 3.6), Cit-AgNPs exposure (33.0% ± 3.2), and Ag^{+} exposure (26.2% ± 1.9). On the other hand, the external cellular fractions (weakly bound and strongly bound), that were liberated with EDTA (*i.e.,* periplasm removal), and subsequently washed off with PBS, were ranging from 35.9% to 44.7% for all forms of Ag exposure. Ag percentage accumulation in the operationally defined internalized fraction

was significantly greater (p =0.0066) in the 2.0 mg L^{-1} Au@Ag NPs exposure at a mean percentage of 16.2% ± 1.8 compared to 9.9% ± 1.1 for 0.2 mg L^{-1} Au@Ag NPs exposure (Table 3.4). However, the highest percentage of Ag accumulation in the operationally defined internalized fraction was detected in Ag^{+} exposure at a value of 31.4% from the original exposure concentration compared to all other forms of Ag exposure (Figure 3.6).

Similarly, Au accumulated preferentially in the abiotic phase at percentages of 23.1% ± 2.7 and 42.0% ± 2.2 for the 2.0 mg L^{-1} Au@Ag NPs exposure and 0.2 mg L^{-1} Au@Ag NPs exposure, respectively. Percentage accumulation was significantly greater (p =0.0007) in the lower exposure concentration. On the other hand, the Au accumulated in the operationally defined internalized fraction was significantly greater (p =0.0008) in the 2.0 mg L^{-1} Au@Ag NPs exposure at an accumulation percentage of 13.2% ± 1.2 compared to 6.6% ± 0.4 in the 0.2 mg L^{-1} Au@Ag NPs exposure. Furthermore, cellular external fraction (operationally defined as weakly bound and strongly sorbed fractions combined) accumulated significantly higher (p =0.0021) percentage of Au in the 2.0 mg L^{-1} Au@Ag NPs exposure at 21.8% ± 2.8 versus 10.1% ± 0.5 in the 0.2 mg L^{-1} Au@Ag NPs exposure.

Most aqueous phase Au remained in particulate form (Figure 3.7), 98.3% in the 2.0 mg L^{-1} Au@Ag NPs exposure and 96.2% in the 0.2 mg L^{-1} Au@Ag NPs exposure. Internalized Au percentages detected were greater for higher concentration exposure at a value of 13.2% ± 1.2 compared to 6.6% ± 0.4 in lower exposure. Cellular external fraction of Au was 10.1% ± 0.5 in the 0.2 mg L^{-1} Au@Ag NPs exposure while it was 21.8% ± 2.8 in the 2.0 mg L^{-1} Au@Ag NPs exposure (Table 3.4).

3.4.4.2 Metallic molar ratios

For all biotic phase fractions, concentration-dependent accumulations of Ag were observed with significantly greater Ag:Au molar ratios at 0.2 mg L^{-1} Au@Ag NPs exposure (Table 3.5) before- and after- periplasm removal except for internalized fraction (p = 0.4726) compared to 2.0 mg L^{-1} Au@Ag NPs exposure. In contrast, significantly lower Ag:Au molar ratios (p = 0.0106) were observed in the total abiotic phase (*i.e.,* aqueous fraction) fraction at 0.2 mg L^{-1} Au@Ag NPs exposure. Ag:Au molar ratios in the total abiotic phase were relatively equal to the pristine molar ratio (5.1 ± 0.6) at both concentrations. However, significantly greater ratios were observed in the dissolved fraction of the abiotic phase at values of 562.1 ± 92.1 (p <0.0001) and 125.9 ± 12.2 (p <0.0001) for higher and lower exposure, respectively (Table 3.5). Before periplasm removal, significant differences were only detected at 0.2 mg L^{-1} Au@Ag NPs exposure (Figure 3.8) in both weakly bound fraction (p <0.0001) and the combined strongly sorbed and internalized fraction (p <0.0001). Whereas after periplasm removal, Ag:Au ratios were not significantly different from pristine NPs ratio in all biotic phase fractions at both exposure concentrations with mean values ranging from 6.9 to 18.2.

3.4.4.3 Mass Balance

Mass balance calculations were conducted for both Ag and Au to calculate the recovery rates in all types of exposure suspensions (Table 3.6). The recovery rates of Ag before periplasm removal (Figure 3.9) were 106.6% ± 7.9 in the 2.0 mg L^{-1} Au@Ag NPs exposure, 88.1% ± 8.1 in the 0.2 mg L^{-1} Au@Ag NPs exposure, 82.7% ± 2.7 in Cit-AgNPs exposure, and 108.1% ± 5.1 in Ag^{+} exposure. Whereas after periplasm removal (Figure 3.10), they

were 115.7% ± 6.0 in the 2.0 mg L^{-1} Au@Ag NPs exposure, 97.6% ± 19.2 in the 0.2 mg L^{-1} Au@Ag NPs exposure, 98.4% ± 4.5 for Cit-AgNPs, and 116.4% ± 15.1 for Ag^{+}.

On the other hand, Au exhibited higher rates of loss from the system. The maximum recovery rate for Au was 58.2% ± 10.5 in the 2.0 mg L^{-1} Au@Ag NPs exposure followed by 52.0% ± 0.2 in the 0.2 mg L^{-1} Au@Ag NPs exposure. Lower recovery rates were achieved before periplasm removal at values of 30.2% ± 1.0 and 37.5% ± 2.2 for the 2.0 mg L^{-1} Au@Ag NPs exposure and 0.2 mg L^{-1} Au@Ag NPs exposure, respectively.

3.5 DISCUSSION

Similar antibacterial activities (*i.e.,* MICs) for bimetallic Au@Ag NPs and monometallic Cit-AgNPs, and insignificant differences in mean viable cell counts between Au@Ag NPs-exposed and Cit-AgNPs-exposed groups suggested similar toxicities and negligible effect of Au core in AgNPs behavior. Therefore, we assume that inferences from Au@Ag NPs interaction with *P. aeruginosa* could be generalized to monometallic AgNPs of comparable physiochemical characteristics. Furthermore, a recent study [179] and our metallic dissolution data (Table 3.3) supports our assumption on relying on the Au as an internal standard that mainly remained in particulate form throughout the interaction with bacteria. However, Au recovery rates were lower than those for Ag which might be attributed to the relatively greater tendency of Au to adhere and be lost to the container walls.

Concentration-dependent dissolution (Figure 3.7) observed is suggesting that Au@Ag NPs are undergoing dynamic changes in the exposure interface which eventually influence their bioavailability and biouptake [288-291]. Dissolution is likely the dominant process occurring at the lower exposure concentration [178, 179], whereas aggregation and deposition seem to be the dominant processes occurring at the higher exposure

concentration which reduced Au@Ag NPs bioavailability to a certain degree [292, 293]. This is indicated by lower Ag:Au molar ratios (Figure 3.8) at higher exposure concentration compared to lower exposure concentration consistently in all biotic phase fractions (*i.e.,* significant in all biotic phase fractions except for internalized (Table 3.5)) accompanied by relatively higher ratios in the abiotic phase (*i.e.,* unbound state). Supported by dissolution data (Figure 3.7), the massive increase of Ag:Au at surface bound fraction (*i.e.,* in the weakly bound before periplasm removal and to a lesser extent in the combined weakly bound and strongly sorbed fraction after periplasm removal) (Figure 3.8), suggests that dissolved Ag^{+} is preferentially binding to cell surface whereas NPs are more bioavailable for internalization, however, this is not necessarily true.

Ag:Au ratios in the operationally defined internalized fractions were relatively equal to the pristine Au@Ag NPs ratio suggesting same amount of Ag and Au being taken up by the organism. Because NPs are dissolving and ionic Ag is enriched on the cell surface, it is quite unlikely that biouptake is solely for the original Au@Ag NPs, and Ag ions are completely excluded from internalization. However, the most likely explanation is that the internalized portion of Ag is the summation of the complex Ag transformations and biouptake. In fact, the weight of evidence suggests that the internalized fraction could be a mixture of completely or partially depleted Au@Ag NPs (with reduced Ag), ionic or re-precipitated Ag^{+} (in form of Ag-Cl complexes or secondary NPs), and the sum of that is coincidentally of an equivalent Ag:Au ratio of the pristine Au@Ag NPs. Therefore, Ag in particulate and ionic forms are both bioavailable and taken up by *P. aeruginosa*. This theory is further supported by other studies conducted to evaluate AgNPs transformation and bioavailability, in which both ionic and particulate Ag found to be bioavailable [294,

295]. This result suggests that AgNPs interact with multiple cellular targets in bacteria simultaneously [45].

Although AgNPs bioavailability compared to Ag^+ has been extensively studied, controversies still abound concerning the relative bioavailability of ions versus particles [172]. For example, in recent studies, bioaccumulation and biouptake was attributed to the particulate form of Ag rather than to dissolved Ag^+ in certain organisms [172, 294, 296]. In contrast, numerous studies that have been conducted attributed biouptake mainly to dissolved Ag [297-299]. However, distinguishing Ag ions from NPs in different bacterial compartment remains complicated because of the limitations associated with current analytical techniques and the lack of valid standardized methodology [179].

Table 3.1 Summary of Au@Ag NPs and AgNPs physiochemical characterization data for pristine nanoparticles represented as mean (SD) of at least three consecutive measurements.

Sample	UV-vis absorbance	DLS	
	Peak Position (nm)	Diameter (nm)	PDI
Au@Ag NPs	439.0 (1.5)	66.5 (1.8)	0.1 (0.01)
Cit-AgNPs	433.0 (1.0)	63.4 (1.0)	0.2 (0.01)

Table 3.2 Cell counts of CLSM images for Au@Ag NPs-exposed and Cit-AgNPs-exposed cells before- and after- periplasm removal along with t-test results of statistical significance of difference between mean values at $p < 0.05$*. Data presented as mean (SD). FOV= Field of View = 238x238 μm.

Sample	Before periplasm removal (cells/ FOV) mean (SD)	After periplasm removal (cells/ FOV) mean (SD)	*p* value
Au@Ag NPs	1493 (109)	1449 (157)	0.2105
Cit-AgNPs	1361 (189)	1475 (123)	0.6033
p value	0.3046	0.8318	

Table 3.3 Metallic molar concentration (μmol) of Ag and Au in all fractions for each type of exposure.

Biotic phase mole concentration (μmol)
mean (SD)

		Au@Ag NPs				Ag^+	Cit-AgNPs
		2.0 mg L^{-1}		0.2 mg L^{-1}			
		Ag	**Au**	**Ag**	**Au**		
Before periplasm removal	**Weakly bound**	59.0 (12.6)	0.8 (0.2)	4.7 (1.0)	0.03 (0.01)	48.6 (7.2)	61.1 (12.0)
	Internalized + Strongly sorbed	12.9 (3.6)	1.0 (0.4)	1.2 (0.1)	0.03 (0.003)	60.9 (1.4)	12.9 (3.4)
After periplasm removal	**Weakly bound + Strongly sorbed**	62.2 (6.1)	5.5 (1.4)	5.9 (2.2)	0.26 (0.03)	80.4 (6.8)	89.9 (7.8)
	Internalized	22.5 (5.1)	3.4 (0.6)	1.4 (0.3)	0.17 (0.02)	58.3 (6.0)	26.5 (9.3)

Abiotic phase mole concentration (μmol)
mean (SD)

		Au@Ag NPs				Ag^+	Cit-AgNPs
		2.0 mg L^{-1}		0.2 mg L^{-1}			
		Ag	**Au**	**Ag**	**Au**		
Aqueous fraction	**Dissolved**	51.1 (17.5)	0.1 (0.02)	5.1 (0.5)	0.04 (0.0004)	51.0 (17.4)	36.5 (3.9)
	Particle	25.1 (8.4)	5.8 (0.7)	1.2 (0.2)	0.9 (0.1)	40.0 (9.9)	42.9 (13.5)
	Total	76.2 (3.2)	5.9 (0.7)	6.3 (0.8)	0.9 (0.1)	91.0 (2.1)	79.4 (18.1)

Table 3.4 Percentage mean mass distribution (%) of Ag and Au of initially added mass in all fractions for each type of exposure.

		Biotic phase percentage mean mass distribution (%) mean (SD)					
		Au@Ag NPs				Ag^+	Cit-AgNPs
		2.0 mg L^{-1}		0.2 mg L^{-1}			
		Ag	**Au**	**Ag**	**Au**		
Before periplasm removal	**Weakly bound**	42.4 (4.5)	3.1 (0.4)	33.9 (3.6)	1.2 (0.2)	26.2 (1.9)	33.0 (3.2)
	Internalized + Strongly sorbed	9.3 (1.3)	4.0 (0.8)	8.6 (0.5)	1.1 (0.1)	32.8 (0.4)	7.0 (0.9)
After periplasm removal	**Weakly bound + Strongly sorbed**	44.7 (2.2)	21.8 (2.8)	42.2 (7.9)	10.1 (0.5)	35.9 (6.6)	41.3 (6.4)
	Internalized	16.2 (1.8)	13.2 (1.2)	9.9 (1.1)	6.6 (0.4)	31.4 (1.6)	14.3 (2.5)

		Abiotic phase percentage mass distribution (%) mean (SD)					
		Au@Ag NPs				Ag^+	Cit-AgNPs
		2.0 mg L^{-1}		0.2 mg L^{-1}			
		Ag	**Au**	**Ag**	**Au**		
Aqueous fraction	**Dissolved**	36.8 (12.6)	0.4 (0.6)	38.3 (3.4)	1.6 (0.02)	27.5 (9.4)	19.7 (2.1)
	Particle	18 (6.0)	22.7 (2.6)	7.2 (1.6)	40.4 (2.2)	21.6 (9.9)	23.1 (10.7)
	Total	54.8 (2.3)	23.1 (2.7)	45.5 (5.9)	42.0 (2.2)	49.1 (1.1)	42.8 (9.8)

Table 3.5 Summary of molar ratios and statistical significance data. Tukey multiple comparison test comparing mean molar ratio of each fraction in both exposure concentrations to pristine Au@Ag NPs molar ratio of 5.1 (0.6), and t-test results for concentration-dependent difference in mean molar ratios in each fraction at significance level p <0.05*. Data represented as mean (SD).

		Biotic phase				
		Molar ratio		**Tukey**		**t-test**
		2.0 mg L^{-1}	0.2 mg L^{-1}	2.0 mg L^{-1}	0.2 mg L^{-1}	
Before periplasm removal	**Weakly bound**	60.2 (8.8)	136.7 (4.1)	0.4760	<0.0001*	0.0002*
	Strongly sorbed + Internalized	13.4 (2.3)	42.7 (2.8)	>0.9999	<0.0001*	0.0002*
After periplasm removal	**Weakly bound + Strongly sorbed**	9.8 (0.3)	18.2 (2.1)	>0.9999	0.0617	0.0024*
	Internalized	6.9 (2.4)	8.3 (1.9)	0.9999	0.9894	0.4726
		Abiotic phase				
		Molar ratio		**Tukey**		**t-test**
		2.0 mg L^{-1}	0.2 mg L^{-1}	2.0 mg L^{-1}	2.0 mg L^{-1}	
Aqueous fraction	**Dissolved**	562.1 (92.1)	125.9 (12.2)	<0.0001*	<0.0001*	0.0012*
	Particle	6.2 (2.2)	2.0 (0.3)	>0.9999	0.9911	0.0306*
	Total	13.1 (1.7)	7.5 (1.3)	>0.9999	0.9981	0.0106*

Table 3.6 Recovery rates % for all types of Ag before- and after- periplasm removal obtained by ICPMS. Data presented as the mean percent recovery (SD) from aqueous phase, weakly bound, strongly sorbed to the surface, and internalized fractions.

		Recovery rate (%)	
	Total mass (μg)	Before periplasm removal (%) Mean (SD)	After periplasm removal (%) Mean (SD)
2.0 mg L^{-1} Cit-AgNPs	20.0	82.7 (2.7)	98.4 (4.5)
Ag^{+} 2.0 mg L^{-1}	20.0	108.1 (5.1)	116.4 (15.1)
Ag in 2.0 mg L^{-1} Au@Ag	15.0	106.6 (7.9)	115.7 (6.0)
Ag in 0.2 mg L^{-1} Au@Ag	1.5	88.1 (8.1)	97.6 (19.2)
Au in 2.0 mg L^{-1} Au@Ag	5.0	30.2 (1.0)	58.2 (10.5)
Au in 0.2 mg L^{-1} Au@Ag	0.5	37.5 (2.2)	52.0 (0.2)

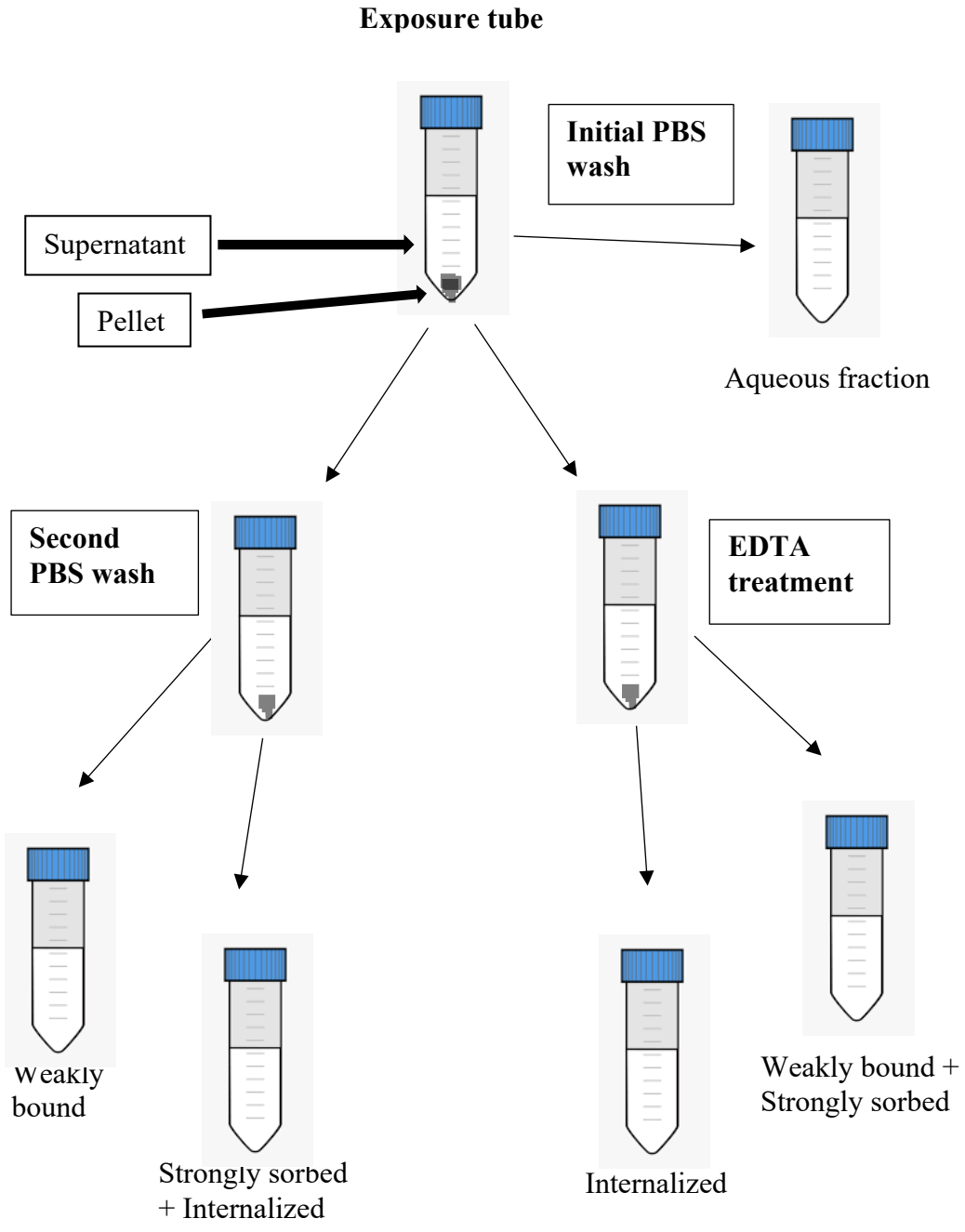

Figure 3.1 Schematic representation for experimental approach showing all fractions and their operational extraction method.

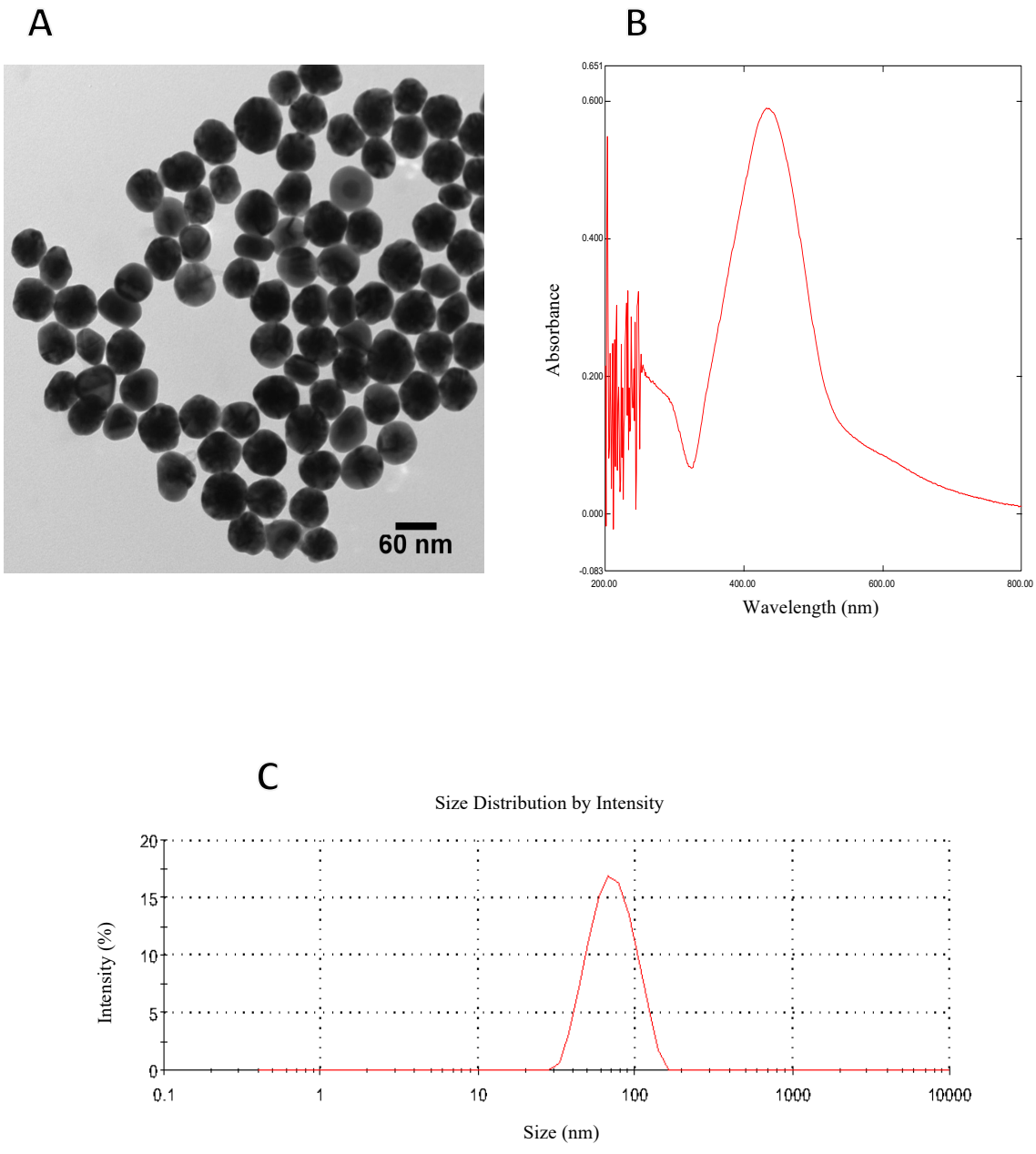

Figure 3.2 Characterization of stock bimetallic Au@Ag NPs. (A) TEM image (obtained from manufacturer nanoComposix)**,** (B) UV-Vis spectra obtained by UV-Vis, (C) size distribution obtained by DLS.

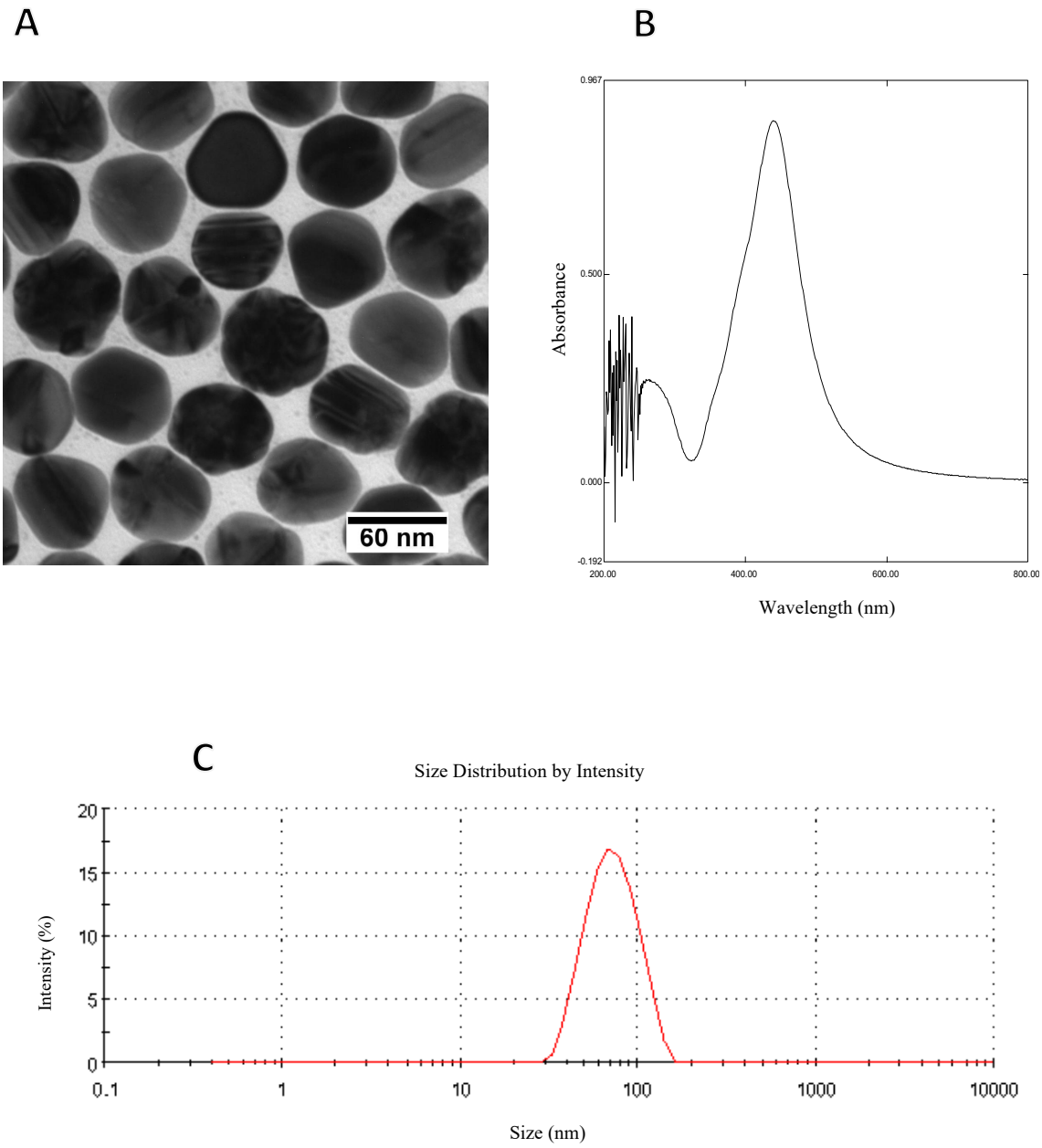

Figure 3.3 Characterization of stock Cit-AgNPs. (A) TEM image (obtained from manufacturer nanoComposix)**,** (B) UV-Vis spectra obtained by UV-Vis, (C) size distribution obtained by DLS.

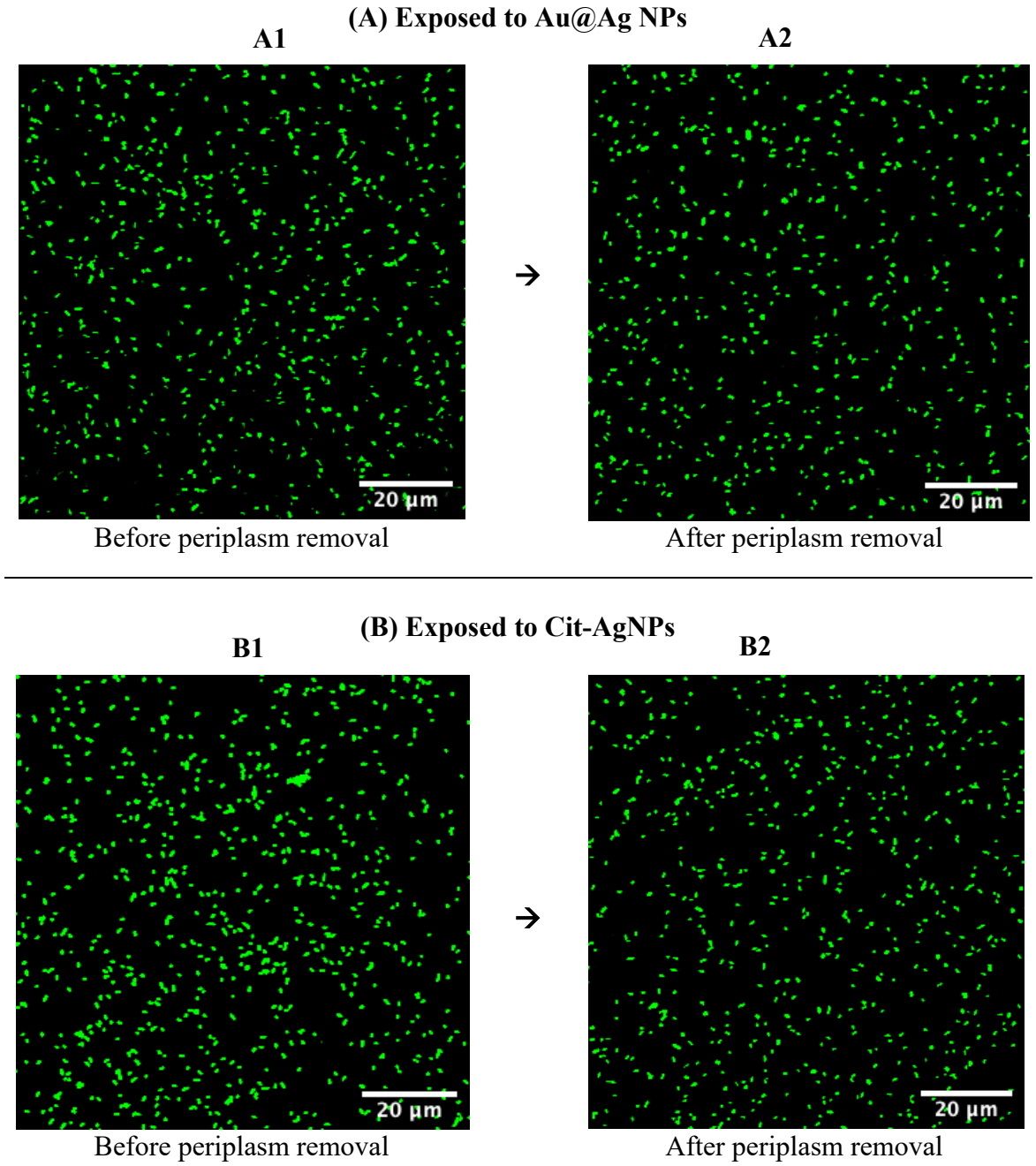

Figure 3.4 Confocal laser scanning microscopy (CLSM) images of fluorescent-stained (LIVE/DEAD *Bac*Light viability kit) *P. aeruginosa* cells before- and after- periplasm removal. (A) exposed to Au@Ag NPs; (B) exposed to Cit-AgNPs; (A1 and B1) before periplasm removal; (A2 and B2) after periplasm removal. Green fluorescence indicates cells with intact membranes (Live cells). There were no significant differences between cell counts before and after periplasm removal in both exposures at significance level $p < 0.05$.

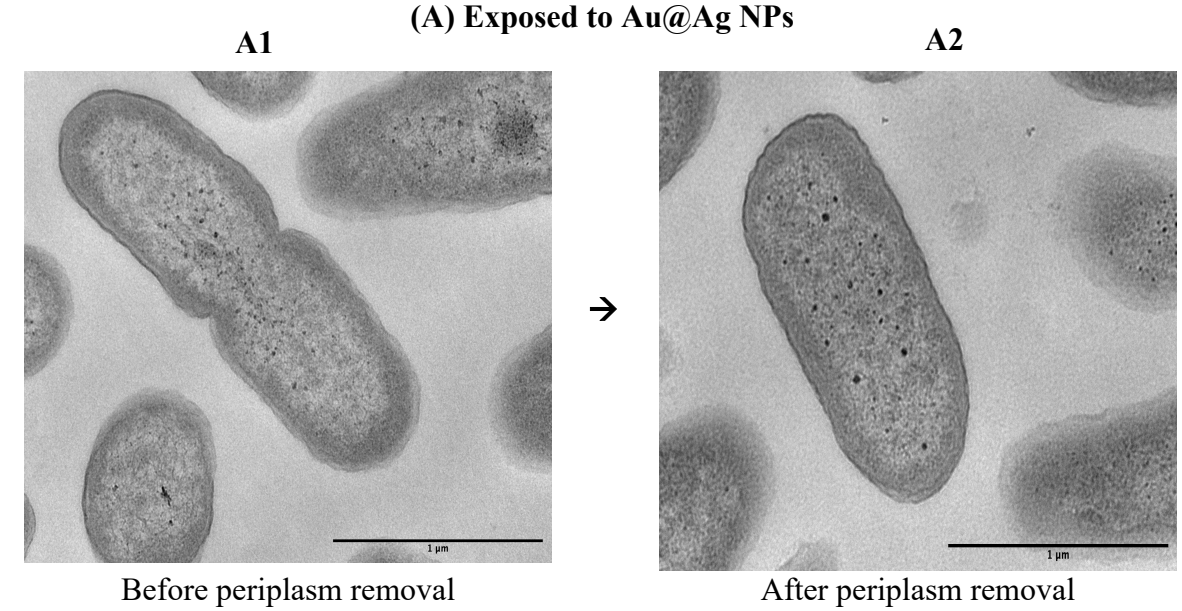

Figure 3.5 TEM ultra-thin sections (~90 nm thick) micrographs of *P. aeruginosa* post-stained with uranyl acetate and lead citrate. (A) exposed to Au@Ag NPs; (B) exposed to Cit-AgNPs; (A1 and B1) before periplasm removal; (A2 and B2) after periplasm removal.

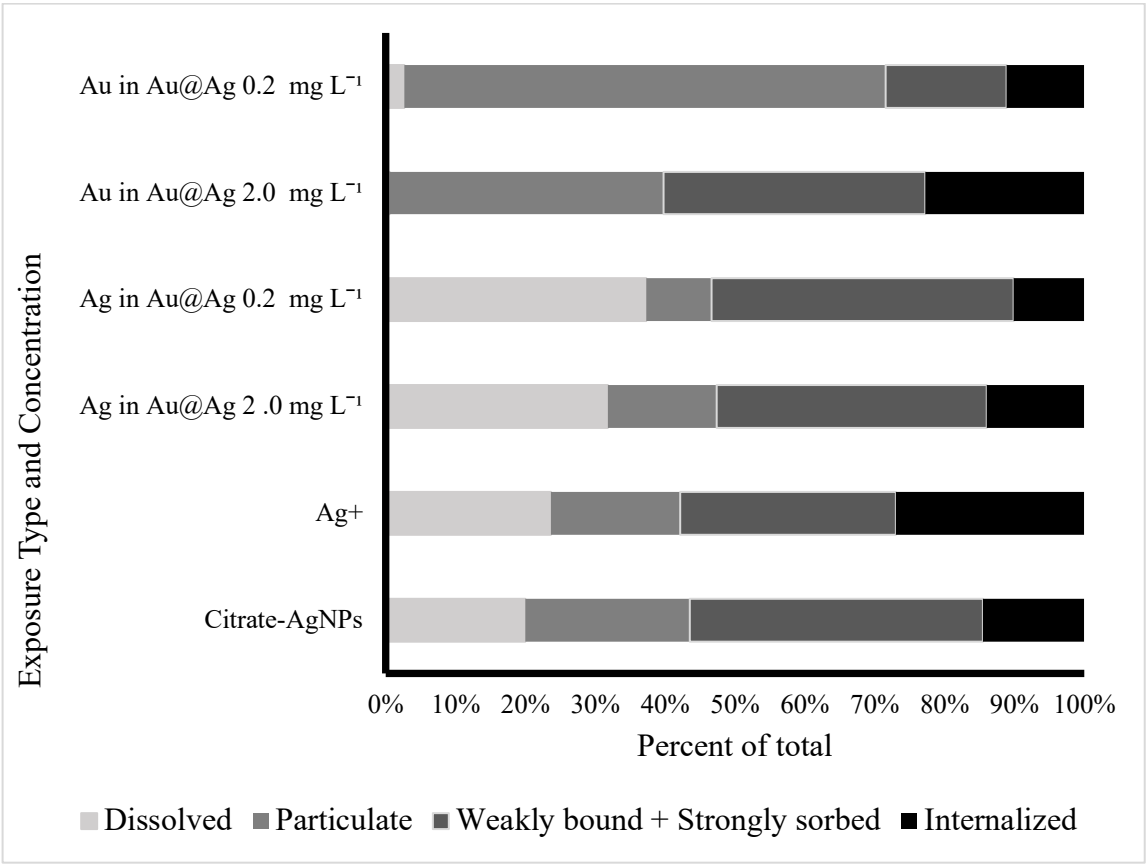

Figure 3.6 Metals mass distribution after periplasm removal presented as 100% stacked bar chart. The sum of dissolved and particulate form constitutes the total metal content in the abiotic phase. The sum of dissolved and particulate forms represents the total metal accumulation in the aqueous phase. (Note that weakly bound and strongly sorbed fractions are combined).

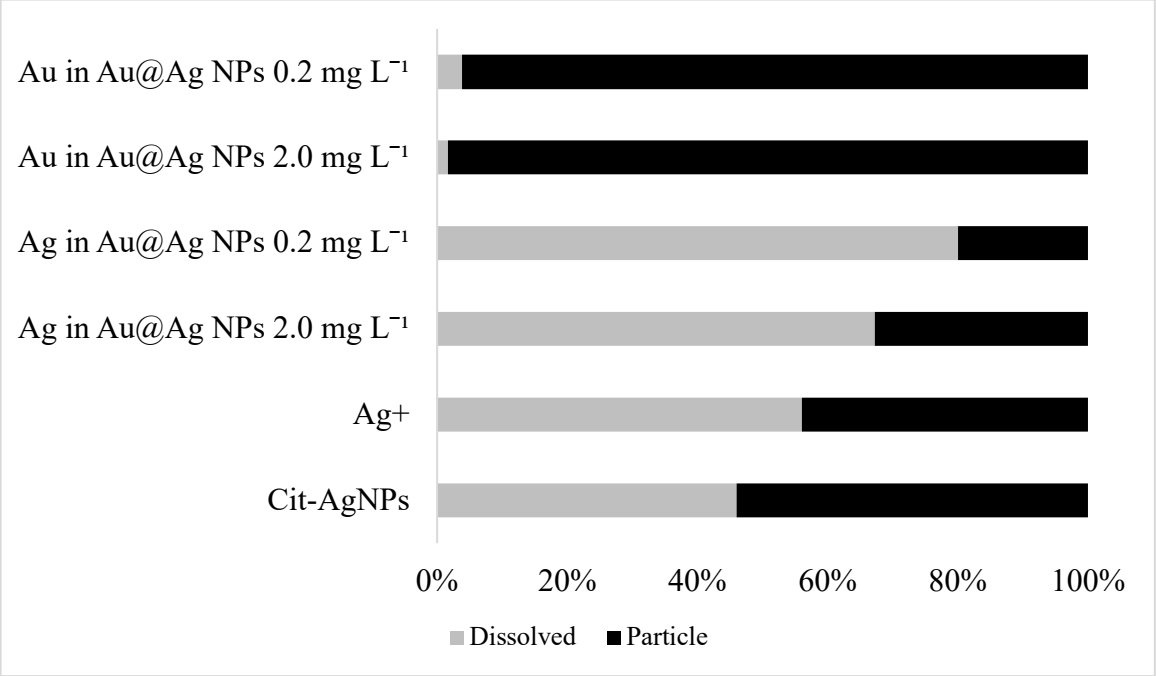

Figure 3.7 Total dissolved and particle form of metals in percent (%) of total mass detected in abiotic phase.

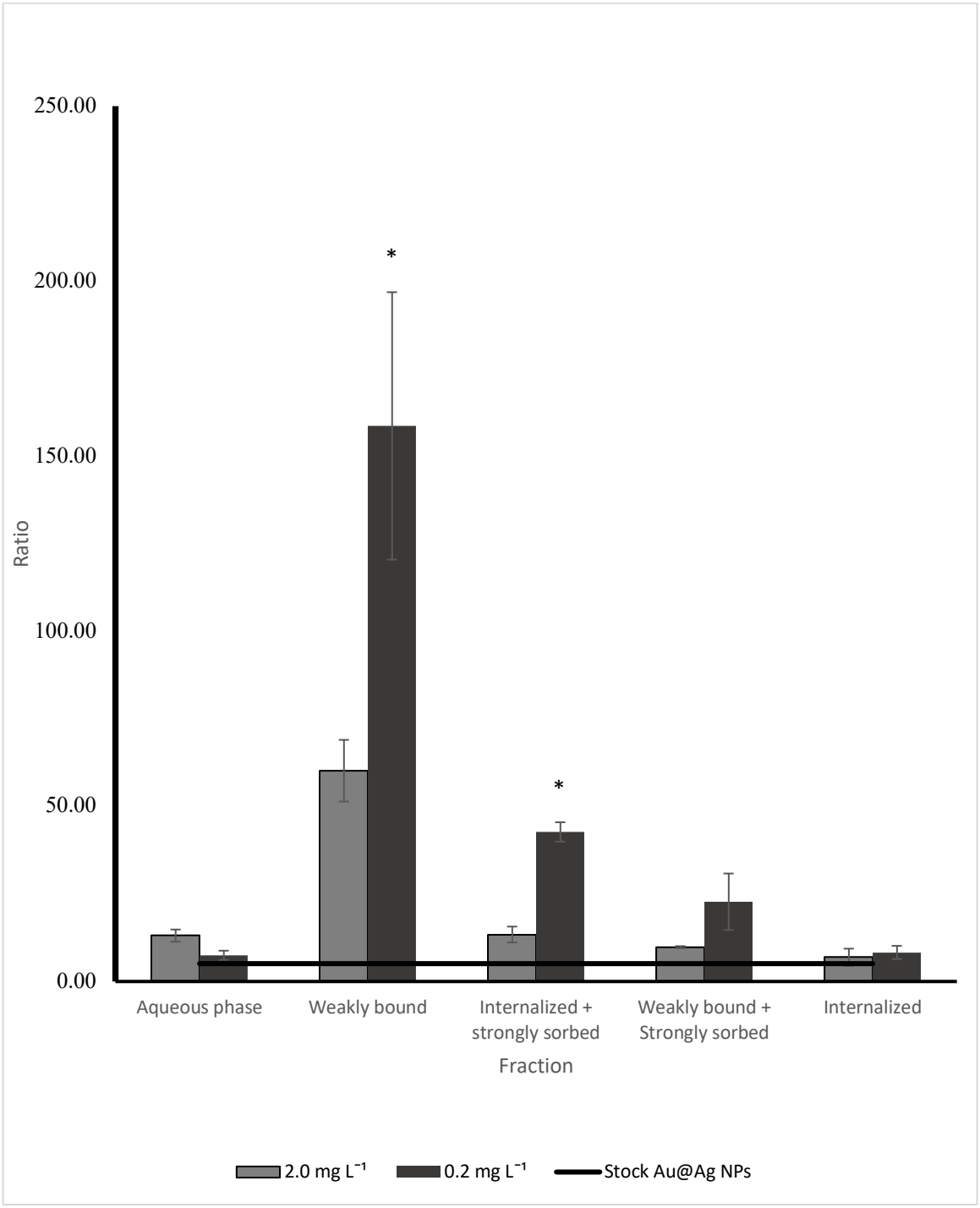

Figure 3.8 Ag:Au molar ratios in bacterial different fractions. The stock Au@Ag NPs Ag:Au ratio is indicated as a straight horizontal line at a value of 5.1. Each bar represents the average of three replicates. Error bars represent standard deviation. The asterisk denotes significantly different ratio from the pristine NPs ratio at significance level p <0.05*.

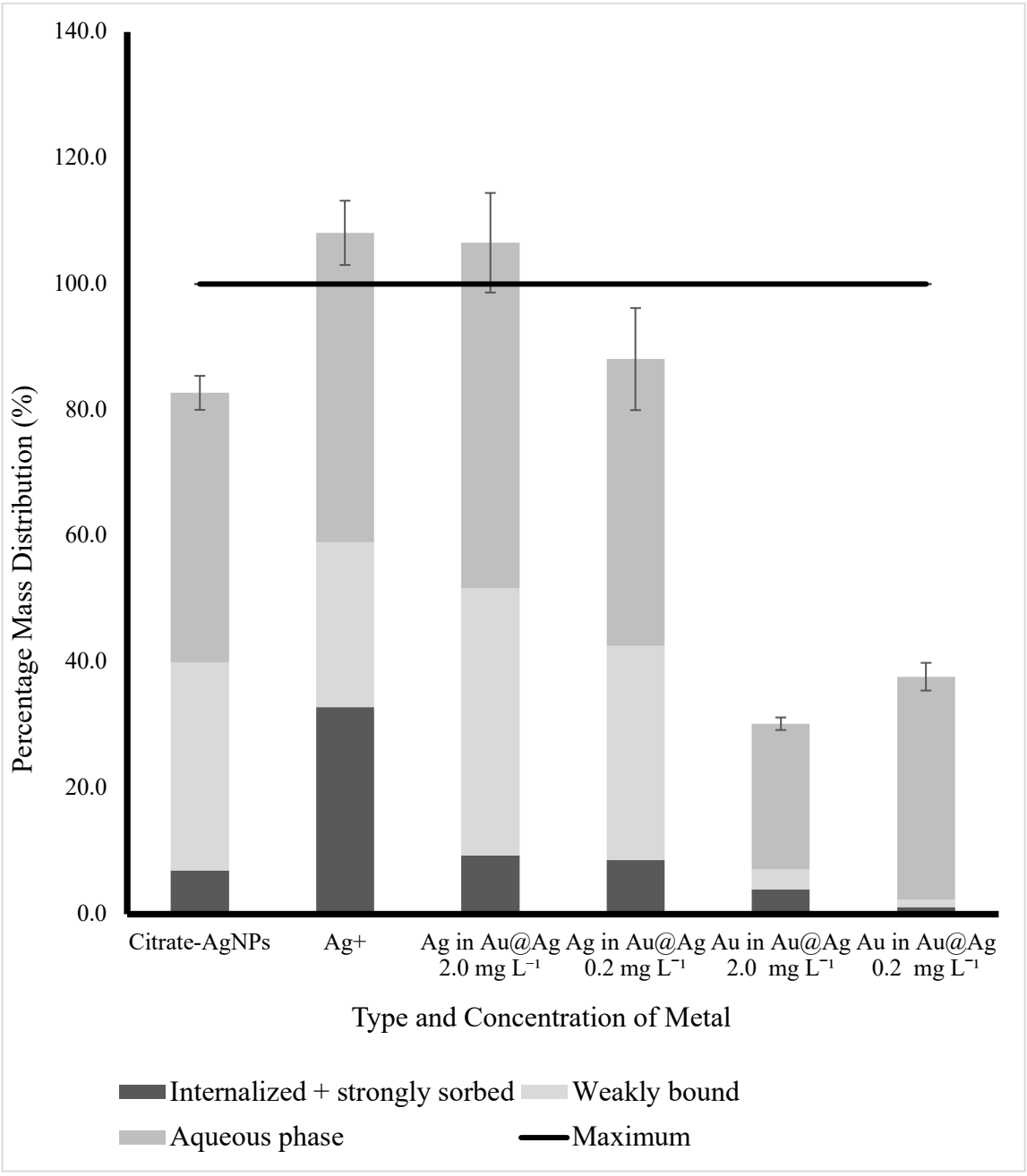

Figure 3.9 Percentage of metals mass distribution before periplasm removal. The original exposure concentration percent is indicated as a straight horizontal line at a value of 100%. Each bar represents the average of three replicates. Error bars represent standard deviation. (Note that internalized and strongly sorbed are combined).

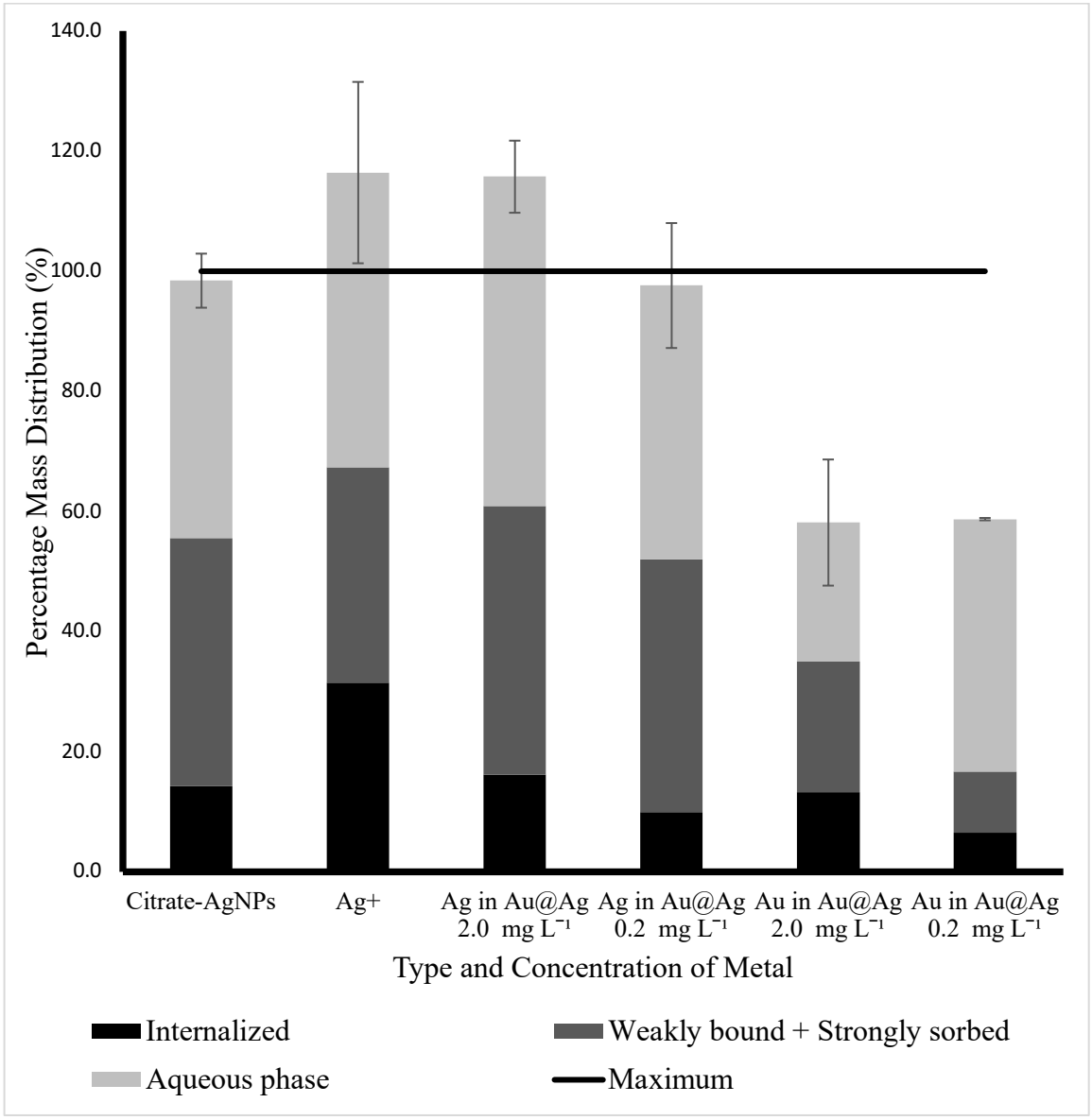

Figure 3.10 Percentage of metals mass distribution after periplasm removal. The original exposure concentration percent is indicated as a straight horizontal line at a value of 100%. Each bar represents the average of three replicates. Error bars represent standard deviation. (Note that weakly bound and strongly sorbed are combined).

CHAPTER 4

CONCLUSION

Bacteria are monocellular yet highly sophisticated and adaptable microorganisms. Their remarkable capacity to adapt stresses and develop resistance against antibiotics resulted in the emergence of MDR. Multiple bacterial mechanisms may contribute to the development of resistance against conventional antimicrobial agents such as alteration in drug target and modifying membrane fluidity and permeability. Although MDR is challenging to treat, the rapidly growing field of nanotechnology could be the solution through utilizing NPs tunable properties. Materials at nanoscale can acquire novel properties as a result of quantum size effect and high specific surface area.

Nanotechnology offers a wide range of revolutionary applications in variety of scientific fields. Particularly, AgNPs were the most studied NPs as a potent broad-spectrum antimicrobial agent that bacteria are less likely to develop resistance against. However, interaction between AgNPs and bacteria is complex and yet to be fully elucidated. Physiochemical properties of AgNPs and exposure media composition determine the ultimate outcome of the interactions. Developing an understanding to the mechanisms of interaction and the role of NPs transformations in AgNPs antimicrobial activity is essential for their potential utilization in medical field. However, this is limited by the combination of the complexity of exposure systems, lack of standardized analytical methods and limitations of current analytical techniques.

In this work, a novel method was developed and validated to separate and quantify AgNPs distribution in different bacterial compartments (*i.e.,* internalized, strongly sorbed, and weakly bound to the external surface of the cell). EDTA, a metal chelator, was applied to specifically binds to the divalent cations that stabilize bacterial outer membrane. Therefore, at the optimal treatment conditions, EDTA will only remove the bacterial

periplasm (*i.e.,* outer cell membrane, cell wall, surface-sorbed-NPs, and NPs contained within this space) of Gram-negative bacterium *P. aeruginosa*, without significantly influencing cells inner membrane integrity.

The validation process was conducted using multimethod approach to falsify our hypothesis of EDTA effect under appropriate treatment condition. Treating cells with 50 mM EDTA for two hours consistently suggested that our proposed method is accurately differentiating and approximating the amount of Ag accumulated over external bacterial surface and/or internalized into bacterial cytoplasm. However, multiple Ag species could accumulate within each fraction.

AgNPs readily undergo dynamic physiochemical transformation and speciation in exposure media. The capability of currently available analytical techniques to differentiate the relative role of AgNPs and Ag^+ in biouptake and bioaccumulation is limited. As a result, it is still not very clear which Ag species is more bioavailable. To better assess that, the previously validated method was applied to quantify Ag:Au distribution after exposing bacterial strain to core-shell NPs, Au@Ag. The Au core in the bimetallic Au@Ag NPs was used as an internal standard due to its relatively higher stability (*i.e.,* remains in particulate form throughout exposure) compared to Ag shell.

Data obtained suggested a remarkable influence of concentration on AgNPs transformations and bioavailability. At lower concentrations, Ag was in a dissolution-dominant process and relatively more bioavailable to be taken up by the microorganism. AgNPs at higher concentrations tend to aggregate and deposit at the bottom of the exposure tube. As particles get larger, their specific surface area gets smaller. Therefore, deposited

particles lower bioavailability might be attributed to that NPs aggregates tend to have smaller specific surface area and deposit away from direct interaction with the organism.

Bacterial cell external surface was Ag-enriched mainly with dissolved Ag whereas various Ag species appeared to make their way to the inside of bacterial cytoplasm. The weight of evidence in this work suggests multiple cellular targets of AgNPs and other Ag species that resulted from AgNPs transformations in exposure system. This multi-target action of AgNPs further support the view of AgNPs promising potential in overcoming MDR bacterial infections. However, uncertainty regarding AgNPs cytotoxicity and the exact mechanism of action remains a major impediment to scientific progress in AgNPs applications.

While this chemical extraction method was successfully validated for *P. aeruginosa* exposed to AgNPs, applying it to another microorganism or using another NPs may require further validation. We recommend applying it to a range of Gram-negative bacteria and NPs with different physiochemical characteristics to increase its external validity. Furthermore, applying the method in another exposure system that simulates the complex composition of human body will further improve its applicability and generalizability.

REFERENCES

1. Logothetidis, S., *Nanotechnology in medicine: the medicine of tomorrow and nanomedicine.* Hippokratia, 2006. **10**(1): p. 7-21.
2. Abbasi, E., et al., *Silver nanoparticles: Synthesis methods, bio-applications and properties.* Crit Rev Microbiol, 2016. **42**(2): p. 173-80.
3. Khan, I., K. Saeed, and I. Khan, *Nanoparticles: Properties, applications and toxicities.* Arabian Journal of Chemistry, 2019. **12**(7): p. 908-931.
4. Feynman, R., *Engineering & Science Magazine.* California Institute of Technology, USA, 1960.
5. Benelmekki, M., *An introduction to nanoparticles and nanotechnology.* Designing Hybrid Nanoparticles, 2015.
6. Cao, X.F., et al., *Improved metal remediation using a combined bacterial and nanoscience approach.* Science of the Total Environment, 2020. **704**.
7. Aguilar, Z.P., *Nanomaterials for Medical Applications.* Nanomaterials for Medical Applications, 2013: p. 1-461.
8. Nagarajan, R., *Nanoparticles: building blocks for nanotechnology*. 2008, ACS Publications.
9. EU. *Definition of a nanomaterial*. European Commission 2011 November/22/2017; Available from: http://ec.europa.eu/environment/chemicals/nanotech/faq/definition_en.htm.
10. Alabresm, A., et al., *Use of PVP-coated magnetite nanoparticles to ameliorate oil toxicity to an estuarine meiobenthic copepod and stimulate the growth of oildegrading bacteria.* Environmental Science-Nano, 2017. **4**(9): p. 1859-1865.
11. Medina, C., et al., *Nanoparticles: pharmacological and toxicological significance.* Br J Pharmacol, 2007. **150**(5): p. 552-8.
12. Sperling, R.A. and W.J. Parak, *Surface modification, functionalization and bioconjugation of colloidal inorganic nanoparticles.* Philosophical Transactions of the Royal Society a-Mathematical Physical and Engineering Sciences, 2010. **368**(1915): p. 1333-1383.
13. Canfarotta, F., M.J. Whitcombe, and S.A. Piletsky, *Polymeric nanoparticles for optical sensing.* Biotechnology Advances, 2013. **31**(8): p. 1585-1599.
14. Ventola, C.L., *Progress in Nanomedicine: Approved and Investigational Nanodrugs.* P T, 2017. **42**(12): p. 742-755.
15. Duncan, R., et al., *ESF scientific forward look on nanomedicine.* European Science Foundation Policy Briefing, 2005: p. 1-6.
16. Auria-Soro, C., et al., *Interactions of Nanoparticles and Biosystems: Microenvironment of Nanoparticles and Biomolecules in Nanomedicine.* Nanomaterials (Basel), 2019. **9**(10).
17. Doroudian, M., et al., *Nanotechnology based therapeutics for lung disease.* Thorax, 2019. **74**(10): p. 965-976

18. Kumar, S., et al., *Carbohydrate-Coated Gold-Silver Nanoparticles for Efficient Elimination of Multidrug Resistant Bacteria and in Vivo Wound Healing.* Acs Applied Materials & Interfaces, 2019. **11**(46): p. 42998-43017.
19. Thambiraj, S., S. Hema, and D.R. Shankaran, *An Overview on Applications of Gold Nanoparticle for Early Diagnosis and Targeted Drug Delivery to Prostate Cancer.* Recent Patents on Nanotechnology, 2018. **12**(2): p. 110-131.
20. Kim, J., et al., *Use of Nanoparticle Contrast Agents for Cell Tracking with Computed Tomography.* Bioconjugate Chemistry, 2017. **28**(6): p. 1581-1597.
21. Kim, B.Y., J.T. Rutka, and W.C. Chan, *Nanomedicine.* New England Journal of Medicine, 2010. **363**(25): p. 2434-2443.
22. Silhavy, T.J., D. Kahne, and S. Walker, *The Bacterial Cell Envelope.* Cold Spring Harbor Perspectives in Biology, 2010. **2**(5).
23. Auer, G.K. and D.B. Weibel, *Bacterial Cell Mechanics.* Biochemistry, 2017. **56**(29): p. 3710-3724.
24. Clifton, L.A., et al., *Effect of Divalent Cation Removal on the Structure of Gram-Negative Bacterial Outer Membrane Models.* Langmuir, 2015. **31**(1): p. 404-412.
25. Huang, G.C., et al., *Interaction between bacterial cell membranes and nano-TiO2 revealed by two-dimensional FTIR correlation spectroscopy using bacterial ghost as a model cell envelope.* Water Research, 2017. **118**: p. 104-113.
26. Raviv, U., *Interacting Bacteria Surfaces.* Biophysical Journal, 2018. **114**(7): p. 1515-1517.
27. Cockayne, A., *Bacterial cell walls.* 1998.
28. Vollmer, W., D. Blanot, and M.A. de Pedro, *Peptidoglycan structure and architecture.* FEMS Microbiol Rev, 2008. **32**(2): p. 149-67.
29. Piddock, L.J.V., *Understanding drug resistance will improve the treatment of bacterial infections.* Nat Rev Microbiol, 2017. **15**(11): p. 639-640.
30. Slavin, Y.N., et al., *Metal nanoparticles: understanding the mechanisms behind antibacterial activity.* Journal of Nanobiotechnology, 2017. **15**.
31. Kapoor, G., S. Saigal, and A. Elongavan, *Action and resistance mechanisms of antibiotics: A guide for clinicians.* J Anaesthesiol Clin Pharmacol, 2017. **33**(3): p. 300-305.
32. Sultan, I., et al., *Antibiotics, Resistome and Resistance Mechanisms: A Bacterial Perspective.* Front Microbiol, 2018. **9**: p. 2066.
33. Santajit, S. and N. Indrawattana, *Mechanisms of Antimicrobial Resistance in ESKAPE Pathogens.* Biomed Research International, 2016.
34. Perovic, S., G. Veinovic, and J. Antic Stankovic, *A Review on Antibiotic Resistance: Origin and Mechanisms of Bacterial Resistance as Biological Phenomenon.* Genetika-Belgrade, 2018. **50**(3): p. 1123-1135.
35. Dodd, M.C., *Potential impacts of disinfection processes on elimination and deactivation of antibiotic resistance genes during water and wastewater treatment.* Journal of Environmental Monitoring, 2012. **14**(7): p. 1754-1771.
36. Domingues, S., G.J. da Silva, and K.M. Nielsen, *Integrons: Vehicles and pathways for horizontal dissemination in bacteria.* Mob Genet Elements, 2012. **2**(5): p. 211-223.
37. Dufour, D., V. Leung, and C.M. Lévesque, *Bacterial biofilm: structure, function, and antimicrobial resistance.* Endodontic Topics, 2010. **22**(1): p. 2-16.

38. Hall-Stoodley, L., J.W. Costerton, and P. Stoodley, *Bacterial biofilms: From the natural environment to infectious diseases.* Nature Reviews Microbiology, 2004. **2**(2): p. 95-108.
39. Donlan, R.M., *Role of biofilms in antimicrobial resistance.* Asaio Journal, 2000. **46**(6): p. S47-S52.
40. Ikuma, K., A.W. Decho, and B.L.T. Lau, *When nanoparticles meet biofilms-interactions guiding the environmental fate and accumulation of nanoparticles.* Frontiers in Microbiology, 2015. **6**.
41. Khameneh, B., et al., *Breakthroughs in bacterial resistance mechanisms and the potential ways to combat them.* Microbial Pathogenesis, 2016. **95**: p. 32-42.
42. Foster, T.J., *Antibiotic resistance in Staphylococcus aureus. Current status and future prospects.* FEMS Microbiol Rev, 2017. **41**(3): p. 430-449.
43. Sandoval-Motta, S. and M. Aldana, *Adaptive resistance to antibiotics in bacteria: a systems biology perspective.* Wiley Interdiscip Rev Syst Biol Med, 2016. **8**(3): p. 253-67.
44. Worthington, R.J. and C. Melander, *Combination approaches to combat multidrug-resistant bacteria.* Trends Biotechnol, 2013. **31**(3): p. 177-84.
45. Wang, L., C. Hu, and L. Shao, *The antimicrobial activity of nanoparticles: present situation and prospects for the future.* Int J Nanomedicine, 2017. **12**: p. 1227-1249.
46. Seil, J.T. and T.J. Webster, *Antimicrobial applications of nanotechnology: methods and literature.* Int J Nanomedicine, 2012. **7**: p. 2767-81.
47. Guo, B.L., et al., *The Antibacterial Activity of Ta-doped ZnO Nanoparticles.* Nanoscale Res Lett, 2015. **10**(1): p. 1047.
48. Wang, G.M., et al., *Antibacterial effects of titanium embedded with silver nanoparticles based on electron-transfer-induced reactive oxygen species.* Biomaterials, 2017. **124**: p. 25-34.
49. Shi, L.E., et al., *Synthesis, antibacterial activity, antibacterial mechanism and food applications of ZnO nanoparticles: a review.* Food Addit Contam Part A Chem Anal Control Expo Risk Assess, 2014. **31**(2): p. 173-86.
50. Vallet-Regi, M., B. Gonzalez, and I. Izquierdo-Barba, *Nanomaterials as Promising Alternative in the Infection Treatment.* Int J Mol Sci, 2019. **20**(15).
51. Huh, A.J. and Y.J. Kwon, *"Nanoantibiotics": A new paradigm for treating infectious diseases using nanomaterials in the antibiotics resistant era.* Journal of Controlled Release, 2011. **156**(2): p. 128-145.
52. Prabhu, S. and E.K. Poulose, *Silver nanoparticles: mechanism of antimicrobial action, synthesis, medical applications, and toxicity effects.* International nano letters, 2012. **2**(1): p. 32.
53. Azam, A., et al., *Antimicrobial activity of metal oxide nanoparticles against Gram-positive and Gram-negative bacteria: a comparative study.* International Journal of Nanomedicine, 2012. **7**: p. 6003-6009.
54. Dos Santos, C.A., et al., *Silver Nanoparticles: Therapeutical Uses, Toxicity, and Safety Issues.* Journal of Pharmaceutical Sciences, 2014. **103**(7): p. 1931-1944.
55. Gao, W.W., et al., *Nanoparticle approaches against bacterial infections.* Wiley Interdisciplinary Reviews-Nanomedicine and Nanobiotechnology, 2014. **6**(6): p. 532-547.

56. Armentano, I., et al., *The Interaction of Bacteria with Engineered Nanostructured Polymeric Materials: A Review.* Scientific World Journal, 2014.
57. Li, H.H., et al., *Enhancing the antimicrobial activity of natural extraction using the synthetic ultrasmall metal nanoparticles.* Scientific Reports, 2015. **5**.
58. Luan, B.Q., T. Huynh, and R.H. Zhou, *Complete wetting of graphene by biological lipids.* Nanoscale, 2016. **8**(10): p. 5750-5754.
59. Anaya, N.M., et al., *Comparative study between chemostat and batch reactors to quantify membrane permeability changes on bacteria exposed to silver nanoparticles.* Sci Total Environ, 2016. **565**: p. 841-848.
60. Zhang, Y., N. Kohler, and M. Zhang, *Surface modification of superparamagnetic magnetite nanoparticles and their intracellular uptake.* Biomaterials, 2002. **23**(7): p. 1553-61.
61. Stoimenov, P.K., et al., *Metal oxide nanoparticles as bactericidal agents.* Langmuir, 2002. **18**(17): p. 6679-6686.
62. Karakoti, A.S., L.L. Hench, and S. Seal, *The potential toxicity of nanomaterials - The role of surfaces.* Jom, 2006. **58**(7): p. 77-82.
63. Sirelkhatim, A., et al., *Review on Zinc Oxide Nanoparticles: Antibacterial Activity and Toxicity Mechanism.* Nanomicro Lett, 2015. **7**(3): p. 219-242.
64. Nakamura, S., et al., *Synthesis and Application of Silver Nanoparticles (Ag NPs) for the Prevention of Infection in Healthcare Workers.* Int J Mol Sci, 2019. **20**(15).
65. Halliwell, B. and C.E. Cross, *Oxygen-derived species: their relation to human disease and environmental stress.* Environ Health Perspect, 1994. **102 Suppl 10**: p. 5-12.
66. Dharmaraja, A.T., *Role of Reactive Oxygen Species (ROS) in Therapeutics and Drug Resistance in Cancer and Bacteria.* Journal of Medicinal Chemistry, 2017. **60**(8): p. 3221-3240.
67. Abdal Dayem, A., et al., *The Role of Reactive Oxygen Species (ROS) in the Biological Activities of Metallic Nanoparticles.* Int J Mol Sci, 2017. **18**(1).
68. Fu, P.P., et al., *Mechanisms of nanotoxicity: generation of reactive oxygen species.* J Food Drug Anal, 2014. **22**(1): p. 64-75.
69. Halliwell, B., *Reactive species and antioxidants. Redox biology is a fundamental theme of aerobic life.* Plant Physiol, 2006. **141**(2): p. 312-22.
70. Wang, D., et al., *Quantitative Analysis of Reactive Oxygen Species Photogenerated on Metal Oxide Nanoparticles and Their Bacteria Toxicity: The Role of Superoxide Radicals.* Environ Sci Technol, 2017. **51**(17): p. 10137-10145.
71. Arakha, M., et al., *Antimicrobial activity of iron oxide nanoparticle upon modulation of nanoparticle-bacteria interface.* Sci Rep, 2015. **5**: p. 14813.
72. Quinteros, M.A., et al., *Oxidative stress generation of silver nanoparticles in three bacterial genera and its relationship with the antimicrobial activity.* Toxicol In Vitro, 2016. **36**: p. 216-223.
73. Kobayashi, R.K.T., et al., *Chapter 6 - Metallic nanoparticles as a potential antimicrobial for catheters and prostheses*, in *Materials for Biomedical Engineering*, A.-M. Holban and A.M. Grumezescu, Editors. 2019, Elsevier. p. 153-196.

74. Shankar, S. and J.W. Rhim, *Facile approach for large-scale production of metal and metal oxide nanoparticles and preparation of antibacterial cotton pads.* Carbohydr Polym, 2017. **163**: p. 137-145.
75. Xie, Y., et al., *Antibacterial activity and mechanism of action of zinc oxide nanoparticles against Campylobacter jejuni.* Appl Environ Microbiol, 2011. **77**(7): p. 2325-31.
76. Moniri Javadhesari, S., et al., *Antibacterial activity of ultra-small copper oxide (II) nanoparticles synthesized by mechanochemical processing against S. aureus and E. coli.* Mater Sci Eng C Mater Biol Appl, 2019. **105**: p. 110011.
77. Badetti, E., et al., *Interaction between Copper Oxide Nanoparticles and Amino Acids: Influence on the Antibacterial Activity.* Nanomaterials (Basel), 2019. **9**(5).
78. Meroni, G., J.F. Soares Filipe, and P.A. Martino, *In Vitro Antibacterial Activity of Biological-Derived Silver Nanoparticles: Preliminary Data.* Vet Sci, 2020. **7**(1).
79. Shaikh, S., et al., *Mechanistic Insights into the Antimicrobial Actions of Metallic Nanoparticles and Their Implications for Multidrug Resistance.* Int J Mol Sci, 2019. **20**(10).
80. Kittler, S., et al., *Toxicity of silver nanoparticles increases during storage because of slow dissolution under release of silver ions.* Chemistry of Materials, 2010. **22**(16): p. 4548-4554.
81. Shen, M., et al., *Antibacterial applications of metal–organic frameworks and their composites.* Comprehensive Reviews in Food Science and Food Safety, 2020. **n/a**(n/a).
82. McQuillan, J.S., et al., *Silver nanoparticle enhanced silver ion stress response in Escherichia coli K12.* Nanotoxicology, 2012. **6**: p. 857-66.
83. Li, W.R., et al., *Antibacterial activity and mechanism of silver nanoparticles on Escherichia coli.* Appl Microbiol Biotechnol, 2010. **85**(4): p. 1115-22.
84. Chen, M., et al., *Antimicrobial activity and the mechanism of silver nanoparticle thermosensitive gel.* Int J Nanomedicine, 2011. **6**: p. 2873-7.
85. Ramalingam, B., T. Parandhaman, and S.K. Das, *Antibacterial Effects of Biosynthesized Silver Nanoparticles on Surface Ultrastructure and Nanomechanical Properties of Gram-Negative Bacteria viz. Escherichia coli and Pseudomonas aeruginosa.* Acs Applied Materials & Interfaces, 2016. **8**(7): p. 4963-4976.
86. Das, B., et al., *Green synthesized silver nanoparticles destroy multidrug resistant bacteria via reactive oxygen species mediated membrane damage.* Arabian Journal of Chemistry, 2017. **10**(6): p. 862-876.
87. Bellio, P., et al., *Cerium oxide nanoparticles as potential antibiotic adjuvant. Effects of CeO2 nanoparticles on bacterial outer membrane permeability.* Biochimica Et Biophysica Acta-Biomembranes, 2018. **1860**(11): p. 2428-2435.
88. Bondarenko, O.M., et al., *Plasma membrane is the target of rapid antibacterial action of silver nanoparticles in Escherichia coli and Pseudomonas aeruginosa.* International Journal of Nanomedicine, 2018. **13**: p. 6779-6790.
89. Jayawardena, H.S.N., et al., *Maltoheptaose promotes nanoparticle internalization by Escherichia coli.* Chemical Communications, 2013. **49**(29): p. 3034-3036.

90. Ali, K., et al., *Aloe vera extract functionalized zinc oxide nanoparticles as nanoantibiotics against multi-drug resistant clinical bacterial isolates.* Journal of Colloid and Interface Science, 2016. **472**: p. 145-156.
91. Leung, Y.H., et al., *Transmission electron microscopy artifacts in characterization of the nanomaterial-cell interactions.* Applied Microbiology and Biotechnology, 2017. **101**(13): p. 5469-5479.
92. Kumar, M., et al., *Insights into cell penetrating peptide conjugated gold nanoparticles for internalization into bacterial cells.* Biophysical Chemistry, 2018. **237**: p. 38-46.
93. Lesniak, A., et al., *Nanoparticle adhesion to the cell membrane and its effect on nanoparticle uptake efficiency.* J Am Chem Soc, 2013. **135**(4): p. 1438-44.
94. Lai, L., et al., *Adhesion of quantum dots-induced membrane damage of Escherichia coli.* J Colloid Interface Sci, 2013. **389**(1): p. 61-70.
95. Kumar, A., et al., *Cellular uptake and mutagenic potential of metal oxide nanoparticles in bacterial cells.* Chemosphere, 2011. **83**(8): p. 1124-32.
96. Hayden, S.C., et al., *Aggregation and interaction of cationic nanoparticles on bacterial surfaces.* J Am Chem Soc, 2012. **134**(16): p. 6920-3.
97. Berry, V., et al., *Deposition of CTAB-terminated nanorods on bacteria to form highly conducting hybrid systems.* J Am Chem Soc, 2005. **127**(50): p. 17600-1.
98. Deschenes, L. and T. Ells, *Bacteria-nanoparticle interactions in the context of nanofouling.* Adv Colloid Interface Sci, 2020. **277**: p. 102106.
99. Dinh, N.X., et al., *Water-dispersible silver nanoparticles-decorated carbon nanomaterials: synthesis and enhanced antibacterial activity.* Applied Physics a-Materials Science & Processing, 2015. **119**(1): p. 85-95.
100. Huang, T., et al., *Engineering highly effective antimicrobial selenium nanoparticles through control of particle size.* Nanoscale, 2019. **11**(31): p. 14937-14951.
101. Truong, V., et al., *Synergistic Antibacterial Activity of Silver-Loaded Graphene Oxide towards Staphylococcus Aureus and Escherichia Coli.* Nanomaterials (Basel), 2020. **10**(2).
102. Ruddaraju, L.K., et al., *A review on anti-bacterials to combat resistance: From ancient era of plants and metals to present and future perspectives of green nano technological combinations.* Asian Journal of Pharmaceutical Sciences, 2019.
103. Dadfar, S.M., et al., *Iron oxide nanoparticles: Diagnostic, therapeutic and theranostic applications.* Advanced Drug Delivery Reviews, 2019. **138**: p. 302-325.
104. Lombardo, D., M.A. Kiselev, and M.T. Caccamo, *Smart Nanoparticles for Drug Delivery Application: Development of Versatile Nanocarrier Platforms in Biotechnology and Nanomedicine.* Journal of Nanomaterials, 2019.
105. Baetke, S.C., T. Lammers, and F. Kiessling, *Applications of nanoparticles for diagnosis and therapy of cancer.* Br J Radiol, 2015. **88**(1054): p. 20150207.
106. Caster, J.M., et al., *Investigational nanomedicines in 2016: a review of nanotherapeutics currently undergoing clinical trials.* Wiley Interdiscip Rev Nanomed Nanobiotechnol, 2017. **9**(1).

107. Patravale, V., P. Dandekar, and R. Jain, *Nanoparticulate Drug Delivery: Perspectives on the Transition from Laboratory to Market.* Nanoparticulate Drug Delivery: Perspectives on the Transition from Laboratory to Market, 2012(17): p. 1-229.
108. Min, Y., et al., *Clinical Translation of Nanomedicine.* Chem Rev, 2015. **115**(19): p. 11147-90.
109. Van Norman, G.A., *Drugs, devices, and the FDA: Part 1: an overview of approval processes for drugs.* JACC: Basic to Translational Science, 2016. **1**(3): p. 170-179.
110. Chen, F., E.B. Ehlerding, and W. Cai, *Theranostic nanoparticles.* J Nucl Med, 2014. **55**(12): p. 1919-22.
111. Ding, X., et al., *Au-Ag core-shell nanoparticles for simultaneous bacterial imaging and synergistic antibacterial activity.* Nanomedicine-Nanotechnology Biology and Medicine, 2017. **13**(1): p. 297-305.
112. Yuan, P., et al., *Plasmon coupling-enhanced two-photon photoluminescence of Au@Ag core-shell nanoparticles and applications in the nuclease assay.* Nanoscale, 2015. **7**(22): p. 10233-9.
113. Michalet, X., et al., *Quantum dots for live cells, in vivo imaging, and diagnostics.* Science, 2005. **307**(5709): p. 538-44.
114. Buss, C.G., et al., *Protease activity sensors noninvasively classify bacterial infections and antibiotic responses.* EBioMedicine, 2018. **38**: p. 248-256.
115. Taymaz, T., et al., *Significance of the detection of influenza and other respiratory viruses for antibiotic stewardship: Lessons from the post-pandemic period.* Int J Infect Dis, 2018. **77**: p. 53-56.
116. Iregui, M., et al., *Clinical importance of delays in the initiation of appropriate antibiotic treatment for ventilator-associated pneumonia.* Chest, 2002. **122**(1): p. 262-8.
117. Caliendo, A.M., et al., *Better tests, better care: improved diagnostics for infectious diseases.* Clin Infect Dis, 2013. **57 Suppl 3**: p. S139-70.
118. Leekha, S., C.L. Terrell, and R.S. Edson, *General Principles of Antimicrobial Therapy.* Mayo Clinic Proceedings, 2011. **86**(2): p. 156-167.
119. Zimdahl, R.L., *Antibiotics.* Six Chemicals That Changed Agriculture, 2015: p. 165-182.
120. Ventola, C.L., *The antibiotic resistance crisis: part 1: causes and threats.* Pharmacy and therapeutics, 2015. **40**(4): p. 277.
121. Gupta, A., et al., *Combatting antibiotic-resistant bacteria using nanomaterials.* Chemical Society Reviews, 2019. **48**(2): p. 415-427.
122. Rai, M.K., et al., *Silver nanoparticles: the powerful nanoweapon against multidrug-resistant bacteria.* Journal of Applied Microbiology, 2012. **112**(5): p. 841-852.
123. Khan, M.H., S. Unnikrishnan, and K. Ramalingam, *Bactericidal potential of silver-tolerant bacteria derived silver nanoparticles against multi drug resistant ESKAPE pathogens.* Biocatalysis and Agricultural Biotechnology, 2019. **18**.
124. Mulani, M.S., et al., *Emerging Strategies to Combat ESKAPE Pathogens in the Era of Antimicrobial Resistance: A Review.* Front Microbiol, 2019. **10**: p. 539.

125. Percival, S.L., P.G. Bowler, and J. Dolman, *Antimicrobial activity of silver-containing dressings on wound microorganisms using an in vitro biofilm model.* International wound journal, 2007. **4**(2): p. 186-91.
126. Percival, S.L., et al., *Healthcare-associated infections, medical devices and biofilms: risk, tolerance and control.* J Med Microbiol, 2015. **64**(Pt 4): p. 323-34.
127. Khatoon, Z., et al., *Bacterial biofilm formation on implantable devices and approaches to its treatment and prevention.* Heliyon, 2018. **4**(12): p. e01067.
128. Ramasamy, M., J.H. Lee, and J. Lee, *Potent antimicrobial and antibiofilm activities of bacteriogenically synthesized gold-silver nanoparticles against pathogenic bacteria and their physiochemical characterizations.* Journal of Biomaterials Applications, 2016. **31**(3): p. 366-378.
129. De Giglio, E., et al., *An innovative, easily fabricated, silver nanoparticle-based titanium implant coating: development and analytical characterization.* Anal Bioanal Chem, 2013. **405**(2-3): p. 805-16.
130. Garino, N., et al., *Zinc oxide nanocrystals as a nanoantibiotic and osteoinductive agent.* RSC Adv, 2019. **9**(20): p. 11312-11321.
131. Mahamuni-Badiger, P.P., et al., *Biofilm formation to inhibition: Role of zinc oxide-based nanoparticles.* Materials Science and Engineering: C, 2019: p. 110319.
132. Tian, J., et al., *Topical delivery of silver nanoparticles promotes wound healing.* ChemMedChem, 2007. **2**(1): p. 129-36.
133. Hussain, S., et al., *Antibiotic-loaded nanoparticles targeted to the site of infection enhance antibacterial efficacy.* Nature Biomedical Engineering, 2018. **2**(2): p. 95-103.
134. Wang, Y., et al., *Targeted delivery of antibiotics to the infected pulmonary tissues using ROS-responsive nanoparticles.* Journal of Nanobiotechnology, 2019. **17**(1).
135. Luk, B.T. and L. Zhang, *Cell membrane-camouflaged nanoparticles for drug delivery.* J Control Release, 2015. **220**(Pt B): p. 600-7.
136. Mitragotri, S., P.A. Burke, and R. Langer, *Overcoming the challenges in administering biopharmaceuticals: formulation and delivery strategies.* Nat Rev Drug Discov, 2014. **13**(9): p. 655-72.
137. Mandal, T.K., *Swelling-controlled release system for the vaginal delivery of miconazole.* Eur J Pharm Biopharm, 2000. **50**(3): p. 337-43.
138. Gao, W.W., et al., *Nanoparticle-based local antimicrobial drug delivery.* Advanced Drug Delivery Reviews, 2018. **127**: p. 46-57.
139. Singh, R. and H.S. Nalwa, *Medical Applications of Nanoparticles in Biological Imaging, Cell Labeling, Antimicrobial Agents, and Anticancer Nanodrugs.* Journal of Biomedical Nanotechnology, 2011. **7**(4): p. 489-503.
140. Torchilin, V.P., *Multifunctional, stimuli-sensitive nanoparticulate systems for drug delivery.* Nat Rev Drug Discov, 2014. **13**(11): p. 813-27.
141. Sanvicens, N. and M.P. Marco, *Multifunctional nanoparticles - properties and prospects for their use in human medicine.* Trends in Biotechnology, 2008. **26**(8): p. 425-433.
142. Henry-Michelland, S., et al., *Attachment of antibiotics to nanoparticles: preparation, drug-release and antimicrobial activity in vitro.* International journal of pharmaceutics, 1987. **35**(1-2): p. 121-127.

143. Couvreur, P., et al., *Intracellular targeting of antibiotics by means of biodegradable nanoparticles.* Journal of controlled release, 1992. **19**(1-3): p. 259-267.
144. Fahmy, T.M., et al., *Design opportunities for actively targeted nanoparticle vaccines.* Nanomedicine, 2008. **3**(3): p. 343-355.
145. Irvine, D.J., et al., *Synthetic Nanoparticles for Vaccines and Immunotherapy.* Chem Rev, 2015. **115**(19): p. 11109-46.
146. Torres-Sangiao, E., A.M. Holban, and M.C. Gestal, *Advanced Nanobiomaterials: Vaccines, Diagnosis and Treatment of Infectious Diseases.* Molecules, 2016. **21**(7).
147. Zhao, L., et al., *Nanoparticle vaccines.* Vaccine, 2014. **32**(3): p. 327-37.
148. Dorosti, H., et al., *Designing self-assembled peptide nanovaccine against Streptococcus pneumoniae: An in silico strategy.* Mol Cell Probes, 2019. **48**: p. 101446.
149. Geho, D.H., et al., *Opportunities for nanotechnology-based innovation in tissue proteomics.* Biomed Microdevices, 2004. **6**(3): p. 231-9.
150. Bai, Y.L., et al., *A rapid method for the detection of foodborne pathogens by extraction of a trace amount of DNA from raw milk based on amino-modified silica-coated magnetic nanoparticles and polymerase chain reaction.* Analytica Chimica Acta, 2013. **787**: p. 93-101.
151. Donmez, M., M.D. Yilmaz, and B. Kilbas, *Fluorescent detection of dipicolinic acid as a biomarker of bacterial spores using lanthanide-chelated gold nanoparticles.* Journal of Hazardous Materials, 2017. **324**: p. 593-598.
152. Chen, H., et al., *Point of care testing for infectious diseases.* Clin Chim Acta, 2019. **493**: p. 138-147.
153. Aarestrup, F.M. and M.G. Koopmans, *Sharing Data for Global Infectious Disease Surveillance and Outbreak Detection.* Trends Microbiol, 2016. **24**(4): p. 241-245.
154. Sanger, P.C., et al., *A Prognostic Model of Surgical Site Infection Using Daily Clinical Wound Assessment.* Journal of the American College of Surgeons, 2016. **223**(2): p. 259-+.
155. Nishanth, A. and T. Thiruvaran, *Identifying Important Attributes for Early Detection of Chronic Kidney Disease.* IEEE Rev Biomed Eng, 2018. **11**: p. 208-216.
156. Fatima, A. and S.S.A. Zaidi, *The Need of NET Diagnostic Biomarkers for Early Detection and Targeted Management. Should Biomarkers Reflect Disease Progression?* Neuroendocrinology, 2019. **108**: p. 118-118.
157. Tao, Y., et al., *Metal nanoclusters: novel probes for diagnostic and therapeutic applications.* Chem Soc Rev, 2015. **44**(23): p. 8636-63.
158. Hu, Y., et al., *Nanodevices in diagnostics.* Wiley Interdiscip Rev Nanomed Nanobiotechnol, 2011. **3**(1): p. 11-32.
159. Huang, X., et al., *Gold nanoparticles: interesting optical properties and recent applications in cancer diagnostics and therapy.* Nanomedicine (Lond), 2007. **2**(5): p. 681-93.
160. Singh, P., et al., *Gold Nanoparticles in Diagnostics and Therapeutics for Human Cancer.* Int J Mol Sci, 2018. **19**(7).
161. Li, W. and X. Chen, *Gold nanoparticles for photoacoustic imaging.* Nanomedicine (Lond), 2015. **10**(2): p. 299-320.

162. un-Sheng Chen, W.F., Seungsoo Kim, Pieter Kruizinga, Kimberly Homan, and Stanislav Emelianov, *Silica-Coated Gold Nanorods as Photoacoustic Signal Nanoamplifiers.* Nano Letters, 2011. **11**(2): p. 348-354
163. Kim, T., et al., *A Gold/Silver Hybrid Nanoparticle for Treatment and Photoacoustic Imaging of Bacterial Infection.* ACS Nano, 2018. **12**(6): p. 5615-5625.
164. Klostranec, J.M., et al., *Convergence of quantum dot barcodes with microfluidics and signal processing for multiplexed high-throughput infectious disease diagnostics.* Nano Letters, 2007. **7**(9): p. 2812-2818.
165. Zhao, X.J., et al., *A rapid bioassay for single bacterial cell quantitation using bioconjugated nanoparticles.* Proceedings of the National Academy of Sciences of the United States of America, 2004. **101**(42): p. 15027-15032.
166. Xu, C., et al., *Applications of Iron Oxide-Based Magnetic Nanoparticles in the Diagnosis and Treatment of Bacterial Infections.* Front Bioeng Biotechnol, 2019. **7**: p. 141.
167. Jiang, C.J., et al., *Relative Contributions of Copper Oxide Nanoparticles and Dissolved Copper to Cu Uptake Kinetics of Gulf Killifish (Fundulus grandis) Embryos.* Environmental Science & Technology, 2017. **51**(3): p. 1395-1404.
168. Loureiro, S., et al., *Chapter 7 - Nanomaterials as Soil Pollutants*, in *Soil Pollution*, A.C. Duarte, A. Cachada, and T. Rocha-Santos, Editors. 2018, Academic Press. p. 161-190.
169. Millour, M., et al., *Does the bacterial media culture chemistry affect the stability of nanoparticles in nanotoxicity assays?* Journal of Xenobiotics, 2015. **5**(2): p. 34-36.
170. De Leersnyder, I., et al., *Influence of growth media components on the antibacterial effect of silver ions on Bacillus subtilis in a liquid growth medium.* Sci Rep, 2018. **8**(1): p. 9325.
171. Smekalova, M., et al., *Culture medium mediated aggregation and re-crystallization of silver nanoparticles reduce their toxicity.* Applied Materials Today, 2018. **12**: p. 198-206.
172. Behra, R., et al., *Bioavailability of silver nanoparticles and ions: from a chemical and biochemical perspective.* Journal of the Royal Society Interface, 2013. **10**(87).
173. von Moos, N., P. Bowen, and V.I. Slaveykova, *Bioavailability of inorganic nanoparticles to planktonic bacteria and aquatic microalgae in freshwater.* Environmental Science-Nano, 2014. **1**(3): p. 214-232.
174. Wu, W.H., et al., *Transformation and Speciation Analysis of Silver Nanoparticles of Dietary Supplement in Simulated Human Gastrointestinal Tract.* Environmental Science & Technology, 2018. **52**(15): p. 8792-8800.
175. El Badawy, A.M., et al., *Impact of Environmental Conditions (pH, Ionic Strength, and Electrolyte Type) on the Surface Charge and Aggregation of Silver Nanoparticles Suspensions.* Environmental Science & Technology, 2010. **44**(4): p. 1260-1266.
176. Guzman, M., J. Dille, and S. Godet, *Synthesis and antibacterial activity of silver nanoparticles against gram-positive and gram-negative bacteria.* Nanomedicine, 2012. **8**(1): p. 37-45.

177. El Badawy, A.M., et al., *The impact of stabilization mechanism on the aggregation kinetics of silver nanoparticles.* Science of the Total Environment, 2012. **429**: p. 325-331.
178. Baalousha, M., et al., *The concentration-dependent behaviour of nanoparticles.* Environmental Chemistry, 2016. **13**(1): p. 1-3.
179. Merrifield, R.C., C. Stephan, and J. Lead, *Determining the Concentration Dependent Transformations of Ag Nanoparticles in Complex Media: Using SP-ICP-MS and Au@Ag Core Shell Nanoparticles as Tracers.* Environmental Science & Technology, 2017. **51**(6): p. 3206-3213.
180. Pal, S., Y.K. Tak, and J.M. Song, *Does the antibacterial activity of silver nanoparticles depend on the shape of the nanoparticle? A study of the Gram-negative bacterium Escherichia coli.* Appl Environ Microbiol, 2007. **73**(6): p. 1712-20.
181. Wang, L., et al., *Morphology-dependent bactericidal activities of Ag/CeO2 catalysts against Escherichia coli.* J Inorg Biochem, 2014. **135**: p. 45-53.
182. Wu, M., et al., *Size-dependent cellular uptake and localization profiles of silver nanoparticles.* Int J Nanomedicine, 2019. **14**: p. 4247-4259.
183. Chambers, B.A., et al., *Effects of Chloride and Ionic Strength on Physical Morphology, Dissolution, and Bacterial Toxicity of Silver Nanoparticles.* Environmental Science & Technology, 2014. **48**(1): p. 761-769.
184. Levard, C., et al., *Effect of Chloride on the Dissolution Rate of Silver Nanoparticles and Toxicity to E. coli.* Environmental Science & Technology, 2013. **47**(11): p. 5738-5745.
185. Shannahan, J.H., et al., *Silver Nanoparticle Protein Corona Composition in Cell Culture Media.* Plos One, 2013. **8**(9).
186. Abo-Zeid, Y. and G.R. Williams, *The potential anti-infective applications of metal oxide nanoparticles: A systematic review.* Wiley Interdiscip Rev Nanomed Nanobiotechnol, 2019: p. e1592.
187. Stensberg, M.C., et al., *Toxicological studies on silver nanoparticles: challenges and opportunities in assessment, monitoring and imaging.* Nanomedicine (Lond), 2011. **6**(5): p. 879-98.
188. Rajeshkumar, S., L. Bharath, and R. Geetha, *Broad spectrum antibacterial silver nanoparticle green synthesis: Characterization, and mechanism of action*, in *Green Synthesis, Characterization and Applications of Nanoparticles*. 2019, Elsevier. p. 429-444.
189. Vishnupriya, S., et al., *Single-Cell Investigations of Silver Nanoparticle–Bacteria Interactions.* Particle & Particle Systems Characterization, 2013. **30**(12): p. 1056-1062.
190. Peck, C.C., et al., *Opportunities for Integration of Pharmacokinetics, Pharmacodynamics, and Toxicokinetics in Rational Drug Development.* Clinical Pharmacology & Therapeutics, 1992. **51**(4): p. 465-473.
191. Nix, D.E., *Toxicokinetics and Toxicodynamics of Anti-infective Agents.* Antibiotic Pharmacodynamics, 2016: p. 159-173.
192. Kumar, A., et al., *A flow cytometric method to assess nanoparticle uptake in bacteria.* Cytometry A, 2011. **79**(9): p. 707-12.

193. Ahmed, B., et al., *Bacterial toxicity of biomimetic green zinc oxide nanoantibiotic: insights into ZnONP uptake and nanocolloid-bacteria interface.* Toxicol Res (Camb), 2019. **8**(2): p. 246-261.
194. Lindfors, K., et al., *Detection and spectroscopy of gold nanoparticles using supercontinuum white light confocal microscopy.* Phys Rev Lett, 2004. **93**(3): p. 037401.
195. van Dijk, M.A., M. Lippitz, and M. Orrit, *Far-field optical microscopy of single metal nanoparticles.* Acc Chem Res, 2005. **38**(7): p. 594-601.
196. Chen, S., et al., *Avoiding artefacts during electron microscopy of silver nanomaterials exposed to biological environments.* J Microsc, 2016. **261**(2): p. 157-66.
197. Goodman, S.R., *Medical cell biology*. 2007: Academic Press.
198. Suzuki, K., *Characterisation of airborne particulates and associated trace metals deposited on tree bark by ICP-OES, ICP-MS, SEM-EDX and laser ablation ICP-MS.* Atmospheric Environment, 2006. **40**(14): p. 2626-2634.
199. Scimeca, M., et al., *Energy Dispersive X-ray (EDX) microanalysis: A powerful tool in biomedical research and diagnosis.* Eur J Histochem, 2018. **62**(1): p. 2841.
200. Mozhayeva, D. and C. Engelhard, *A critical review of single particle inductively coupled plasma mass spectrometry–A step towards an ideal method for nanomaterial characterization.* Journal of Analytical Atomic Spectrometry, 2020.
201. Pyrgiotakis, G., C.O. Blattmann, and P. Demokritou, *Real-Time Nanoparticle-Cell Interactions in Physiological Media by Atomic Force Microscopy.* ACS Sustain Chem Eng, 2014. **2**(7): p. 1681-1690.
202. Bulska, E. and B. Wagner, *Quantitative aspects of inductively coupled plasma mass spectrometry.* Philos Trans A Math Phys Eng Sci, 2016. **374**(2079).
203. Hu, J., et al., *Single nanoparticle analysis by ICPMS: a potential tool for bioassay.* Journal of Analytical Atomic Spectrometry, 2018. **33**(1): p. 57-67.
204. Kefayat, A., et al., *Alive attenuated Salmonella as a cargo shuttle for smart carrying of gold nanoparticles to tumour hypoxic regions.* Journal of Drug Targeting, 2019. **27**(3): p. 315-324.
205. Ramkorun-Schmidt, B., et al., *Investigation of a Combined Microdroplet Generator and Pneumatic Nebulization System for Quantitative Determination of Metal-Containing Nanoparticles Using ICPMS.* Analytical Chemistry, 2015. **87**(17): p. 8687-8694.
206. May, T.W. and R.H. Wiedmeyer, *A table of polyatomic interferences in ICP-MS.* ATOMIC SPECTROSCOPY-NORWALK CONNECTICUT-, 1998. **19**: p. 150-155.
207. Mitrano, D.M., et al., *Detecting nanoparticulate silver using single-particle inductively coupled plasma-mass spectrometry.* Environmental Toxicology and Chemistry, 2012. **31**(1): p. 115-121.
208. Montano, M.D., et al., *Single Particle ICP-MS: Advances toward routine analysis of nanomaterials.* Anal Bioanal Chem, 2016. **408**(19): p. 5053-74.
209. Laborda, F., E. Bolea, and J. Jimenez-Lamana, *Single particle inductively coupled plasma mass spectrometry for the analysis of inorganic engineered nanoparticles in environmental samples.* Trends in Environmental Analytical Chemistry, 2016. **9**: p. 15-23.

210. Qiu, T.A., et al., *Growth-Based Bacterial Viability Assay for Interference-Free and High-Throughput Toxicity Screening of Nanomaterials.* Anal Chem, 2017. **89**(3): p. 2057-2064.
211. Park, J.C., et al., *Effect of the size and shape of silver nanoparticles on bacterial growth and metabolism by monitoring optical density and fluorescence intensity.* Biotechnology and Bioprocess Engineering, 2017. **22**(2): p. 210-217.
212. Alavi, M., N. Karimi, and I. Salimikia, *phytosynthesis of zinc oxide nanoparticles and its antibacterial, antiquorum sensing, antimotility, and antioxidant capacities against multidrug resistant bacteria.* Journal of Industrial and Engineering Chemistry, 2019. **72**: p. 457-473.
213. Lyu, Y.B., et al., *Synthesis of silver nanoparticles using oxidized amylose and combination with curcumin for enhanced antibacterial activity.* Carbohydrate Polymers, 2020. **230**.
214. Wu, L., et al., *Silver nanoparticles inhibit denitrification by altering the viability and metabolic activity of Pseudomonas stutzeri.* Sci Total Environ, 2020. **706**: p. 135711.
215. Bankier, C., et al., *A comparison of methods to assess the antimicrobial activity of nanoparticle combinations on bacterial cells.* PLoS One, 2018. **13**(2): p. e0192093.
216. Han, C., et al., *Enzyme-encapsulating polymeric nanoparticles: A potential adjunctive therapy in Pseudomonas aeruginosa biofilm-associated infection treatment.* Colloids and Surfaces B: Biointerfaces, 2019. **184**: p. 110512.
217. Roth, B.L., et al., *Bacterial viability and antibiotic susceptibility testing with SYTOX green nucleic acid stain.* Appl Environ Microbiol, 1997. **63**(6): p. 2421-31.
218. Berney, M., et al., *Assessment and interpretation of bacterial viability by using the LIVE/DEAD BacLight Kit in combination with flow cytometry.* Appl Environ Microbiol, 2007. **73**(10): p. 3283-90.
219. Pfaller, M.A., et al., *Comparison of European Committee on Antimicrobial Susceptibility Testing (EUCAST) and Etest methods with the CLSI broth microdilution method for echinocandin susceptibility testing of Candida species.* J Clin Microbiol, 2010. **48**(5): p. 1592-9.
220. Egervarn, M., et al., *Effects of inoculum size and incubation time on broth microdilution susceptibility testing of lactic acid bacteria.* Antimicrob Agents Chemother, 2007. **51**(1): p. 394-6.
221. Luber, P., et al., *Comparison of broth microdilution, E Test, and agar dilution methods for antibiotic susceptibility testing of Campylobacter jejuni and Campylobacter coli.* J Clin Microbiol, 2003. **41**(3): p. 1062-8.
222. Woehl, T.J., et al., *Correlative Electron and Fluorescence Microscopy of Magnetotactic Bacteria in Liquid: Toward In Vivo Imaging.* Scientific Reports, 2014. **4**.
223. Myers, J.A., B.S. Curtis, and W.R. Curtis, *Improving accuracy of cell and chromophore concentration measurements using optical density.* Bmc Biophysics, 2013. **6**.
224. Sutton, S., *Accuracy of plate counts.* Journal of validation technology, 2011. **17**(3): p. 42-46.
225. Hazan, R., et al., *A method for high throughput determination of viable bacteria cell counts in 96-well plates.* Bmc Microbiology, 2012. **12**.

226. Martinez-Gutierrez, F., et al., *Synthesis, characterization, and evaluation of antimicrobial and cytotoxic effect of silver and titanium nanoparticles.* Nanomedicine, 2010. **6**(5): p. 681-8.
227. Perez-Diaz, M.A., et al., *Silver nanoparticles with antimicrobial activities against Streptococcus mutans and their cytotoxic effect.* Materials Science & Engineering C-Materials for Biological Applications, 2015. **55**: p. 360-366.
228. Li, M., L.Z. Zhu, and D.H. Lin, *Toxicity of ZnO Nanoparticles to Escherichia coli: Mechanism and the Influence of Medium Components.* Environmental Science & Technology, 2011. **45**(5): p. 1977-1983.
229. Simon-Deckers, A., et al., *Size-, composition- and shape-dependent toxicological impact of metal oxide nanoparticles and carbon nanotubes toward bacteria.* Environ Sci Technol, 2009. **43**(21): p. 8423-9.
230. Ren, G.G., et al., *Characterisation of copper oxide nanoparticles for antimicrobial applications.* International Journal of Antimicrobial Agents, 2009. **33**(6): p. 587-590.
231. Amiri, M., et al., *Antimicrobial Effect of Copper Oxide Nanoparticles on Some Oral Bacteria and Candida Species.* J Dent Biomater, 2017. **4**(1): p. 347-352.
232. Jiang, W., H. Mashayekhi, and B. Xing, *Bacterial toxicity comparison between nano- and micro-scaled oxide particles.* Environ Pollut, 2009. **157**(5): p. 1619-25.
233. Lipovsky, A., et al., *Antifungal activity of ZnO nanoparticles--the role of ROS mediated cell injury.* Nanotechnology, 2011. **22**(10): p. 105101.
234. Heinlaan, M., et al., *Toxicity of nanosized and bulk ZnO, CuO and TiO2 to bacteria Vibrio fischeri and crustaceans Daphnia magna and Thamnocephalus platyurus.* Chemosphere, 2008. **71**(7): p. 1308-1316.
235. Kubacka, A., et al., *Understanding the antimicrobial mechanism of TiO(2)-based nanocomposite films in a pathogenic bacterium.* Sci Rep, 2014. **4**: p. 4134.
236. Leung, Y.H., et al., *Toxicity of ZnO and TiO2 to Escherichia coli cells.* Sci Rep, 2016. **6**: p. 35243.
237. Meghana, S., et al., *Understanding the pathway of antibacterial activity of copper oxide nanoparticles.* Rsc Advances, 2015. **5**(16): p. 12293-12299.
238. Agarwala, M., B. Choudhury, and R.N. Yadav, *Comparative study of antibiofilm activity of copper oxide and iron oxide nanoparticles against multidrug resistant biofilm forming uropathogens.* Indian J Microbiol, 2014. **54**(3): p. 365-8.
239. Depelteau, J.S., S. Brenzinger, and A. Briegel, *Bacterial and Archaeal Cell Structure*, in *Encyclopedia of Microbiology (Fourth Edition)*, T.M. Schmidt, Editor. 2019, Academic Press: Oxford. p. 348-360.
240. MAURIN, M. *Antibiotics, antibiotic resistance and environment*. 2020 January 27, 2020]; Available from: https://www.encyclopedie-environnement.org/en/health/antibiotics-antibiotic-resistance-and-environment/.
241. Wyeth, J., *The importance of infection control in tackling the antimicrobial resistance crisis.* Br J Nurs, 2019. **28**(5): p. 284-286.
242. O'neill, J., *Antimicrobial resistance: tackling a crisis for the health and wealth of nations.* Rev. Antimicrob. Resist, 2014. **20**: p. 1-16.
243. Govindaraj Vaithinathan, A. and A. Vanitha, *WHO global priority pathogens list on antibiotic resistance: an urgent need for action to integrate One Health data.* Perspect Public Health, 2018. **138**(2): p. 87-88.

244. Tacconelli, E., et al., *Discovery, research, and development of new antibiotics: the WHO priority list of antibiotic-resistant bacteria and tuberculosis.* The Lancet Infectious Diseases, 2018. **18**(3): p. 318-327.
245. Care, D.f.H.a.S., *Tackling antimicrobial resistance 2019 to 2024*. 2019: The UK's 5-year action plan for antimicrobial resistance 2019 to 2024.
246. Rai, M., A. Yadav, and A. Gade, *Silver nanoparticles as a new generation of antimicrobials.* Biotechnology Advances, 2009. **27**(1): p. 76-83.
247. Franci, G., et al., *Silver Nanoparticles as Potential Antibacterial Agents.* Molecules, 2015. **20**(5): p. 8856-8874.
248. Alexander, J.W., *History of the Medical Use of Silver.* Surgical Infections, 2009. **10**(3): p. 289-292.
249. Dakal, T.C., et al., *Mechanistic Basis of Antimicrobial Actions of Silver Nanoparticles.* Front Microbiol, 2016. **7**: p. 1831.
250. Percival, S.L., P.G. Bowler, and D. Russell, *Bacterial resistance to silver in wound care.* J Hosp Infect, 2005. **60**(1): p. 1-7.
251. Maneerung, T., S. Tokura, and R. Rujiravanit, *Impregnation of silver nanoparticles into bacterial cellulose for antimicrobial wound dressing.* Carbohydrate Polymers, 2008. **72**(1): p. 43-51.
252. Sim, W., et al., *Antimicrobial Silver in Medicinal and Consumer Applications: A Patent Review of the Past Decade (2007(-)2017).* Antibiotics (Basel), 2018. **7**(4).
253. Reidy, B., et al., *Mechanisms of Silver Nanoparticle Release, Transformation and Toxicity: A Critical Review of Current Knowledge and Recommendations for Future Studies and Applications.* Materials (Basel), 2013. **6**(6): p. 2295-2350.
254. Lead, J.R., et al., *Nanomaterials in the environment: Behavior, fate, bioavailability, and effects-An updated review.* Environ Toxicol Chem, 2018. **37**(8): p. 2029-2063.
255. Kim, J.S., et al., *Antimicrobial effects of silver nanoparticles.* Nanomedicine-Nanotechnology Biology and Medicine, 2007. **3**(1): p. 95-101.
256. Marambio-Jones, C. and E.M.V. Hoek, *A review of the antibacterial effects of silver nanomaterials and potential implications for human health and the environment.* Journal of Nanoparticle Research, 2010. **12**(5): p. 1531-1551.
257. Bae, E., et al., *Bacterial uptake of silver nanoparticles in the presence of humic acid and AgNO3.* Korean Journal of Chemical Engineering, 2011. **28**(1): p. 267-271.
258. Jena, P., et al., *Toxicity and antibacterial assessment of chitosan-coated silver nanoparticles on human pathogens and macrophage cells.* International Journal of Nanomedicine, 2012. **7**: p. 1805-1818.
259. Eckhardt, S., et al., *Nanobio Silver: Its Interactions with Peptides and Bacteria, and Its Uses in Medicine.* Chemical Reviews, 2013. **113**(7): p. 4708-4754.
260. Romer, I., et al., *Aggregation and dispersion of silver nanoparticles in exposure media for aquatic toxicity tests.* J Chromatogr A, 2011. **1218**(27): p. 4226-33.
261. Tejamaya, M., et al., *Stability of Citrate, PVP, and PEG Coated Silver Nanoparticles in Ecotoxicology Media.* Environmental Science & Technology, 2012. **46**(13): p. 7011-7017.
262. Hitchman, A., et al., *The effect of environmentally relevant conditions on PVP stabilised gold nanoparticles.* Chemosphere, 2013. **90**(2): p. 410-6.

263. Scown, T.M., et al., *Effects of aqueous exposure to silver nanoparticles of different sizes in rainbow trout.* Toxicol Sci, 2010. **115**(2): p. 521-34.
264. Wiegand, I., K. Hilpert, and R.E. Hancock, *Agar and broth dilution methods to determine the minimal inhibitory concentration (MIC) of antimicrobial substances.* Nat Protoc, 2008. **3**(2): p. 163-75.
265. Grishagin, I.V., *Automatic cell counting with ImageJ.* Anal Biochem, 2015. **473**: p. 63-5.
266. Graham, L.L. and T.J. Beveridge, *Evaluation of Freeze-Substitution and Conventional Embedding Protocols for Routine Electron-Microscopic Processing of Eubacteria.* Journal of Bacteriology, 1990. **172**(4): p. 2141-2149.
267. Repaske, R., *Lysis of Gram-Negative Organisms and the Role of Versene.* Biochimica Et Biophysica Acta, 1958. **30**(2): p. 225-232.
268. Osborn, M.J. and R. Munson, *Separation of the inner (cytoplasmic) and outer membranes of Gram-negative bacteria.* Methods Enzymol, 1974. **31**: p. 642-53.
269. Nikaido, H., *Molecular basis of bacterial outer membrane permeability revisited.* Microbiol Mol Biol Rev, 2003. **67**(4): p. 593-656.
270. Matsushita, K., et al., *Isolation and Characterization of Outer and Inner Membranes from Pseudomonas-Aeruginosa and Effect of Edta on Membranes.* Journal of Biochemistry, 1978. **83**(1): p. 171-181.
271. Miller, C., et al., *SOS response induction by beta-lactams and bacterial defense against antibiotic lethality.* Science, 2004. **305**(5690): p. 1629-1631.
272. Torres-Barcelo, C., et al., *The SOS response increases bacterial fitness, but not evolvability, under a sublethal dose of antibiotic.* Proceedings of the Royal Society B-Biological Sciences, 2015. **282**(1816).
273. Irazoki, O., et al., *SOS System Induction Inhibits the Assembly of Chemoreceptor Signaling Clusters in Salmonella enterica.* PLoS One, 2016. **11**(1): p. e0146685.
274. Lee, B.K., Y.H. Yun, and K. Park, *Smart Nanoparticles for Drug Delivery: Boundaries and Opportunities.* Chem Eng Sci, 2015. **125**: p. 158-164.
275. Jeevanandam, J., et al., *Review on nanoparticles and nanostructured materials: history, sources, toxicity and regulations.* Beilstein J Nanotechnol, 2018. **9**: p. 1050-1074.
276. Monowar, T., et al., *Silver Nanoparticles Synthesized by Using the Endophytic Bacterium Pantoea ananatis are Promising Antimicrobial Agents against Multidrug Resistant Bacteria.* Molecules, 2018. **23**(12).
277. Duran, N., et al., *Silver nanoparticles: A new view on mechanistic aspects on antimicrobial activity.* Nanomedicine, 2016. **12**(3): p. 789-799.
278. Faiz, M.B., et al., *Nanosilver and the microbiological activity of the particulate solids versus the leached soluble silver.* Nanotoxicology, 2018. **12**(3): p. 263-273.
279. Pareek, V., R. Gupta, and J. Panwar, *Do physico-chemical properties of silver nanoparticles decide their interaction with biological media and bactericidal action? A review.* Materials Science and Engineering: C, 2018. **90**: p. 739-749.
280. Ban, D.K. and S. Paul, *Protein corona over silver nanoparticles triggers conformational change of proteins and drop in bactericidal potential of nanoparticles: Polyethylene glycol capping as preventive strategy.* Colloids Surf B Biointerfaces, 2016. **146**: p. 577-84.

281. Pareek, V., R. Gupta, and J. Panwar, *Do physico-chemical properties of silver nanoparticles decide their interaction with biological media and bactericidal action? A review.* Mater Sci Eng C Mater Biol Appl, 2018. **90**: p. 739-749.
282. Dong, F. and Y. Zhou, *Differential transformation and antibacterial effects of silver nanoparticles in aerobic and anaerobic environment.* Nanotoxicology, 2019. **13**(3): p. 339-353.
283. Riaz Ahmed, K.B., et al., *Silver nanoparticles: Significance of physicochemical properties and assay interference on the interpretation of in vitro cytotoxicity studies.* Toxicol In Vitro, 2017. **38**: p. 179-192.
284. López-Heras, M., et al., *Towards understanding the antibacterial activity of Ag nanoparticles: electron microscopy in the analysis of the materials-biology interface in the lung.* Environmental Science: Nano, 2015. **2**(4): p. 312-326.
285. Huang, J., et al., *Ag dendrite-based Au/Ag bimetallic nanostructures with strongly enhanced catalytic activity.* Langmuir, 2009. **25**(19): p. 11890-6.
286. Ghosh Chaudhuri, R. and S. Paria, *Core/shell nanoparticles: classes, properties, synthesis mechanisms, characterization, and applications.* Chem Rev, 2012. **112**(4): p. 2373-433.
287. Lopez-Heras, M., et al., *Towards understanding the antibacterial activity of Ag nanoparticles: electron microscopy in the analysis of the materials-biology interface in the lung.* Environmental Science-Nano, 2015. **2**(4): p. 312-326.
288. Azimzada, A., N. Tufenkji, and K.J. Wilkinson, *Transformations of silver nanoparticles in wastewater effluents: links to Ag bioavailability.* Environmental Science: Nano, 2017. **4**(6): p. 1339-1349.
289. Lasat, M.M., et al., *Advancing the Understanding of Environmental Transformations, Bioavailability and Effects of Nanomaterials, an International US Environmental Protection Agency-UK Environmental Nanoscience Initiative Joint Program.* J Environ Prot (Irvine, Calif), 2018. **9**(4): p. 385-404.
290. Choi, Y., et al., *Comparative toxicity of silver nanoparticles and silver ions to Escherichia coli.* Journal of Environmental Sciences, 2018. **66**: p. 50-60.
291. Zhang, W.C., et al., *Fate and toxicity of silver nanoparticles in freshwater from laboratory to realistic environments: a review.* Environmental Science and Pollution Research, 2019. **26**(8): p. 7390-7404.
292. Oliver, A.L.S., et al., *Does water chemistry affect the dietary uptake and toxicity of silver nanoparticles by the freshwater snail Lymnaea stagnalis?* Environmental Pollution, 2014. **189**: p. 87-91.
293. Dong, F., E. Valsami-Jones, and J.U. Kreft, *New, rapid method to measure dissolved silver concentration in silver nanoparticle suspensions by aggregation combined with centrifugation.* J Nanopart Res, 2016. **18**(9): p. 259.
294. Stoiber, T., et al., *Influence of hardness on the bioavailability of silver to a freshwater snail after waterborne exposure to silver nitrate and silver nanoparticles.* Nanotoxicology, 2015. **9**(7): p. 918-927.
295. Luoma, S.N., et al., *Effect of cysteine and humic acids on bioavailability of Ag from Ag nanoparticles to a freshwater snail.* Nanoimpact, 2016. **2**: p. 61-69.
296. Navarro, E., et al., *Toxicity of silver nanoparticles to Chlamydomonas reinhardtii.* Environ Sci Technol, 2008. **42**(23): p. 8959-64.

297. Piccapietra, F., et al., *Intracellular Silver Accumulation in Chlamydomonas reinhardtii upon Exposure to Carbonate Coated Silver Nanoparticles and Silver Nitrate.* Environmental Science & Technology, 2012. **46**(13): p. 7390-7397.
298. Leclerc, S. and K.J. Wilkinson, *Bioaccumulation of Nanosilver by Chlamydomonas reinhardtii-nanoparticle or the free ion?* Environ Sci Technol, 2014. **48**(1): p. 358-64.
299. Ellis, D.H., et al., *Silver nanoparticle antibacterial efficacy and resistance development in key bacterial species.* Biomedical Physics & Engineering Express, 2019. **5**(1).